Interaction between Highly-Anisotropic 4f System and Photo-Excited Cyclic π –systems in Lanthanide-Porphyrin Complexes with Varied Non-Aromatic Ligands

A doctorate thesis

Langit Cahya Adi

CHEMISTRY DEPARTMENT
GRADUATE SCHOOL OF SCIENCE
OSAKA UNIVERSITY

Abstract

In this doctorate thesis report, the electronic interaction in tetraphenylporphyrinato-lanthanides (Ln) complexes with different various non-aromatic ligands or simply called as the second ligands and Ln denotes Tb(III), Dy(III), and Y(III) as the reference were measured by using variable-temperature variable-magnetic field (VTVH) magnetic circular dichroism (MCD) spectrophotometer. Here, the mentioned electronic interaction is the interaction between the angular momentum of porphyrin (**L**) with the total momentum of the lanthanide (**J**), symbolized as Δ_{JL}. The second ligands used in this research are 12-crown-4 ether, 1-aza-12-crown-4 ether, and 2,2′-Ethylenebis(nitrilomethylidene)diphenol, *N*,*N*′-Ethylenebis(salicylimine) or salen. The purpose of this research is to investigate how the values of Δ_{JL} on Q(0,0), Q(1,0), and B(0,0) bands can be varied with different symmetry of the second ligands. The interaction was determined by using simulation-based fitting to the experimental $\mathcal{A}_1/\mathcal{D}_0$ ratios. Even though the angular momentum values of the complexes were not significantly changed, different interaction magnitude were observed as indicated by the different Δ_{JL}. The results are tabulated below.

Compound	B(0,0)		Q(0,0)		Q(1,0)	
	L_z	Δ_{JL}	L_z	Δ_{JL}	L_z	Δ_{JL}
[Y(TPP)Crown]Cl	0.54	-	3.44	-	2.35	-
[Tb(TPP)Crown]Cl	0.63	0.81	3.61	5.24	2.83	3.63
[Dy(TPP)Crown]Cl	0.84	-3.19	3.53	-0.39	2.26	-0.26
[Y(TPP)Azacrown]Cl	0.61	-	3.5	-	2.25	-
[Tb(TPP)Azacrown]Cl	0.54	1.02	3.68	6.77	3.9	4.37
[Dy(TPP)Azacrown]Cl	0.28	-4.19	3.44	-3.24	1.03	-1.74
[Y(TPP)Salen]Cl	0.66	-	4.53	-	2.66	-
[Tb(TPP)Salen]Cl	0.53	0.66	6.26	9.31	3.45	5.77
[Dy(TPP)Salen]Cl	0.59	-3.50	4.85	-1.29	2.85	-0.71

CONTENTS

Chapter 1

Introduction

1.1 General Introduction

Porphyrins or porphyrinoid compounds can be understood as a macrocyclic compound consisted of four tetrapyrroles connected with methine bridge. They have been long known regarding their major roles in nature such as chlorophyll and pheophytin in photosynthesis, haemoglobin for oxygen transport process, cytochrome for electrons transfer, myoglobin for oxygen storage, or they are simply used as pigments[1,2]. Since the mentioned porphyrins in their natural occurrences are metalated, therefore metalated porphyrins draw attention for researchers to develop more. For example, there was research studying platinum-porphyrin and extended porphyrin regarding their near-infrared phosphorescent properties[3]. Others reported the prospects of metal-porphyrin as electronic material[4], polymerization catalyst[5], and as well as that, porphyrins' electrochemical properties[6,7]. The development metal-porphyrin has been developing not limited in transition metal only, but expanded to lanthanide(Ln)-porphyrin directed to be magnetic materials or more specifically to investigate their single-molecular magnetism potential[8-10].

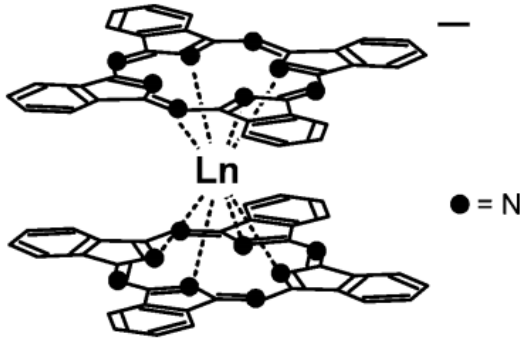

Figure 1.1 Scheme of $[Pc_2Ln]^-$ with Ln = Tb(III) or Dy(III)

The interest of investigating Ln-metalated porphyrin roots from the finding based on previous report[11-12]. In a molecular system of phtalocyanine, another type of tetrapyrrole compound, named $[Pc2Ln]^-•TBA^+$ (TBA: tetrabuthylammine) in homoleptic structure, it is discovered that among metal ions in Ln series of Tb, Dy, Ho, Er, Tm, and Yb, Tb and Dy indicated strong single-molecular magnetism character and furthermore, such results

indicate magnetic anisotropy of Tb and Dy, indicated by large total angular momentum symbolized as J_z values of the sublevels of the ground multiplets of square-antiprismatic molecular systems. In particular, the ligand field splitting calculation of the Ln-phtalocyanine were calculated and J_z values of Tb and Dy were reported to be equal ±6 and $\pm\frac{13}{2}$ respectively, in which the two values are the two biggest values compared to the other Ln metals. The magnetic anisotropy of Tb and Dy is also confirmed by another report[13], stating that strong angular dependence electronic structures of Tb and Dy is the key.

This finding is an important foundation for deeper investigation of another complexes with square-antiprismatic geometry. Recently, synthesis of Ln-porphyrin (Ln: Tb, Dy, Ho, Er, Tm, Yb, and Y) with crystal structure determinations was reported[14]. Here, Ln metals formed complexes with 5,10,15,20-tetraphenylporphyrinato (TPP) and 1,4,7,10-tetraazacyclododecane (cyclen) or named as [Ln(TPP)cyclen]Cl where both organic moieties bind with the metals via their N atoms, forming a sandwich-like structure where the skew angles are close to 45° which means that square-antiprismatic structure can be obtained with tetradentate non-aromatic ligand or simply called as the second ligand.

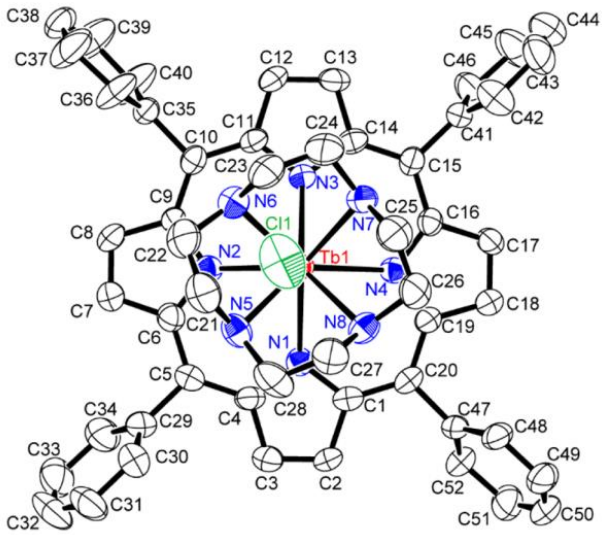

Figure 1.2 Crystal structure of [Tb(TPP)cyclen]Cl

By obtaining single-crystal structure, ligand-field splitting of Ln-porphyrin can be calculated by both experiment and computational chemistry calculation[15]. Through comparison between the results of experiment and calculation, it is understood that ligand-field estimation difference is very slight and in fact, computational chemistry calculation can

be carried out as a mean to predict the multilevel energy in ground states in Ln-porphyrin systems. In that mentioned work, the energy difference of [Tb(TPP)cyclen]Cl between the lowest state and the second-lowest state is relatively smaller compared with $[Pc2Tb]^{-}\bullet TBA^{+}$. In addition to that, the lowest and the second-lowest J_z value of Dy complex was respectively equal $\pm\frac{11}{2}$ and $\pm\frac{13}{2}$ slightly different with $[Pc2Dy]^{-}\bullet TBA^{+}$ where the lowest and the second-lowest J_z value were $\pm\frac{13}{2}$ and $\pm\frac{11}{2}$. The energy diagram of [Tb(TPP)cyclen]Cl and [Dy(TPP)cyclen]Cl are given as follow.

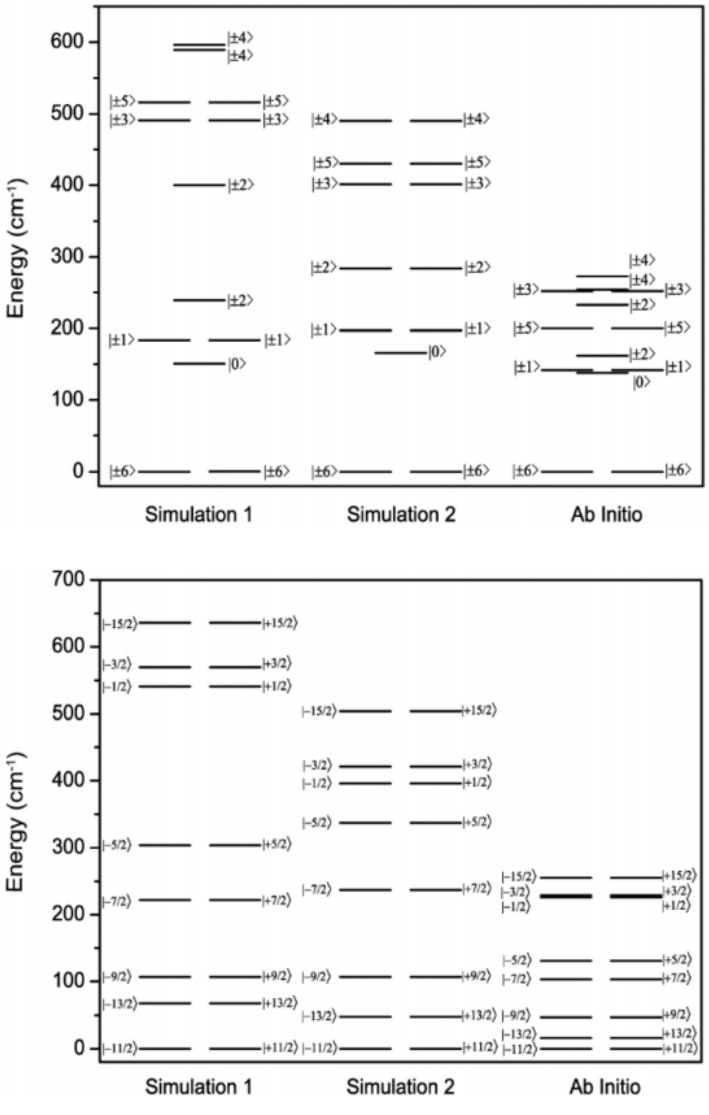

Figure 1.3 Energy diagram for the multilevel ground-state of [Tb(TPP) cyclen]Cl **(a)** and [Dy(TPP)cyclen]Cl **(b)**. Simulations 1 and 2 are produced with C_4 and D_{4d} symmetry, respectively.

Regarding their optical-electronic characters, metal-porphyrins exhibit characteristic spectra under ultraviolet (UV) and visible wavelength (300-800 nm) with two groups of bands[7,14,16,17]. The first band is located close to UV region named B band, identified with its intense, sharp appearance and the other one is observed in the visible wavelength named Q bandss, consisted of Q(0,0) and Q(1,0) bands. The Q bandss appear to be small and much less intense than B band. Those bands are associated with the highest-occupied molecular orbital (HOMO) to lowest-unoccupied molecular orbital (LUMO) or ascribed to the π–π* transition within porphyrin. More specifically, B band is yielded from allowed transition with the total angular momentum (ΔL) = ±1 while on the other side, Q bands originates from forbidden transition with ΔL = ±9. That is also why B band appears considerably higher and sharper compared to Q bands[18-20].

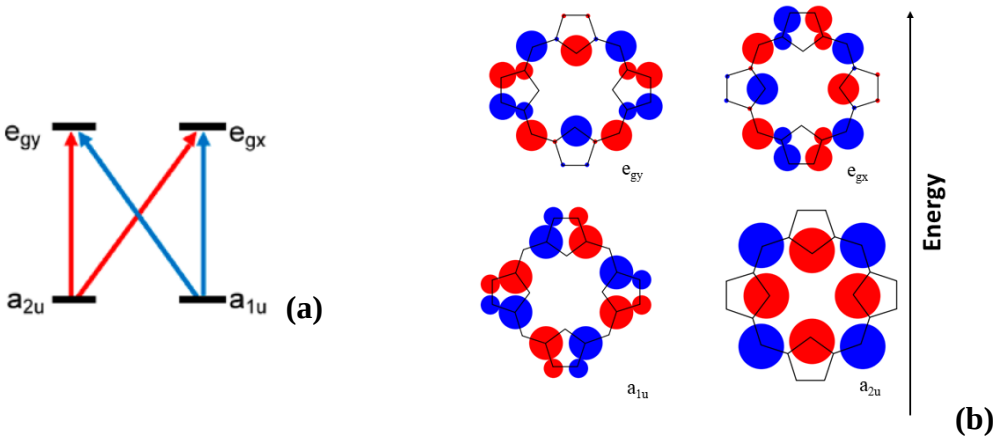

Figure 1.4 The electronic transition scheme of porphyrin **(a)** and molecular orbital of porphyrin according to the Gouterman's four-orbital model **(b)**

However, in order to perform examination at a molecular level, higher sensitivity tool needs to be used. Thus, magnetic circular dichroism (MCD) spectroscopy is then advantageous. From the work of Ceulemans et al.[21], MCD measurement is reported to measure the angular momentum of metalated porphyrin with different axial ligation for both B and Q bandss. By using the four-orbital model by Gouterman[19], the report also explains that electronic transition from a_{2u} and a_{1u} to e_{gy} and e_{gx} yield four combinations i.e. **(1)** ($a_{2u} \rightarrow e_{gx}$) − ($a_{1u} \rightarrow e_{gy}$), **(2)** ($a_{2u} \rightarrow e_{gy}$) + ($a_{1u} \rightarrow e_{gx}$), **(3)** ($a_{2u} \rightarrow e_{gx}$) + ($a_{1u} \rightarrow e_{gy}$), and **(4)** ($a_{2u} \rightarrow e_{gy}$) − ($a_{1u} \rightarrow e_{gx}$). While **(1)** and **(2)** are corresponding with B band, the rest are associated with Q bands. Because of the configuration mixing, B band has higher intensity but smaller angular momentum and Q bands gains lower intensity with greater angular momentum.

On the other hand, some principles of MCD analysis are necessary to be described first. The measured is performed in all matter by applying a uniform magnetic field (*H*) parallel to the light propagating through the sample. Hence, the Zeeman perturbation will be introduced and the electronic state degeneracy will be lifted. While maintaining Zeeman splitting of the electronic states, molecules in sample are irradiated with circularly polarized light. The instrument measures difference between left circularly polarized light (lcp) and right circularly polarized light (rcp) that each corresponds to the transitions between the Zeeman components. Such difference is formulated as $\Delta\varepsilon = \varepsilon_{lcp} - \varepsilon_{rcp}$ where ε_{lcp} and ε_{rcp} each means molar absorptivity for left circularly polarized light and right circularly polarized light. In MCD analysis for porphyrins, signals are recorded as superposition of $\mathcal{A}_1$, $\mathcal{B}_0$, and $\mathcal{C}_0$ terms. $\mathcal{A}_1$ term originates from degenerate level of excited states is split due to magnetic field and lcp induces transition to the higher split state and rcp induces transition to the lower split state. $\mathcal{B}_0$ term arises from the mixing in ground and excited states. $\mathcal{C}_0$ term is present caused by degenerate ground state and thus, strongly depends on temperature[22,23].

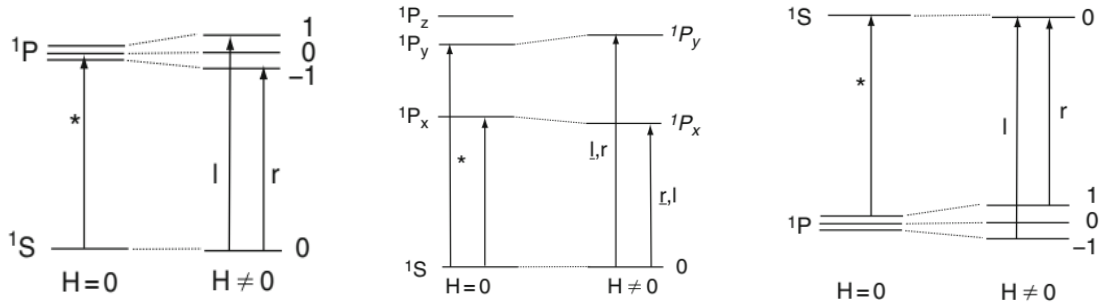

(a) **(b)** **(c)**

Figure 1.5 The illustration of the transition in $\mathcal{A}_1$ term (a), $\mathcal{B}_0$ term (b), and $\mathcal{C}_0$ term (c).

The application of MCD has been expanded and recently by our group, it is employed to measure the electronic interaction between total angular momentum of lanthanide from the 4f electrons, symbolised as **J**, and the angular momentum of porphyrin **L** (denoted as Δ_{JL}) in [Tb(TPP)cylen]Cl[24] and [Dy(TPP)cyclen][25]. The measurement was carried out by incorporating the complex samples into poly(methyl methacrylate), resulting frozen solutions. The analysis was performed with varied temperature and varied magnetic field (VTVH) and by deconvolution technique, the values of $\mathcal{A}_1/\mathcal{D}_0$ as the angular momentum of the porphyrinoid molecular systems at each temperature set and under certain magnetic field

will be estimated. Then, by using simulation fitting to the experimental data of VTVH $\mathcal{A}_1/\mathcal{D}_0$, Δ_{JL} was estimated and compared with the theoretical result.

On the other hand, our group also analysed how $|L_z|$ or the angular momenta along the z-axis and Δ_{JL} values of tetrapyrollic compounds differ with different second ligand by MCD spectroscopy measurement. In a previous report[26], MCD analysis was carried out for $[Pc_2Tb]^-$ and it was concluded that the values of $|L_z|$ and Δ_{JL} for two Q-bands i.e. Q_H and Q_L are different between each other. With Q_L and Q_H are respectively lower- and higher-energy, $|L_z|$ and Δ_{JL} values are determined to be $|L_z| = 2.3\hbar$ and $\Delta_{JL} = 1.4$ cm^{-1} for Q_L while $|L_z| = 2.2\hbar$ and $\Delta_{JL} = 2.6$ cm^{-1} for Q_H. When one phtalocyanine was replaced with cyclen with maintaining the sandwich-like structure resulting [Tb(Pc)cyclen]Cl[27], only one absorption peak appeared meaning different electronic transition was observed when a non-aromatic ligand replaced the other aromatic macrocyclic ligand due to reduction of the number of electronic transition from 2 to 1. As well as that, from the MCD analysis, $|L_z|$ and Δ_{JL} values each were determined to be $2.0\hbar$ and 2.6 cm^{-1}.

1.2 This Thesis Report

From the description in Section 1.1, it can be inferred that different electronic transition in Ln-phtalocyanine was observed due to the effect of the second ligand. However, this observation was discovered particularly for Ln-phtalocyanine molecular system. So far, there is still no study about the electronic interaction alters with different second ligand in Ln-porphyrin complexes. Thus, this thesis is going to address that problem by referring to the work investigating the electronic interaction within [Ln(TPP)cylen]Cl conducted by our group[24,25]. Here, different organic moieties containing different atoms electronegativities and symmetry with tetradentate binding mode are used to bind with Ln-porphyrin as in [Ln(TPP)cyclen]Cl. The reason why different symmetry of the second ligand is attempted to be in the Ln-porphyrin complexes is because it is necessary to understand how the **J–L** interaction is altered with more distorted ligand inside the compounds.

In Chapter 2, MCD analysis of Ln-porphyrin with cyclododecane ligands and Ln: Tb, Dy, and Y will be reported and explained. The ligands are 1,4,7,10-tetraoxacyclododecane or 12-crown-4 ether and 1,4,7-trioxa-10-azacyclododecane or 1-aza-12-crown-4 ether and they were selected because of the presence of 4 oxygen atoms replacing 4 nitrogen atoms in cyclen with analogous molecular structure which will introduce different electron affinity while for 1-aza-12-crown-4 ether, one of 4 oxygen atoms

in 12-crown-4 ether is replaced with 1 nitrogen which results reduced molecular symmetry. In order to understand the electronic energy states and the orientation of the electronic interaction, *ab-initio* calculation is carried out and described as well.

In Chapter 3, the effect of lower molecular symmetry of the second ligand toward the **J–L** interaction from MCD analysis will be explained. Here, the second ligand is 2,2′-Ethylenebis(nitrilomethylidene)diphenol, *N*,*N*′-Ethylenebis(salicylimine) or salen instead of other compound from cyclododecane group. As salen has more distorted structure compared 1-aza-12-crown-4 ether, more significant **J–L** interaction difference is expected according to the results of MCD measurement. As well as in Chapter 2, computational calculation will be reported in order to analyze the electronic state energy level and also the orientation of the electronic interaction.

1.3 References

1. A.R. Battersby., *Nat. Prod. Rep.*, 2000, **17**, 507–526.
2. J.A. Shelnutt, X.Z., Song, J.G., Ma, S.L. Jia, W. Jentzen, C.J. Medforth, *Chem. Soc. Rev.*, 1998, **27**, 31-42.
3. J.A. Sommer, A.H. Shelton, A. Parthasarathy, I. Ghiviriga, J.R. Reynolds, K.S. Schanze, *Chem. Mater.*, 2011, **23**, 5296-5304.
4. I. Gimeno, A. Urtizberea, J. Roman-Roche, D. Zueco, A. Camon, P.J. Alonso, O. Roubeau, F. Luis, *Chem. Sci.*, 2021, **12**, 5621-5630.
5. S. Praban, P. Piromjitpong, V. Balasanthiran, S. Jayaraj, M.H. Chisholm, J. Tantirungrotechai, K. Phomphrai, *Dalton Trans.*, 2019, **48**, 3223-3230.
6. L. Ye, Y. Fang, Z. Ou, S. Xue, K.M. Kadish, *Inorg. Chem*., 2017, **56**, 13613-13626.
7. M. Fathi-Rasekh, G.T. Rohde, M.D. Hart, T. Nakakita, Y.V. Zatsikha, R.R. Valiev, M.V. Barybin, V.N. Nemykin, *Inorg. Chem.*, 2019, **58**, 9316-9325.
8. J.J. Le Roy, J. Cremers, I.A. Thomlinson, M. Slota, W.K. Myers, P.H. Horton, S.J. Coles, H.L. Anderson, L. Bogani, *Chem. Sci.*, 2018, **9**, 8474–8481.
9. T. Inose, D. Tanaka, H. Tanaka, O. Ivasenko, T. Nagata, Y. Ohta, S. de Feyter, N. Ishikawa, T. Ogawa, *Chem. Eur. J.*, 2014, **20**, 11362-11369.
10. D. Tanaka, T. Inose, H. Tanaka, S. Lee, N. Ishikawa, T. Ogawa, *Chem. Commun*., 2012, **48**, 7796-7798.
11. N. Ishikawa, M. Sugita, T. Okubo, N. Tanaka, T. Iino, Y. Kaizu, *Inorg. Chem.*, 2003, **42**, 2440-2446.

12. N. Ishikawa, M. Sugita, T. Ishikawa, S. Koshihara, Y. Kaizu, *J. Am. Chem. Soc.*, 2003, **125**, 8694-8695.
13. D.N. Woodruff, R.E.P. Winpenny, R.A. Layfield, *Chem. Rev*., 2013, **113**, 5110-5148.
14. A. Santria, A. Fuyuhiro, T. Fukuda, N. Ishikawa, *Inorg. Chem.*, 2017, **56**, 10625-10632.
15. A. Santria, A. Fuyuhiro, T. Fukuda, N. Ishikawa, *Dalton Trans.*, 2019, **48**, 7685-7692.
16. V.K.K. Praneeth, F. Neese, N. Lehnert, *Inorg, Chem.*, 2005, **44**, 2570-2572.
17. P. Singh, A.K. Das, B. Sarkar, M. Niemeyer, F. Roncaroli, J.A. Olabe, J. Fiedler, S. Zalis, W. Kaim, *Inorg. Chem.*, 2008, **47**, 7106-7113.
18. M. Gouterman, *J. Chem. Phys.*, 1960, **33**, 1523-1529.
19. M. Gouterman, *J. Mol. Spectrosc.*, 1961, **6**, 138-163.
20. J. Mack, M.J. Stillman, N. Kobayashi, *Coord. Chem. Rev.*, 2007, **251**, 429-453.
21. A. Ceulemans, W. Oldenhof, C. Görller-Walrand, L. G. Vanquickenborne, *J. Am. Chem. Soc.*, 1986, **108**, 1155−1163.
22. C. Görller-Walrand and L. Fluyt, in *Handbook on the Physics and Chemistry of Rare Earths*, ed. K. A. Gschneidner Jr., J.-C. G. Bünzli and V. K. Pecharsky, North Holland, Elsevier B.V., Amsterdam, 2010, ch. 244, vol. 40.
23. J. Mack, M.J. Stillman, N. Kobayashi, *Coord. Chem. Rev.*, 2007, **251**, 429-453.
24. A. Santria and N. Ishikawa, *Inorg. Chem*., 2020, **59**, 14326-14336.
25. A. Santria and N. Ishikawa, *Inorg. Chem*., 2021, **60**, 14418-14425.
26. K. Kizaki, H. Ozawa, T. Kobayashi, R. Matsuoka, Y. Sakaguchi, A. Fuyuhiro, T. Fukuda, N. Ishikawa, *Chem. Commun*., 2017, **53**, 6168-6171.
27. K. Kizaki, A. Santria, N. Ishikawa, *Inorg. Chem.*, 2020, **60**, 2037-2044.

Chapter 2

Investigation of J-L Interaction in Excited States of Lanthanide-porphyrin with Cyclododecane Ligands by Using Magnetic Circular Dichroism

2.1 Introduction

Magnetic Circular Dichroism (MCD) spectroscopy has long been known for its useful role to examine electronic transition with high sensitivity and it is also independent from chirality unlike CD. The electronic transition is closely related with the differential absorption between left and right-handed circularly polarized light which is caused by a static magnetic field when light beam propagates[1,2]. With the results of positive and negative bands, thus overlapping electronic transition can be identified and be resolved. However, such attempt can be achieved usually with coupling MCD analysis with computational calculation as well[3].

MCD spectroscopy is also used to study electronic transition in various porphyrinoid compounds with different structure. Previously, MCD spectroscopy was applied to analyze angular momenta of cobalt-octaethylporphyrin complexes with various oxidation states[4] and to examine electronic transition within porphyrin attached with electron-withdrawing groups[5]. By Galinato et al.[6] and Rhoda et al[7], MCD spectroscopy analysis was coupled with density functional theory (DFT) and time-dependent density functional theory (TDDFT)calculation in order to study the electronic transition in various transition metal-porphyrin in different conformation. From their results, they proved also that the computational calculation can elucidate the energy states of each π–π^* transition in several substituents in porphyrins complexes. By Andruschenko et al.[8], trivalent lanthanide-porphyrin complexes were studied with comparing between tetraphenylporphyrin (TPP) and octaethylporphyrin (OEP) and the ions were Y, La, Eu, Tb, Dy, Ho, Er, Tm, Yb and Lu. The results revealed that while the magnitude of the MCD signals were relatively constant with different metal ions in either TPP complexes or in OEP complexes, Q bands of OEP complexes exhibit only one A-term signal which is contrast to Q bands of TPP complexes which had two A-term signals which each corresponded to Q(0,0) and Q(1,0) peaks. Such

results are indication that MCD can distinguish different electronic transition in porphyrinoid macrocycles.

On the other hand, lanthanide-crown ether complexes are also interesting as a magnetic material candidate. As well as that, crown ether compounds are known for their facile nature of the organic compound to bind with lanthanide ions strongly through coordination bonding by all O donors[9]. Also according to other reports[10-12], such bonding mode were confirmed from the single-crystal characterization. However, lanthanide ions were not bind exactly in the middle of diameter cavity of crown ether but rather forming sandwich-like or pseudo-sandwich structure with crown ether in one layer and anions on the other layer. On the other hand, 1-aza-12-crown-4 ether crystallized with metal in similar mode where the ammine site donated its electron to create coordination bonding together with oxygen atoms[13].

In this chapter, MCD analysis of Ln-porphyrin complexes with 12-crown-4 ether and 1-aza-12-crown-4 ether are going to be explained and compared. The aim is to understand how different symmetry of the second ligand of cyclododecane ligands will affect the L_z and Δ_{JL} values of Tb and Dy in porphyrin molecular systems with Y complexes as references. In order to examine the electronic structure and direction of the interaction more thoroughly, *ab initio* calculations are explained as well.

2.2 Experimental Methods

2.2.1 Materials and synthesis

The synthesis of complexes is referring to previous publication[14] with replacing cyclen with 12-crown-4 ether to get [Y(TPP)Crown]Cl, [Tb(TPP)Crown]Cl, and [Dy(TPP)Crown]Cl and with 1-aza-12-crown-4 ether to obtain [Y(TPP)Azacrown]Cl, [Tb(TPP)Azacrown]Cl, and [Dy(TPP)Azacrown]Cl. Absorption spectra were measured by using a Thermo Scientific Evolution 220 UV-Visible spectrophotometer. For elemental analysis (C, H, and N), the analysis was done with a Yanaco CHN Corder MT-5 and MT-6 Elemental Analyzer. Mass spectra were measured using a Kratos PC Axima CFR V.2.3.5 (Shimadzu Corporation) operated in reflectron mode. MCD measurements were performed at room temperature (298 K, for solution samples) under permanent magnet of 1.6 T while samples in PMMA films, measurements were performed at varying temperatures from 100 to 1.5 K and with magnetic field range of 0−6 T using a JASCO J-720W spectrodichrometer equipped with an Oxford Instruments SM4000 Spectromag cryostat.

In the unit of mass/charge (m/z), the cationic peaks were found as 877.09, 947.1, 952.17, 876.19, 946.25, and 951.25 that are respectively corresponding to $[Y(TPP)Crown]^+$, $[Tb(TPP)Crown]^+$, $[Dy(TPP)Crown]^+$ $[Y(TPP)Azacrown]^+$, $[Tb(TPP)Azacrown]^+$, and $[Dy(TPP)Azacrown]^+$. Elemental analysis of C, H, and N gave calculation results as C: 62.68, H: 5.99, N: 4.96 (calcd. C: 62.68, H: 5.96, N: 5.22) for [Y(TPP)Crown]Cl. For [Tb(TPP)Crown]Cl, C: 61.88, H: 5.36, N: 5.29 (calculated C: 61.81, H: 5.49, N: 5.20). For [Dy(TPP)Crown]Cl, C: 55.32, H: 4.69, N: 5.14 (calculated C: 55.25, H: 4.87, N: 5.10).

For [Y(TPP)Azacrown]Cl, measured C: 56.28, H: 6.37, and N: 7.25 (calculated C: 56.21, H: 6.17, and N: 7.15) and for [Tb(TPP)Azacrown]Cl, measured C: 54.29, H: 4.68, and N: 5.87 (calculated C: 54.30, H: 4.83, and N: 5.88). While for [Dy(TPP)Azacrown]Cl, measured C: 55.82, H: 6.81, and N: 7.54 (calculated C: 55.77, H: 6.61, and N: 7.39).

As much as 150 mg of PMMA was dissolved in 2 mL of chloroform containing complex to be analysed prior to the MCD measurements. The dried films then would be subjected to the instrument.

2.2.2 Methods for MCD analysis

The absorption and MCD spectra were measured at different temperatures and magnetic field and analysed quantitatively as $\mathcal{A}_1/\mathcal{D}_0$ ratio where $\mathcal{A}_1$ denotes the A-term intensity and $\mathcal{D}_0$ corresponds to the oscillator strength of the band. The $\mathcal{A}_1/\mathcal{D}_0$ values were obtained by fitting of the spectra shape to the following equation[15]

$$\frac{\Delta A}{E} = \gamma \mu_{Bohr} B \left[\mathcal{A}_1 \left(\frac{-\delta f(E)}{\delta E} \right) + \left(\mathcal{B}_0 + \frac{\mathcal{C}_0}{k_B T} \right) f(E) \right]$$

$$\frac{A}{E} = \gamma D_0 f(E)$$

Here, ΔA is the difference between absorbance of left and right circularly polarized light, lcp and rcp, in a magnetic field, E is energy in cm^{-1}, B is the magnetic field in tesla (T), μ_{Bohr} is Bohr magneton (magnetic moment), γ = 326.5cl (c = concentration in mol/L, l is path length which in this case is thickness of sample film in cm), $\mathcal{A}_1$ is MCD A-term, $\mathcal{B}_0$ is MCD B-term, $\mathcal{C}_0$ is MCD C-term, $\mathcal{D}_0$ is oscillator strength, and $f(E)$ is the band shape function[16].

However, the temperature and the magnetic field of $\mathcal{A}_1/\mathcal{D}_0$ ratio can be explained using theoretical model that previously has been explained in other works[17-21]. In PMMA matrix, sample is expected same absorbance spectra as in dichloromethane solvent. Zeeman energy of **J** and **L** have a component of θ because the z axis of the molecule in the matrix is

assumed to be randomly distributed in the range from 0 to 90° and the relations can be stated with $g_J\mu_B J_z B\cos\theta$ and $g_J\mu_B L_z B\cos\theta$ respectively. Here, θ is the angle between the direction of the magnetic field B and the z axis. The transition moments from ground states to the π–π* excited states at $\theta = 0$ are represented by the equations below.

$$\left|\langle\alpha|\hat{m}_{\pm1}|\alpha\ \mp\rangle\right|^2 = \left|\langle\alpha\ \pm|\hat{m}_{\pm1}|\alpha\rangle\right|^2 \equiv M^2$$

$$\left|\langle\alpha|\hat{m}_{\pm1}|\alpha\ \pm\rangle\right|^2 = \left|\langle\alpha\ \mp|\hat{m}_{\pm1}|\alpha\rangle\right|^2 \equiv 0$$

$$\hat{m}_{\pm1} = \mp\left(\frac{1}{\sqrt{2}}\right)(\hat{m}_x \pm i\hat{m}_y)$$

with α is either + or -, $\hat{m}_{\pm1}$ is the transition moment operator defined by Piepho and Schatz[15]. The spatially averaged $\mathcal{D}_0$ related with M is formulated below.

$$\mathcal{D}_0 = \left(\frac{1}{3}\right)\mathcal{D}_0(\theta = 0) = \left(\frac{2}{3}\right)M^2$$

When $\theta \neq 0$ the equation will be

$$|\langle\alpha|\hat{m}_{-1}|\alpha\ \mp\rangle_\theta|^2 = |\langle\alpha\ |\hat{m}_{+1}|\alpha\ \mp\rangle_\theta|^2 = \frac{(M^2(1\ \pm\cos\theta)^2)}{4}$$

Also, there is a transition from $|\boldsymbol{\alpha}\rangle$ to $|\boldsymbol{\alpha}, \pm\rangle$ whose energy is shifted by Zeeman term and by interaction between **J** and **L** denoted as $\Delta_{\mathbf{JL}}$. These can be represented as

$$\mu_{Bohr}B\langle\alpha\lambda|L_z|\alpha\lambda\rangle\cos\theta + \delta_{\alpha\lambda}\Delta_{JL}$$

where α and λ are either $+$ or $-$ and

$$\delta_{\alpha\lambda} = \begin{cases} +1, & \text{for } \alpha \neq \lambda \\ -1, & \text{for } \alpha = \lambda \end{cases}$$

By including the thermal population to the ground states, $\mathcal{A}_1(\theta)$ thus will be written as following

$$\mathcal{A}_1(\theta) = \sum_{\alpha=-,+}\{\sum_{\lambda=-,+}\left(\langle\alpha\lambda|L_z|\alpha\lambda\rangle\cos\theta + \frac{\delta_{\alpha\lambda}\Delta_{JL}}{\mu_{Bohr}B}\right) \times (|\langle\alpha|\hat{m}_{-1}|\alpha\lambda\rangle|^2 - |\langle\alpha\ |\hat{m}_{+1}|\alpha\lambda\rangle|^2)\cos\theta\} \times \frac{\exp\left(\frac{-g_J\mu_{Bohr}\langle\alpha|J_z|\alpha\rangle B\cos\theta}{k_BT}\right)}{\sum_{\alpha=-,+}exp\left(\frac{-g_J\mu_{Bohr}\langle\alpha|J_z|\alpha\rangle B\cos\theta}{k_BT}\right)}$$

Both **J** and **L** have components along z-axis which each is symbolized as J_z and L_z. There are six states which are assumed to be diagonal in $\hat{J}_z$ and $\hat{L}_z$ and are non-zero matrix elements for the angular momentum operators are

$$\langle-|\hat{J}_z|-\rangle = \langle-+|\hat{J}_z|-+\rangle = \langle--|\hat{J}_z|--\rangle = -|J_z|$$

$$\langle+|\hat{J}_z|+\rangle = \langle++|\hat{J}_z|++\rangle = \langle+-|\hat{J}_z|+-\rangle = +|J_z|$$

$$\langle + + |\hat{L}_z| + + \rangle = \langle - + |\hat{L}_z| - + \rangle = +|L_z|$$
$$\langle + - |\hat{L}_z| + - \rangle = \langle - - |\hat{L}_z| - - \rangle = -|L_z|$$

2.2.3 Computational Chemistry Calculations

The calculations were conducted using Open Molcas v 19.11 program package with the molecular structure was optimized using Gaussian09 software. The basis set used in the calculations are ANO-RCC contracted with VTZP for the metals and ANO-RCC-MB was applied on the common atoms. The calculations also used state averaged RASSCF (restricted active space self-consistent field) wave functions and employed RASSI (restricted active space state interaction) and single_aniso calculation to get oscillator strength and spin-orbit (S.O) coupling states.

2.3 Results and Discussion

2.3.1 Analysis of Y complexes

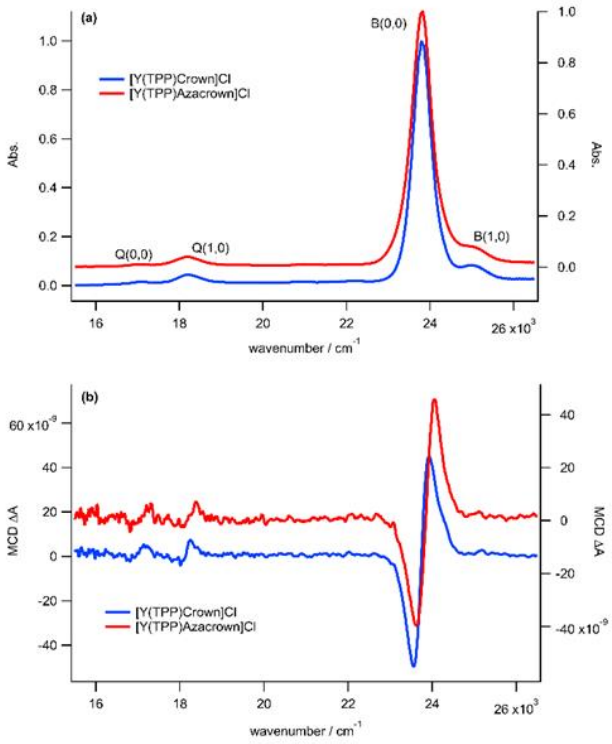

Figure 2.1 UV-Vis spectra (**a**) and room temperature MCD spectra (**b**) of Y complexes

Prior to the investigation of the electronic interaction in lanthanide-porphyrin molecular systems, MCD measurement on Y is necessary to be performed first since Y(III) has diamagnetic character which is treated as the reference for Tb and Dy complexes.

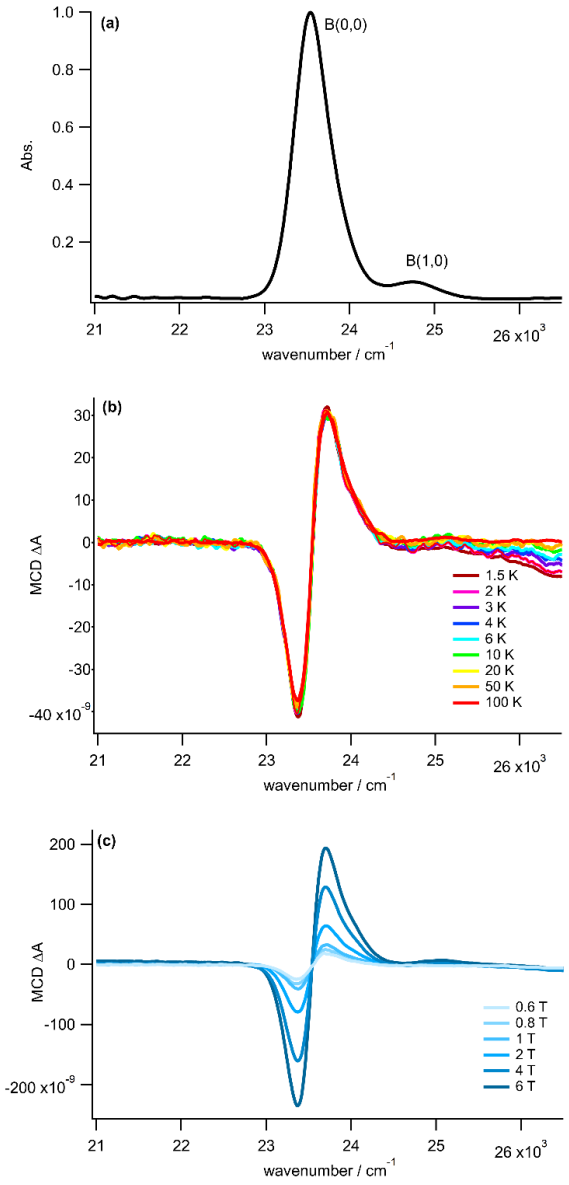

igure 2.2 (a) Absorption, (b) temperature-dependent MCD spectra measured at temperatures of 1.5-100 K under a magnetic field of 1 T, and (c) magnetic field-dependent MCD spectra measured at temperatures of 1.5 K of B band in [Y(TPP)Crown]Cl in PMMA film.

From Figure 2.1(a), both [Y(TPP)Crown]Cl and [Y(TPP)Azacrown]Cl have four absorption peak i.e. Q(0,0), Q(1,0), B(0,0), and B(1,0) bands, in which all of them are associated to

the π–π* electronic transitions, with their positions are located approximately at the same wavenumber. Corresponding to this, both Y complexes were measured by using MCD

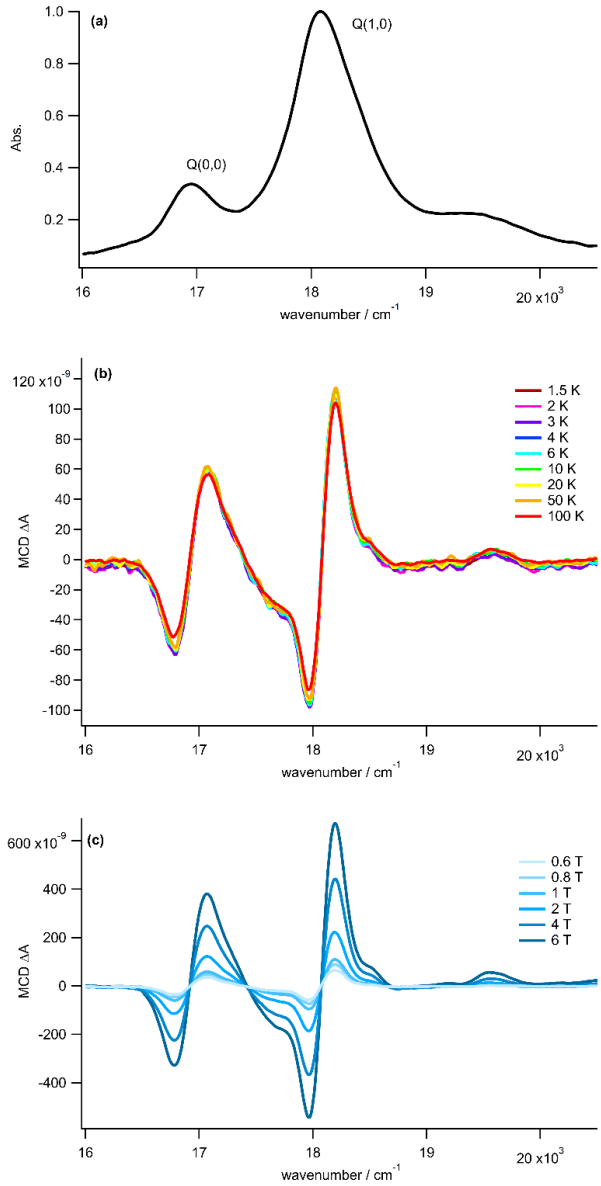

Figure 2.3 (a) Absorption, (b) temperature-dependent MCD spectra measured at temperatures of 1.5-100 K under a magnetic field of 1 T, and (c) magnetic field-dependent MCD spectra measured at temperatures of 1.5 K of Q bands in [Y(TPP)Crown]Cl in PMMA film.

spectrophotometer at room temperature where three positive A-term profiles were detected and the profile related to B(0,0) band of [Y(TPP)Azacrown]Cl was shifted to higher wavenumber compared to that [Y(TPP)Crown]Cl. The presence of the positive A-term band in the MCD signal is associated with the existence of degenerate LOMO excited states within porphyrin compound. However, in their room temperature MCD spectra in Figure 2.1(b), no MCD signal corresponding to B(1,0) band was observed. Thus, it can be inferred that

different symmetry between 12-crown-4 ether and 1-aza-12-crown-4 ether does not alter electronic structure in porphyrin complexes.

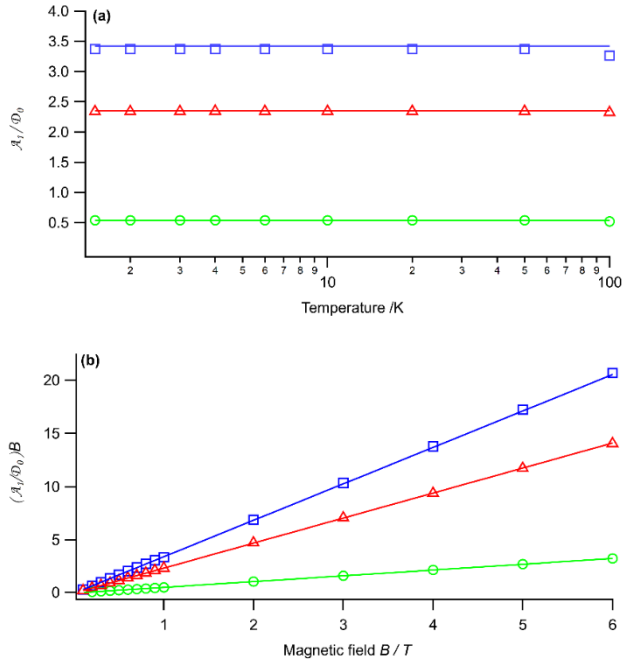

Figure 2.4 Experimental values (squares, triangles, and circles) and calculated value (straight line) of $\mathcal{A}_1/\mathcal{D}_0$ of [Y(TPP)Crown]Cl for B(0,0) in green, Q(1,0) in red, and Q(0,0) in blue under 1 T of magnetic field with varied temperature (a) and under varied magnetic field (b).

Under VT-VH-MCD measurement, some differences in [Y(TPP)Crown]Cl and [Y(TPP)Azacrown]Cl are noticed. In Figure 2.2 and 2.3, both B and Q bandss show no change of positive ΔA intensity of A-term profile under varied temperature from 100 until 1.5 K. Contrary to that, at temperature 1.5 K, the intensity undergoes variation under different magnetic field and it also depends proportionally with the magnetic of the applied field. By applying deconvolution of all spectra measured at different temperature and under varied magnetic field, the values of $\mathcal{A}_1/\mathcal{D}_0$ for all bands were calculated and determined and the results are shown in Figure 2.4.

From the deconvolution of all bands, $\mathcal{A}_1/\mathcal{D}_0$ were found to be constant when the temperature was diminished from 100 K until 1.5 K. As well as that, when the magnetic field is increased from 0.1 T to 6 T, the values of $(\mathcal{A}_1/\mathcal{D}_0)B$ demonstrating the diamagnetic character of Y(III). From the simulation calculation, L_z values for B(0,0), Q(0,0), and Q(1,0)

bands are estimated to be 0.54$\hbar$, 3.44$\hbar$, and 2.35$\hbar$ respectively. Those values are practically very close to the values in previous work with [Y(TPP)Cyclen]Cl by Santria and Ishikawa[17] where L_z for B(0,0), Q(0,0), and Q(1,0) bands are 0.66$\hbar$, 3.59$\hbar$, and 2.61$\hbar$.

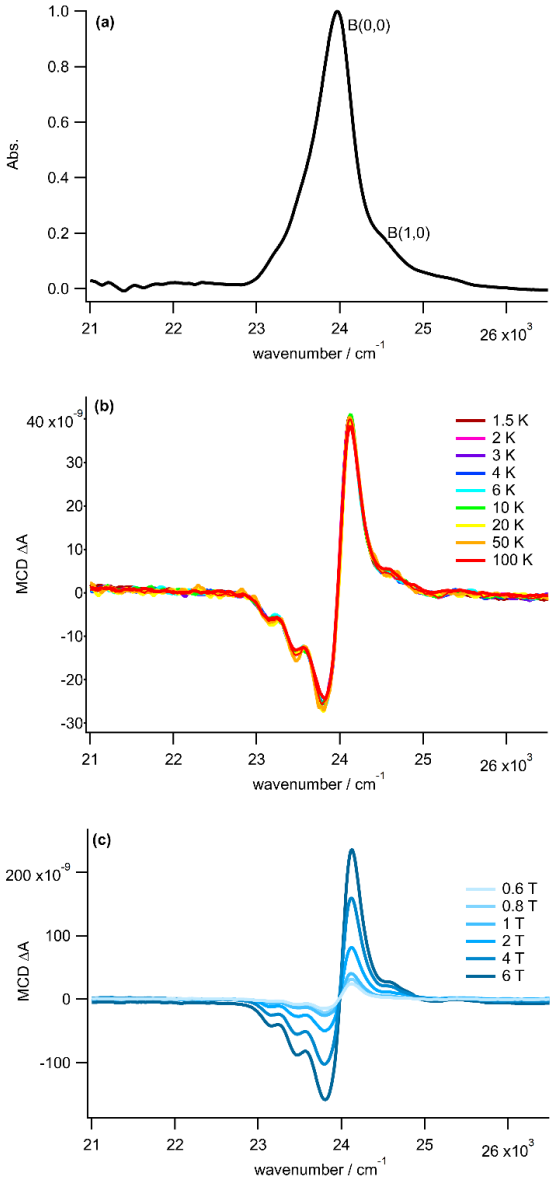

Figure 2.5 (a) Absorption, (b) temperature-dependent MCD spectra measured at temperatures of 1.5-100 K under a magnetic field of 1 T, and (c) magnetic field-dependent MCD spectra measured at temperatures of 1.5 K of B band in [Y(TPP)Azacrown]Cl in PMMA film.

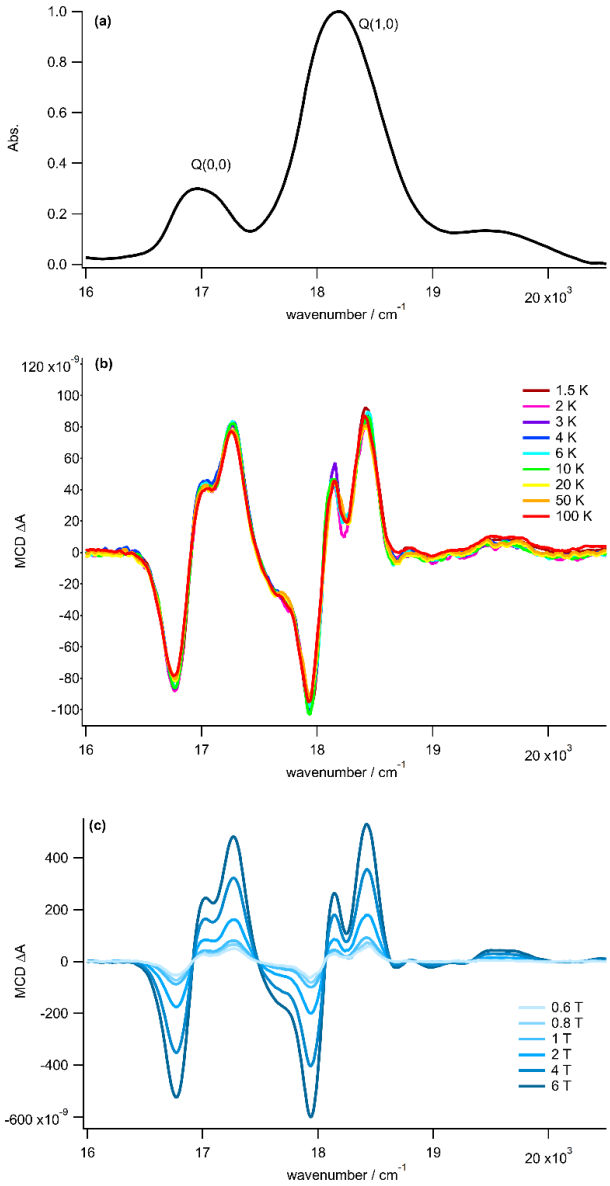

Figure 2.6 (a) Absorption, (b) temperature-dependent MCD spectra measured at temperatures of 1.5-100 K under a magnetic field of 1 T, and (c) magnetic field-dependent MCD spectra measured at temperatures of 1.5 K of B band in [Y(TPP)Azacrown]Cl in PMMA film.

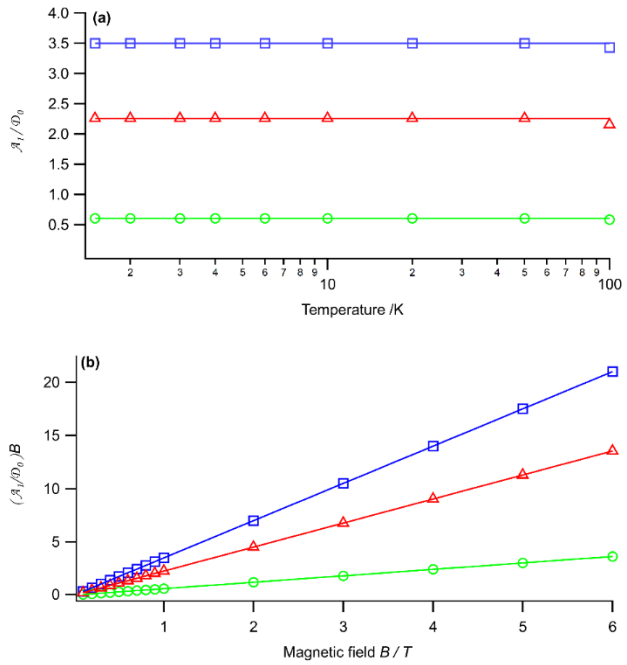

Figure 2.7 Experimental values (squares, triangles, and circles) and calculated value (straight line) of $\mathcal{A}_1/\mathcal{D}_0$ of [Y(TPP)Azacrown]Cl for B(0,0) in green, Q(1,0) in red, and Q(0,0) in blue under 1 T of magnetic field with varied temperature (a) and under varied magnetic field at 1.5 K (b).

However, the results of [Y(TPP)Azacrown]Cl have distinct differences in contrast to [Y(TPP)Crown]. The shape of B-band spectra shown in Figure 2.5(a) was broadened and shoulder band of B(1,0) is less noticeable to that of [Y(TPP)Crown]Cl. Moreover, in Figure 2.5(b) and (c), the negative lobe in MCD spectra of positive A-term have additional shoulder, creating a staircase-like pattern which is still observable during temperature lowering and under different applied magnetic field. For Q(0,0) and Q(1,0) bands, the spectra shape were not as sharp as their counterparts in [Y(TPP)Crown]Cl like shown in Figure 2.6(a) and as well as that, additional shoulders were also detected in positive A-term spectral shape of both bands in all various temperature and magnetic field (see Figure 2.6(b) and Figure 2.6(c)). Those results can be linked to partial aggregation of porphyrinoid complexes in PMMA matrix. Nonetheless, best deconvolution of both B and Q bandss in all VT-VH-MCD measurements give constant values of $\mathcal{A}_1/\mathcal{D}_0$ at different temperature and linear correlation between $(\mathcal{A}_1/\mathcal{D}_0)B$ and the magnetic field as shown in Figure 2.6. Based on the simulation, L_z values of B(0,0), Q(0,0), and Q(1,0) bands each are estimated to be $0.61\hbar$, $3.50\hbar$, and

2.25$\hbar$. It can be inferred that replacing the second ligand with reduced symmetry did not change the L_z of the porphyrinoid complexes. The results can be tabulated as follows.

Compound	Lz ($\hbar$)			
	B band	Q(0,0) band	Q(1,0) band	
[Y(TPP)Crown]Cl	0.54	3.44	2.35	***a***
[Y(TPP)Azarown]Cl	0.61	3.5	2.25	***a***
[Y(TPP)cyclen]Cl	0.66	3.59	2.61	***b***

Table 2.1 Results of Lz for Y complexes with ***a*** as experimental results while ***c*** was from reference[17].

2.3.2 Analysis of Tb complexes

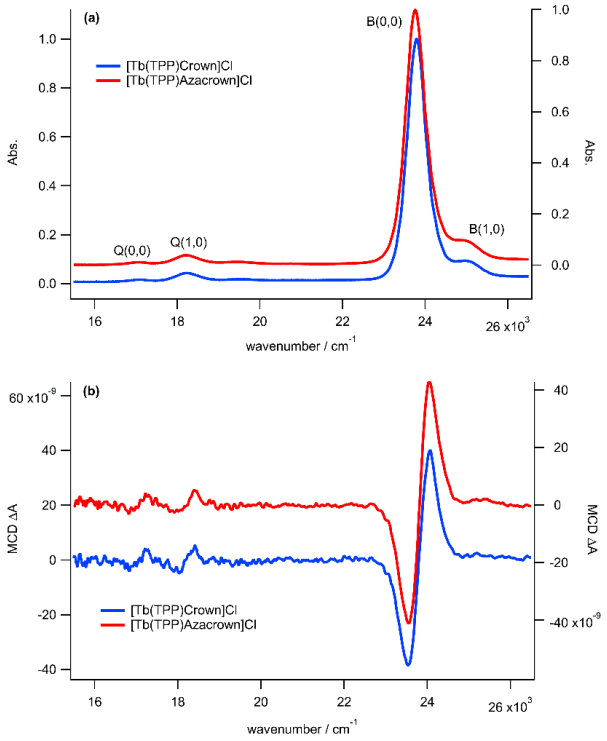

Figure 2.8 UV-vis spectra (a) and room-temperature MCD spectra under 1.6 T permanent magnet (b) of [Tb(TPP)Crown]Cl and [Tb(TPP)Azacrown]Cl in CH_2Cl_2.

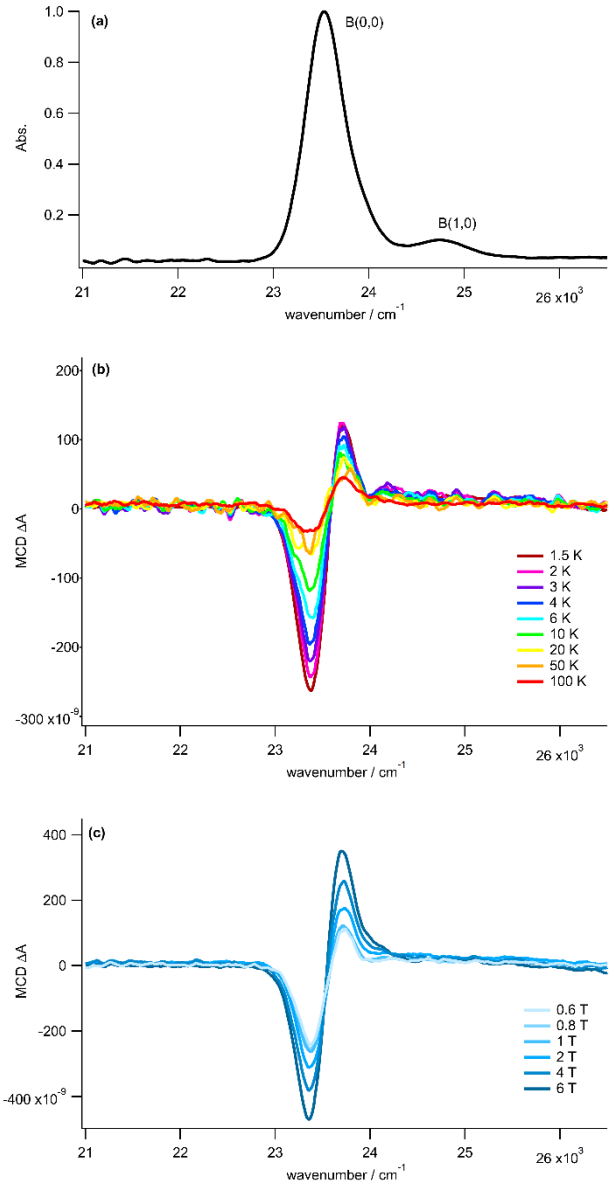

Figure 2.9 (a) Absorption, (b) temperature-dependent MCD spectra measured at temperatures of 1.5-100 K under a magnetic field of 1 T, and (c) magnetic field-dependent MCD spectra measured at temperatures of 1.5 K of B band in [Tb(TPP)Crown]Cl in PMMA film.

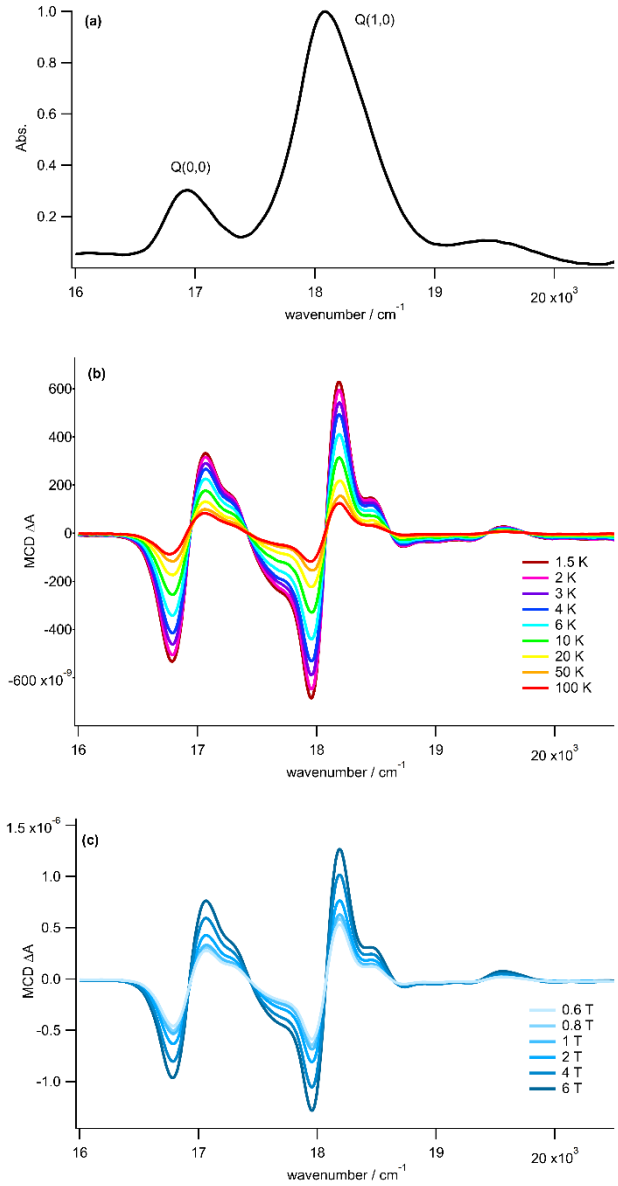

Figure 2.10 (a) Absorption, (b) temperature-dependent MCD spectra measured at temperatures of 1.5-100 K under a magnetic field of 1 T, and (c) magnetic field-dependent MCD spectra measured at temperatures of 1.5 K of Q bands in [Tb(TPP)Crown]Cl in PMMA film.

Contrast to Y(III) complexes as in [Y(TPP)Crown]Cl and [Y(TPP)Azacrown]Cl, Tb(III) have different character in which it has ferromagnetic nature. Therefore, performing MCD measurement for both [Tb(TPP)Crown]Cl and [Tb(TPP)Azacrown]Cl in various temperature points are significantly important in order to investigate how their electronic interaction may differ to each other. From the UV-Vis spectra and room temperature MCD spectra as demonstrated in Figure 2.7, the two Tb-porphyrin complexes show four bands in their UV-Vis spectra (Figure 2.8(a)) consisted of Q(0,0), Q(1,0), B(0,0), and B(1,0) according to ascending energy. In Figure 2.8(b), three positive A-term pattern are detected which are associated to Q(0,0), Q(1,0), and B(0,0) bands. Moreover, the positive A-term band of B band of both Tb complexes detected between 22,000-26,000 cm^{-1} is not shifted as observed in [Y(TPP)Crown]Cl and [Y(TPP)Azacrown]Cl.

However, when [Tb(TPP)Crown]Cl was incorporated to PMMA matrix and subjected to VT-VH-MCD analysis. For both B and Q bandss, positive A-term profiles were exhibited by the complex with more intense ΔA values as the temperature was decreased until 1.5 K, leading to more prominent spectra with lower temperature (Figure 2.9(b) and Figure 2.10(b)). Also, [Tb(TPP)Crown]Cl exhibited magnetic dependence intensity which changed in a non-uniform way with varied applied magnetic field as shown in Figure 2.9(c) and Figure 2.10(c). Those results are indication that there is a ferromagnetic electronic interaction between 4f electrons in Tb(III) with the π-conjugated system in TPP[17]. While MCD spectra of B band are relatively dominated with the negative lobe, those of Q bandss have similar partition between the negative and the positive lobes.

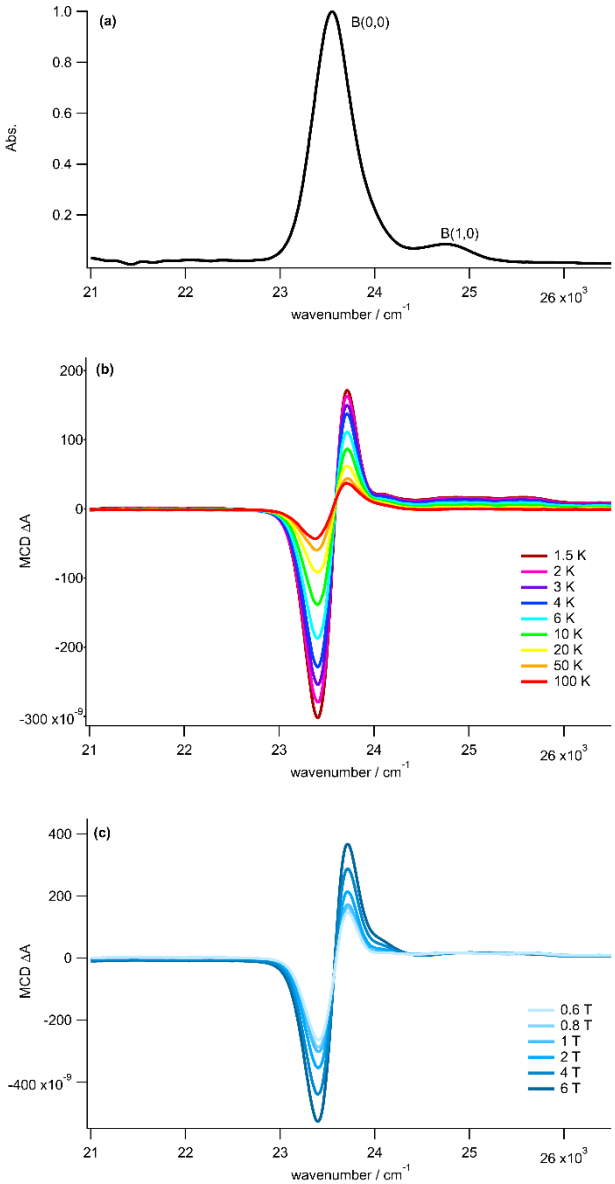

Figure 2.11 (a) Absorption, (b) temperature-dependent MCD spectra measured at temperatures of 1.5-100 K under a magnetic field of 1 T, and (c) magnetic field-dependent MCD spectra measured at temperatures of 1.5 K of B band in [Tb(TPP)Azacrown]Cl in PMMA film.

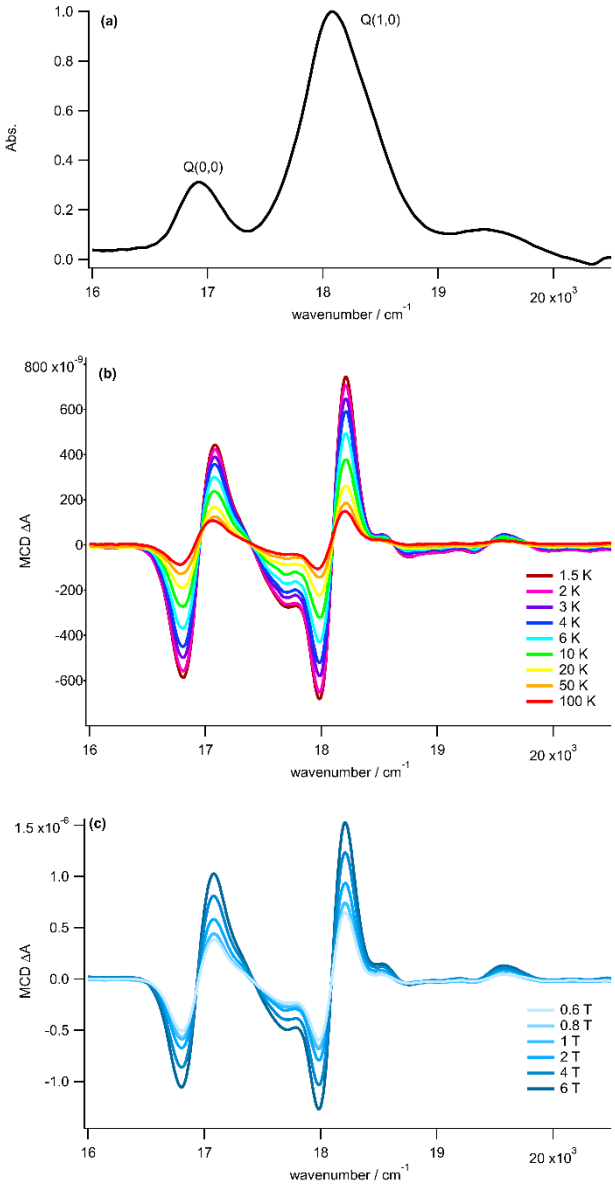

Figure 2.12 (a) Absorption, (b) temperature-dependent MCD spectra measured at temperatures of 1.5-100 K under a magnetic field of 1 T, and (c) magnetic field-dependent MCD spectra measured at temperatures of 1.5 K of Q bands in [Tb(TPP)Azacrown]Cl in PMMA film.

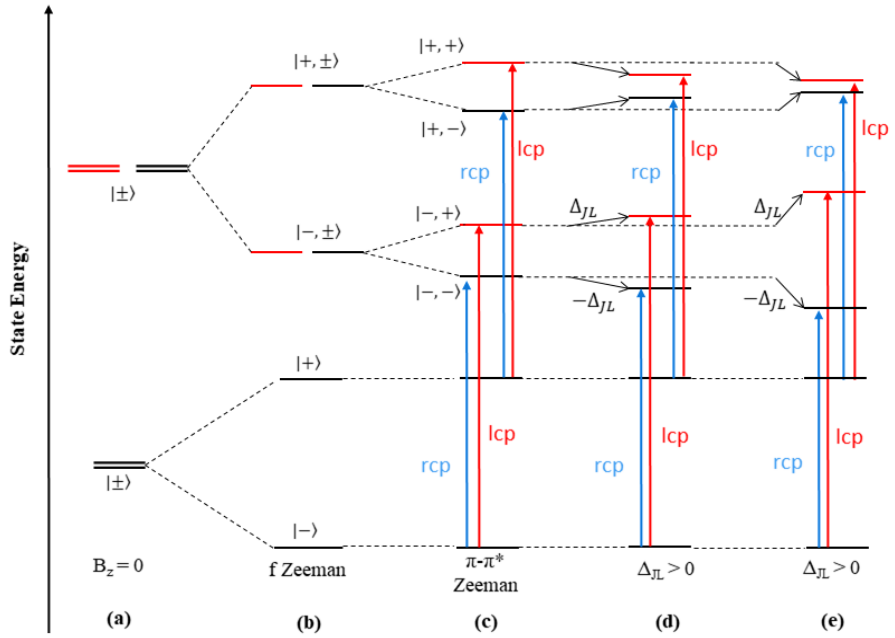

Figure 2.13 Schematic energy of the ground and the excited states of [Tb(TPP)Crown]Cl and [Tb(TPP)Azacrown]Cl.

When VT-VH-MCD investigation was carried out for [Tb(TPP)Azacrown]Cl, any indication of partial aggregation as in [Y(TPP)Azacrown]Cl was not observed in both B and Q bandss (Figure 2.11 and Figure 2.12). As well as MCD spectra of [Tb(TPP)Crown]Cl, B and Q bandss of [Tb(TPP)Azacrown]Cl yield positive A-term that each is associated to B(0,0), Q(0,0), and Q(1,0) bands. For B bands of both complexes, the MCD signals do not undergo reversal from positive A-term into negative A-term within reduced temperature as reported in [Tb(TPP)Cyclen]Cl[17]. From Figure 2.11(b), temperature-dependence MCD spectra for B band of [Tb(TPP)Azacrown]Cl do not present any noise, contrast to that of [Tb(TPP)Crown]Cl. The temperature-dependence MCD spectra of [Tb(TPP)Azacrown]Cl as shown in Figure 2.11(b) and 2.12(b) indicate maximum intensity reaching nearly 200 × 10^{-9} for B band and 800 × 10^{-9} for Q(1,0) and these values are greater than [Tb(TPP)Crown]Cl, which implies greater electronic interaction is likely to be presence in [Tb(TPP)Azacrown]Cl.

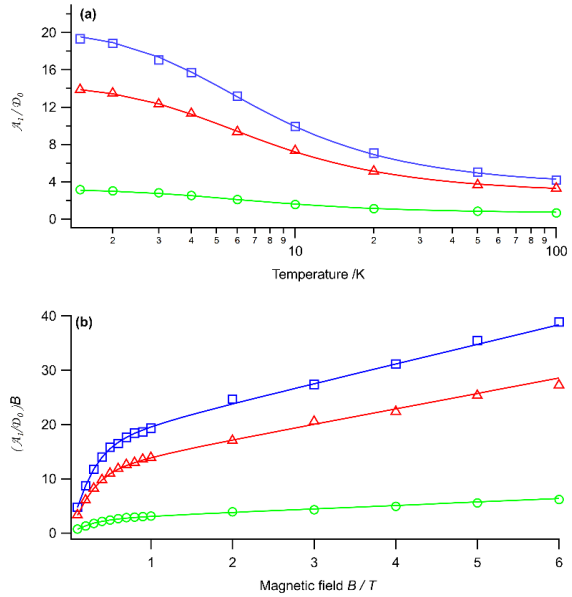

Figure 2.14 Experimental values (squares, triangles, and circles) and calculated value (straight line) of $\mathcal{A}_1/\mathcal{D}_0$ of [Tb(TPP)Crown]Cl for B(0,0) in green, Q(1,0) in red, and Q(0,0) in blue under 1 T of magnetic field with varied temperature (a) and under varied magnetic field.

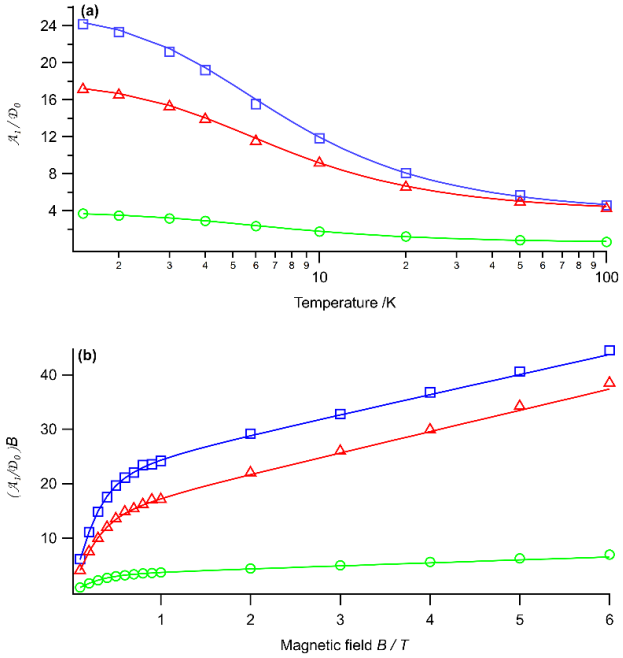

Figure 2.15 Experimental values (squares, triangles, and circles) and calculated value (straight line) of $\mathcal{A}_1/\mathcal{D}_0$ of [Tb(TPP)Azacrown]Cl for B(0,0) in green, Q(1,0) in red, and Q(0,0) in blue under 1 T of magnetic field with varied temperature (a) and under varied magnetic field at 1.5 K.

The phenomenon of the states in [Tb(TPP)Crown]Cl and [Tb(TPP)Azacrown]Cl can be explained by using Figure 2.13 above. The molecular systems contain doubly degenerate ground state and 4-fold degenerate π-π* excited state is symbolized as $|J_z\rangle = |\pm\rangle$ and $|J_z, L_z\rangle = |\pm, \pm\rangle$, where J_z is the z component of **J** while L_z is the component of total angular momentum, **L**, along the z-axis of 4-fold molecular symmetry. The degeneracy in both ground and excited states is split as an external magnetic field is applied (see Figure 2.13(b)) and simultaneously π-π* excited state lost its degeneracy by L_z as in Figure 2.13(c). During this π-π* excitation, the J_z of the 4f system is unchanged and the $|-\rangle \rightarrow |-, \pm\rangle$ and $|+\rangle \rightarrow |+, \pm\rangle$ will occur. Because the $|-\rangle$ state has a larger thermal population than $|+\rangle$, therefore the $|-\rangle \rightarrow |-, \pm\rangle$ transition gains more contribution as temperature is lowered. There are two possible J_z and L_z interactions in excited state. The states in which J_z and L_z have the same sign are stabilized, and those with opposite sign are destabilized, the energy difference between $|-, +\rangle$ and $|-, -\rangle$ becomes larger and causes a larger A-term strength for the $|-\rangle \rightarrow |-, \pm\rangle$ transition and smaller for the other one. As the $|-\rangle \rightarrow |-, \pm\rangle$ transition becomes more dominant at lower temperature range, the magnitude of A-term intensity increases particularly in B and Q-band regions. The tendency becomes more prominent in the case of [Tb(TPP)Azacrown]Cl as indicated in Figure 2.13(e) compared to [Tb(TPP)Crown]Cl. Consequently, all of $\mathcal{A}_1/\mathcal{D}_0$ values rise as the temperatures is diminished as they correspond with the presence of the ferromagnetic-type interaction between **J** and **L** in the excited states.

In order to calculate **J–L** interaction denoted as Δ_{JL}, L_z is to be determined and J_z is constant determined from calculation with the structures of [Tb(TPP)Crown]Cl and [Tb(TPP)Azacrown]Cl are assumed to be resembling [Tb(TPP)Cyclen]Cl[17] and J_z was determined to be ± 6. Based on Figure 2.14 and Figure 2.15, both Tb complexes in all bands have $\mathcal{A}_1/\mathcal{D}_0$ values which are non-linearly related on the temperature and they tend to increase with reduced temperature, consistent with the increased intensity as previously displayed in Figure 2.9(b), Figure 2.10(b), Figure 2.11(b), and Figure 2.12(b). Furthermore, $(\mathcal{A}_1/\mathcal{D}_0)B$ values are no longer linear with magnetic field like in the Y complexes but increase with higher magnetic field and significant drop is observed in the range of 0.8-0.6 T.

In general, the $L_z$values and Δ_{JL} of all Tb complexes can be summed up by the table below.

Compound	B(0,0)		Q(0,0)		Q(1,0)		Note
	L_z ($\hbar$)	Δ_{JL} (cm^{-1})	L_z ($\hbar$)	Δ_{JL} (cm^{-1})	L_z ($\hbar$)	Δ_{JL} (cm^{-1})	
[Tb(TPP)Crown]Cl	0.63	0.81	3.61	5.24	2.83	3.63	***a***
[Tb(TPP)Azacrown]Cl	0.54	1.02	3.68	6.77	3.9	4.37	***a***
[Tb(TPP)Cyclen]Cl	0.64	-1.01	3.86	4.42	2.62	5.01	***b***

Table 2.2 The value of **J-L** interaction (Δ_{JL}) of complexes with ***a*** is the reported work and ***b*** is taken from reference 19.

From Table 2.2 above, it can be said that changing one oxygen atom in 12-crown-4 ether with ammine group as in 1-aza-12-crown-4 ether has caused increased Δ_{JL} in Tb complexes with relatively unchanged L_z, similar to the case of the Y complexes.

2.3.3 Analysis of Dy complexes

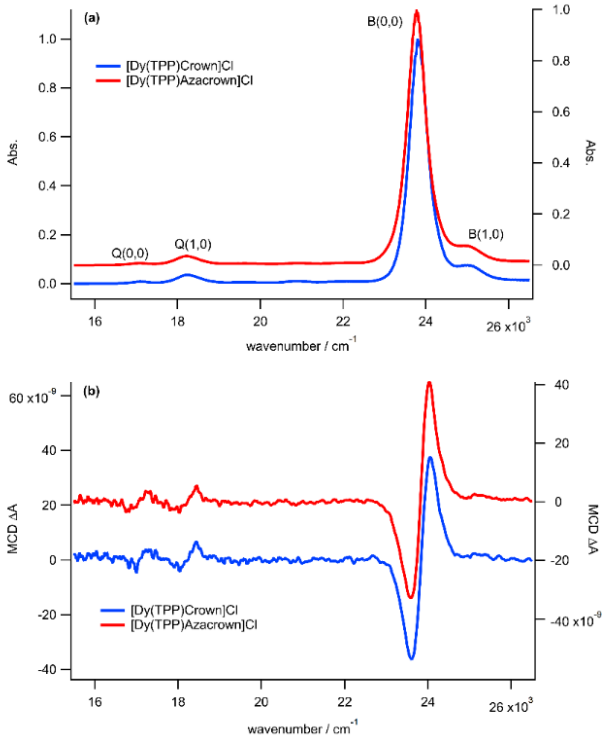

Figure 2.16 UV-vis spectra (a) and room-temperature MCD spectra under 1.6 T permanent magnet (b) of [Dy(TPP)Crown]Cl and [Dy(TPP)Azacrown]Cl in CH_2Cl_2

Besides Tb, Dy is considered as a high-anistropic element and hence, investigating the electronic interaction in [Dy(TPP)Crown]Cl and [Dy(TPP)Azacrown]Cl will be reported in this section. The room temperature MCD analysis was also conducted for those complexes and the results are presented in Figure 2.16. From UV-Vis spectra in Figure 2.16(a), both compounds exhibit four absorption bands i.e. Q(0,0), Q(1,0), B(0,0), and B(1,0) with relatively no wavenumber shift. As well as that, the room temperature MCD show no shift or different spectral shape in which high intensity positive A-term associated with B(0,0) band was detected in the range of 22,000-26,000 cm^{-1} and smaller intensity of two A-term pattern appear in the range of 16,000-20,000 cm^{-1}.

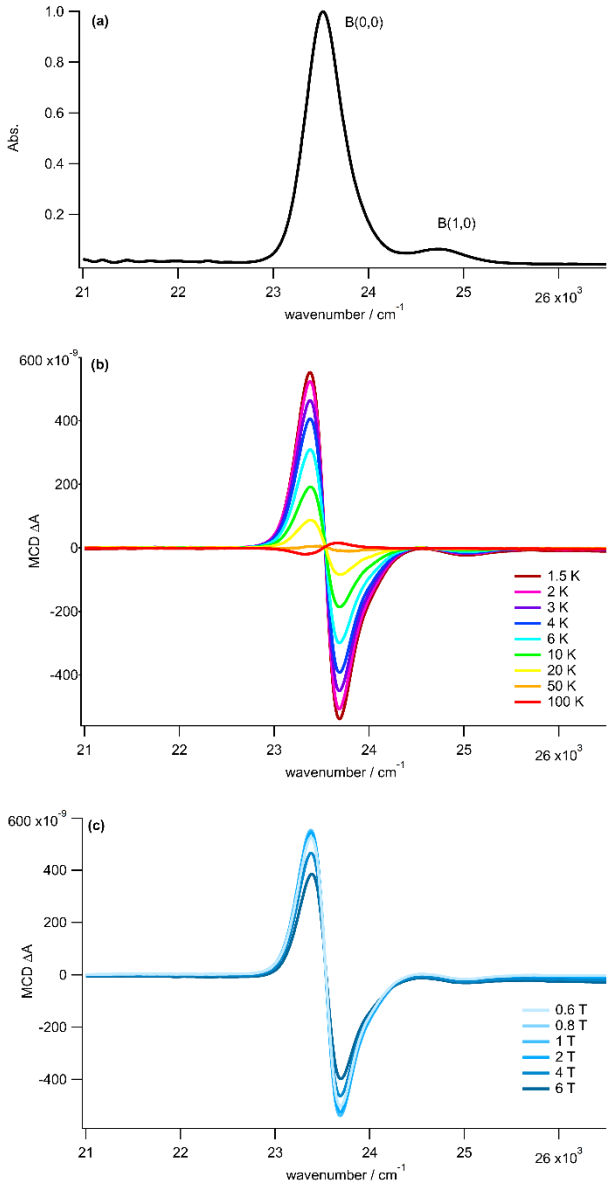

Figure 2.17 a) Absorption, (b) temperature-dependent MCD spectra measured at temperatures of 1.5-100 K under a magnetic field of 1 T, and (c) magnetic field-dependent MCD spectra measured at temperatures of 1.5 K of B band in [Dy(TPP)Crown]Cl in PMMA film.

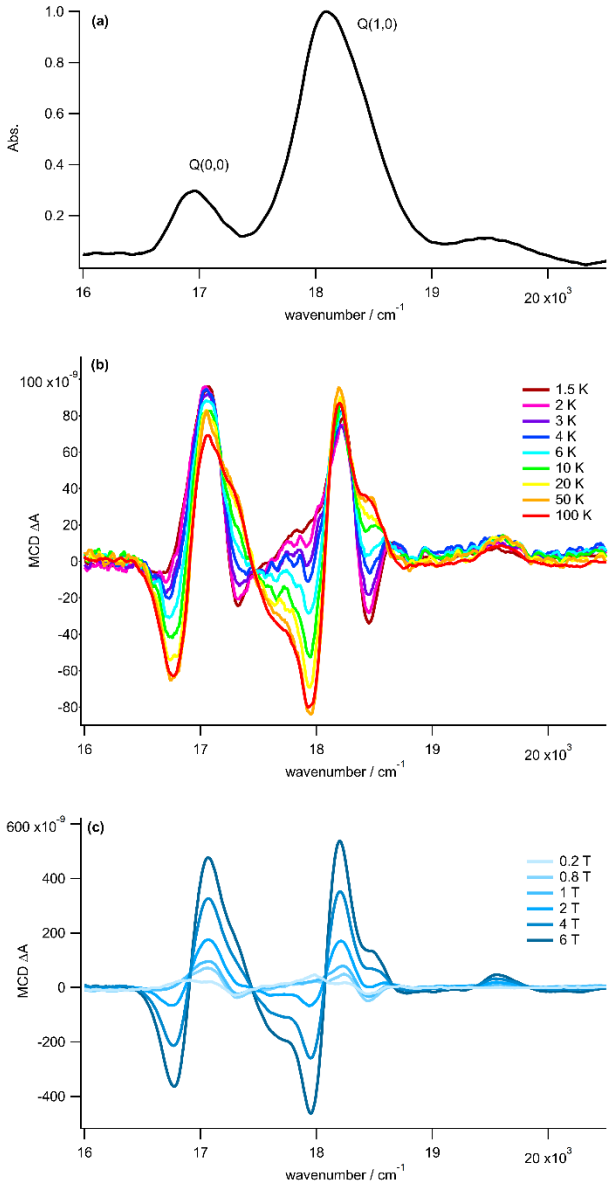

Figure 2.18 a) Absorption, (b) temperature-dependent MCD spectra measured at temperatures of 1.5-100 K under a magnetic field of 1 T, and (c) magnetic field-dependent MCD spectra measured at temperatures of 1.5 K of Q bands in [Dy(TPP)Crown]Cl in PMMA film.

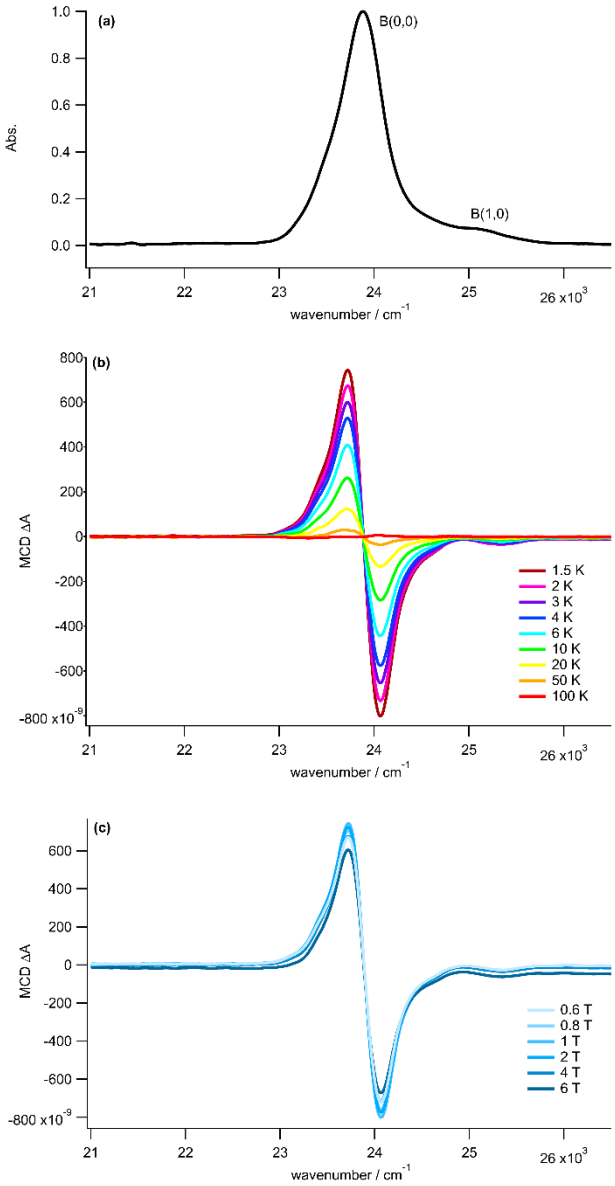

Figure 2.18 a) Absorption, (b) temperature-dependent MCD spectra measured at temperatures of 1.5-100 K under a magnetic field of 1 T, and (c) magnetic field-dependent MCD spectra measured at temperatures of 1.5 K of B band in [Dy(TPP)Azacrown]Cl in PMMA film.

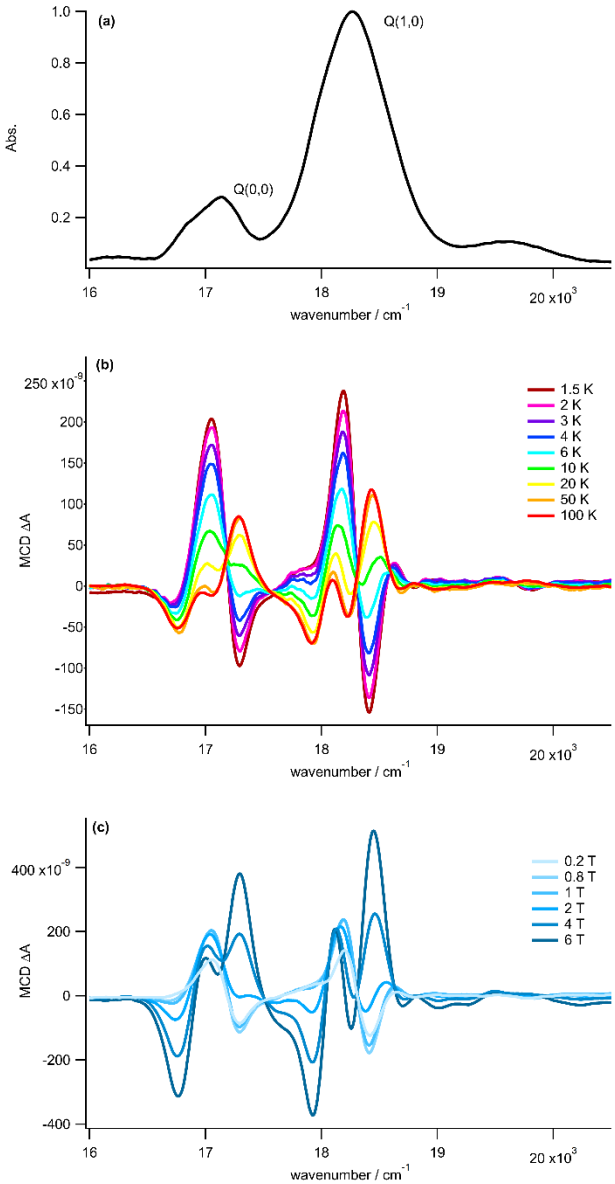

Figure 2.19 a) Absorption, (b) temperature-dependent MCD spectra measured at temperatures of 1.5-100 K under a magnetic field of 1 T, and (c) magnetic field-dependent MCD spectra measured at temperatures of 1.5 K of Q bands in [Dy(TPP)Azacrown]Cl in PMMA film.

When [Dy(TPP)Crown]Cl was incorporated into PMMA matrix to be measured with VT-VH-MCD, several distinguishing aspects compared to the room temperature spectra were detected during the measurement. As shown in Figure 2.17, B(1,0) band did not yield any term during different temperature and applied magnetic field. At 100 K, B(0,0) band yielded positive A-term with ΔA MCD close to 1.5×10^{-8} but underwent reversal to negative A-term profile at 50 K with intensity near 6×10^{-9} and the negative A-term pattern reached approximately 6×10^{-7} at 1.5 K (Figure 2.17(b)). Within decreased magnetic field in Figure 2.16(c), the negative A-term MCD spectral shape was observed with a tendency to increase with lowered applied field.

For Q bands of [Dy(TPP)Crown]Cl demonstrated in Figure 2.18, there are several aspects necessary to discuss. In Figure 2.18(b), both Q(0,0) and Q(1,0) bands resulted positive A-term pattern from 100 K to 1.5 K and this pattern has smaller ΔA MCD intensity until 1.5 K without any reversal to negative A-term shape as in B band. Furthermore, the positive A-term MCD spectra were maintained at 1.5 K with varied magnetic field, shown in Figure 2.18(c) with small intensity was detected as the sample received smaller field.

In the case of [Dy(TPP)Azacrown]Cl, B band showed positive A-term associated to B(0,0) band with ΔA MCD approximately 6×10^{-9} as shown by Figure 2.18(a). As well as in the case of [Dy(TPP)Crown]Cl, the positive A-term pattern was reversed into negative one at 50 K and it reached 7×10^{-7} at 1.5 K. The varied magnetic field did not change negative A-term pattern (Figure 2.18(c)). Q bands interestingly demonstrated different behavior contrast to [Dy(TPP)Crown]Cl. In Figure 2.19(b), at 1.5 K, both Q(0,0) and Q(1,0) bands showed associated MCD spectra with higher intensity than those of [Dy(TPP)Crown]Cl, nearly equal 2×10^{-7}. Furthermore, the spectra have negative A-term profile and this negative A-term underwent smaller intensity at higher temperature. At 6 K, the negative lobes of Q(0,0) and Q(1,0) bands almost disappeared into a completely straight line. At 10 K, the negative lobes were inversed to positive, creating shoulders on the positive lobes of formerly positive A-term patterns of Q(0,0) and Q(1,0) bands. At 100 K, the shoulders gain higher intensity and the main positive part did not undergo reversal into negative A-term band. Such occurrences were also observed in varied magnetic field MCD measurement (Figure 2.19(c)) where the negative lobes of formerly positive A-term band were inversed into shoulders of the positive lobes and the shoulders had higher energy with greater external magnetic field. However, there were no straight reversal from positive A-term into negative A-term in Q(0,0) and Q(1,0) bands of [Dy(TPP)Azacrown]Cl.

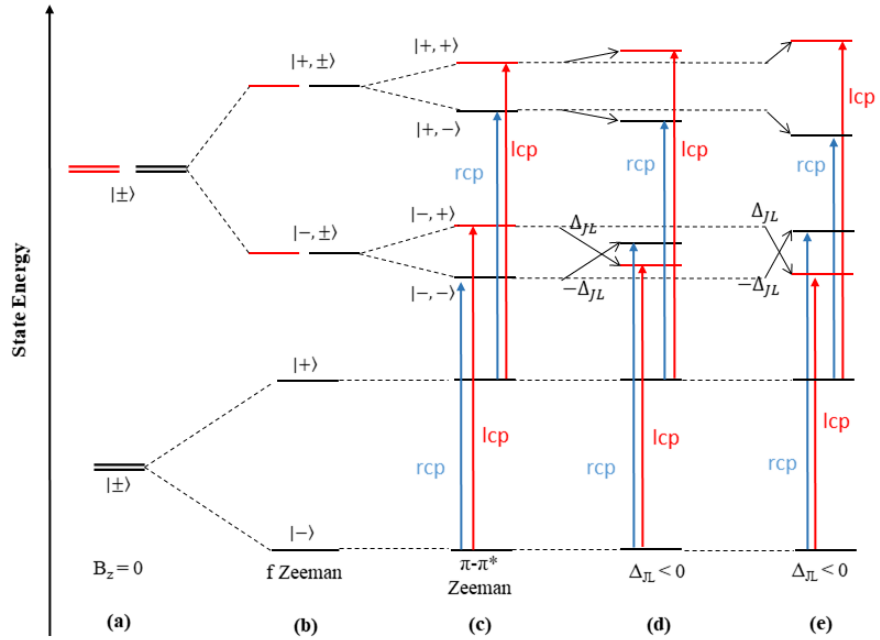

Figure 2.20 Schematic energy of the ground and the excited states of [Tb(TPP)Crown]Cl and [Tb(TPP)Azacrown]Cl.

In general, the reversal of A-term MCD bands were detected in VT-VH-MCD of [Dy(TPP)Crown]Cl and [Dy(TPP)Azacrown]Cl and it is attributed to the antiferromagnetic character of Dy-porphyrin molecular system[18]. As a comparison, complete reversal from positive A-term pattern to negative A-term was observed in both B and Q bandss in [Dy(TPP)Cyclen] as reported before[18]. Besides that, higher ΔA of both B and Q bandss of [Dy(TPP)Azacrown]Cl in comparison with [Dy(TPP)Crown]Cl is expected as an indication of greater electronic interaction was present in [Dy(TPP)Azacrown]Cl than [Dy(TPP)Crown]Cl. The temperature dependence of ΔA values can be explained using the schemes in Figure 2.20. Both **J** and **L** have components on z-axis denoted as J_z and L_z. The doubly degenerate ground state thus can be stated as $|J_z\rangle = |\pm\rangle$ while the fourfold degenerate π–π* excited states are denoted as $|J_z, L_z\rangle = |\pm, \pm\rangle$ (Figure 2.20(a)). The introduction of external magnetic field caused the degeneracy to be lifted (Figure 2.20(b)) and π–π* excited states are split as much as L_z (Figure 2.20(c)). The $|-\rangle \rightarrow |-, \pm\rangle$ and $|+\rangle \rightarrow |+, \pm\rangle$ transitions will occur because J_z is constant during π–π* excitation. At lower temperature, $|-\rangle$ has more population than $|+\rangle$ and thus $|-\rangle \rightarrow |-, \pm\rangle$ transition is more dominant than its counterpart. The interaction between **J** and **L** in excited states is antiferromagnetic. Because

stabilization occurs in the states where J_z and L_z have the same sign and destabilization occurs in those with opposite sign, therefore the energy difference between $|-,+\rangle$ and $|-,-\rangle$ becomes smaller and causes more significant negative A-term magnitude as the $|-\rangle \rightarrow |-,\pm\rangle$ transition has bigger contribution. However, the contribution is found bigger in [Dy(TPP)Azacrown]Cl shown in Figure 2.20(e) than its counterpart (Figure 2.20(d)).

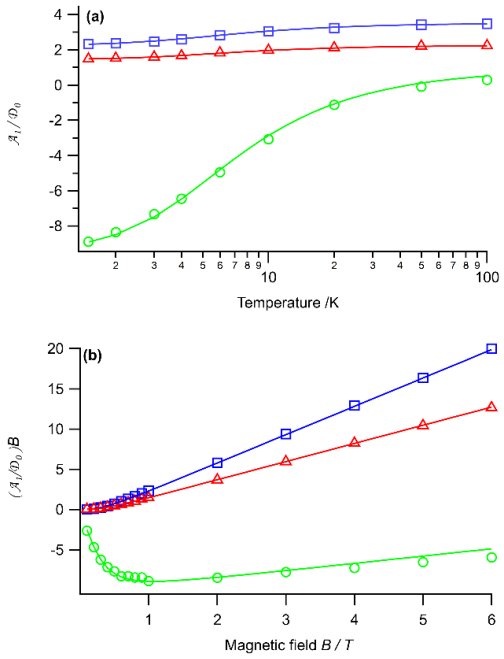

Figure 2.21 Experimental values (squares, triangles, and circles) and calculated value (straight line) of $\mathcal{A}_1/\mathcal{D}_0$ of [Dy(TPP)Crown]Cl for B(0,0) in green, Q(1,0) in red, and Q(0,0) in blue under 1 T of magnetic field with varied temperature (a) and under varied magnetic field.

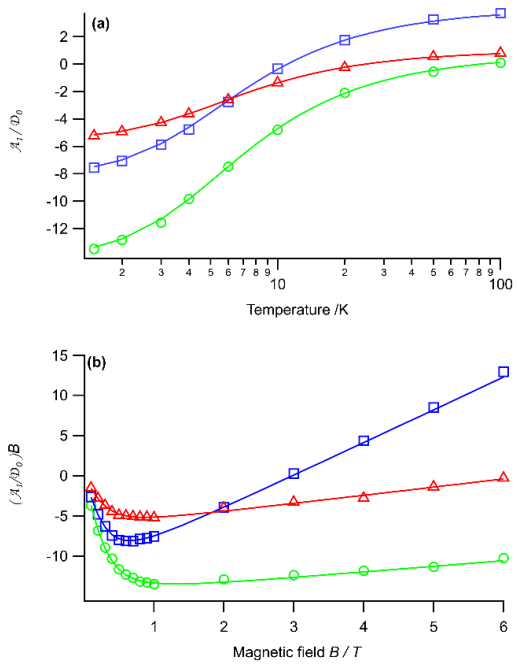

Figure 2.22 Experimental values (squares, triangles, and circles) and calculated value (straight line) of $\mathcal{A}_1/\mathcal{D}_0$ of [Dy(TPP)Azacrown]Cl for B(0,0) in green, Q(1,0) in red, and Q(0,0) in blue under 1 T of magnetic field with varied temperature (a) and under varied magnetic field.

According to Figure 2.21(a) where $\mathcal{A}_1/\mathcal{D}_0$ ratios were plotted against temperature and magnetic field, $\mathcal{A}_1/\mathcal{D}_0$ values of Q(0,0) and Q(1,0) have a steady decrement from 100 K to 1.5 K with all values are always in the positive points, while in Figure 2.21(b), lowest $(\mathcal{A}_1/\mathcal{D}_0)B$ value of Q(0,0) at 0.1 T is 0.03 and that of Q(1,0) is 0.02. Also, $(\mathcal{A}_1/\mathcal{D}_0)B$ of B and Q bands did not have direct correlation with the applied field and reduced field led $(\mathcal{A}_1/\mathcal{D}_0)B$ to reduce non-linearly. This confirms that during lowering temperature and reduced magnetic field, Q bands did not undergo reversal to negative A-term pattern and still maintain its positive A-term profile. In addition to that, B band had $\mathcal{A}_1/\mathcal{D}_0$ values in negative range, confirming the reversal of positive A-term in VT-VH-MCD spectra Figure 2.17. In the case of [Dy(TPP)Azacrown]Cl shown in Figure 2.22, best deconvolution gave positive $\mathcal{A}_1/\mathcal{D}_0$ values at 20 K for Q(0,0) and for Q(1,0) while negative values were obtained for lower temperature points. For B band, positive $\mathcal{A}_1/\mathcal{D}_0$ was obtained at 100 K. Such trend was still present for varied magnetic field with $(\mathcal{A}_1/\mathcal{D}_0)B$ of Q(0,0) was positive at 3 T and it was positive at 5 T for Q(1,0).

In order to calculate Δ_{JL}, simulation was performed with J_z = 6.5 by computational chemistry calculation by *ab initio* method. The simulation results are presented as line in Figure 2.21 for [Dy(TPP)Crown]Cl and in Figure 2.22 for [Dy(TPP)Azacrown]Cl. All of L_z and Δ_{JL} results are tabulated in Table 2.3 below.

Compound	B(0,0)		Q(0,0)		Q(1,0)		Note
	L_z ($\hbar$)	Δ_{JL} (cm^{-1})	L_z ($\hbar$)	Δ_{JL} (cm^{-1})	L_z ($\hbar$)	Δ_{JL} (cm^{-1})	
[Dy(TPP)Crown]Cl	0.84	-3.19	3.53	-0.39	2.26	-0.26	***a***
[Dy(TPP)Azacrown]Cl	0.28	-4.19	3.44	-3.24	1.03	-1.74	***a***
[Dy(TPP)Cyclen]Cl	0.88	-5.99	3.71	-3.40	2.38	-2.61	***b***

Table 2.3 The value of **J-L** interaction (Δ_{JL}) of Dy complexes with ***a*** is the reported work and ***c*** is cited from reference 19.

From Table 2.3, different symmetry between 12-crown-4 ether and 1-aza-12-crown-4 ether did not alter L_z of both B and Q bandss in the Dy complexes and the values are consistent with L_z of previous work with [Dy(TPP)Cyclen]Cl. Nevertheless, different non-aromatic ligands as the second ligands with different atoms binding on the lanthanide ion caused different Δ_{JL}. More specifically, higher Δ_{JL} were gained in the Dy-porphyrin molecular systems with more distorted symmetry as in 1-aza-12-crown-4 ether than in regular symmetry as in 12-crown-4 ether. In addition to that, Δ_{JL} of B band can be made as an ordering according to an ascending magnitude with Δ_{JL} [Dy(TPP)Cyclen] > [Dy(TPP)Azacrown]Cl > [Dy(TPP)Crown]Cl. However, such trend cannot be summed for Q(0,0) as Δ_{JL} of [Dy(TPP)Azacrown]Cl and that of [Dy(TPP)Cyclen] are almost equal.

2.3.4 Computational Chemistry Analysis

In this thesis report, *ab-initio* computational chemistry was performed in order to gain deeper insight about the electronic states energy level at ground state and the **J–L** interaction in the lanthanide molecular systems at excited state. Furthermore, to achieve that purpose, $[Y(TPP)Crown]^+$ and $[Y(TPP)Azacrown]^+$ are used as the references as well as in the experimental analysis. The calculations were performed with basis set ANO-RCC-VTZP for the lanthanides coupled with Pople-type 6-31** for the common atoms.

[Y(TPP)Crown]$^+$				
S.O state	Energy (cm^{-1})	g_z	L_z	S_z
1	0	-	-	-
2	26049.06	8.14	4.07	0.00
3	26051.52			
4	47392.89	0.36	0.18	0.00
5	47431.71			
[Y(TPP)Azacrown]$^+$				
S.O state	Energy (cm^{-1})	g_z	L_z	S_z
1	0	-	-	-
2	26030.76	8.07	4.03	0.00
3	26063.59			
4	47151.07	0.37	0.19	0.00
5	47212.79			

Table 2.4 Angular Momenta from RASSCF/RASSI/single_aniso calculations for [Y(TPP)Crown]$^+$ and [Y(TPP)Azacrown]$^+$

In the case of [Y(TPP)Crown]$^+$ results, 8 transitions and 5 spin-orbit (S.O) states were observed. Based on Table 2.4, S.O state 2 and 3 (the lowest doublet states) has higher energy difference compared to [Y(TPP)Cyclen]$^+$ and the energy difference is more significant between S.O state 4 and 5 or the highest doublet states. This is linked to the symmetry of [Y(TPP)Crown]$^+$ used in this calculation which is smaller than that of [Y(TPP)Cyclen]$^+$ [17]. The energy difference within the lowest and within the highest doublet states increased when 12-crown-4 ether was replaced to 1-aza-12-crown-4 ether due to smaller symmetry of the non-aromatic ligand. However, the energy of the S.O states between the two cyclododecanes were practically unchanged regardless the different symmetry. From Table 2.4 for [Y(TPP)Crown]$^+$ and [Y(TPP)Azacrown]$^+$, transition from singlet state to the first doublet state corresponds to B(0,0) band and transition from singlet state to the second doublet state is associated with Q(0,0) band. Moreover, the different structure between 12-crown-4 ether and 1-aza-12-crown-4 ether did not influence the oscillator strength and the angular momentum of the porphyrin $L_z(\pi)$ in both bands. The values of $L_z(\pi)$ are 4.07$\hbar$ and 0.18$\hbar$ for Q(0,0) and B(0,0) bands respectively in [Y(TPP)Crown]$^+$ while for [Y(TPP)Azacrown]$^+$ $L_z(\pi)$ of Q(0,0) and B(0,0) are 4.03$\hbar$ and 0.19$\hbar$ respectively, consistent with the experimental results where $L_z(\pi)$ are unchanged with different second ligands.

[Tb(TPP)Crown]$^+$		[Tb(TPP)Azacrown]$^+$	
Energy (cm^{-1})	*States*	*Energy (cm^{-1})*	*States*
0.000	$0.99\|\pm6\rangle$	0.000	$0.98\|\pm6\rangle$
0.179	$0.99\|\pm6\rangle$	0.058	$0.98\|\pm6\rangle$
120.229	$0.48\|\pm5\rangle$ $0.38\|\pm1\rangle$	144.860	$0.77\|\pm5\rangle$
120.229	$0.48\|\pm5\rangle$ $0.38\|\pm1\rangle$	146.052	$0.78\|\pm5\rangle$
127.393	$0.66\|0\rangle$ $0.34\|\pm4\rangle$	185.998	$0.28\|\pm4\rangle$ $0.24\|\pm3\rangle$ $0.20\|0\rangle$
136.541	$0.98\|\pm2\rangle$	197.469	$0.20\|\pm5\rangle$ $0.31\|\pm3\rangle$ $0.21\|\pm1\rangle$
154.392	$0.50\|\pm5\rangle$ $0.26\|\pm3\rangle$ $0.25\|\pm1\rangle$	205.889	$0.57\|\pm2\rangle$ $0.19\|0\rangle$
154.392	$0.50\|\pm5\rangle$ $0.26\|\pm3\rangle$ $0.25\|\pm1\rangle$	220.344	$0.18\|\pm3\rangle$ $0.54\|\pm1\rangle$
194.587	$1\|\pm4\rangle$	248.459	$0.71\|\pm4\rangle$ $0.21\|\pm3\rangle$
231.000	$0.98\|\pm2\rangle$	283.594	$0.36\|\pm4\rangle$ $0.42\|0\rangle$
232.305	$0.66\|\pm4\rangle$ $0.34\|0\rangle$	296.282	$0.43\|\pm3\rangle$ $0.18\|\pm2\rangle$ $0.31\|\pm1\rangle$
232.470	$0.62\|\pm3\rangle$ $0.36\|\pm1\rangle$	313.474	$0.29\|\pm3\rangle$ $0.34\|\pm2\rangle$ $0.18\|\pm1\rangle$
232.470	$\|\pm3\rangle$ $\|\pm1\rangle$	317.366	$0.44\|\pm3\rangle$ $0.40\|\pm2\rangle$

Table 2.5 Energy level of the multiplet states in [Tb(TPP)Crown]$^+$ and [Tb(TPP)Azacrown]$^+$

In study of the Tb complexes, computational chemistry analysis was performed to analyze the energy level of the multiplet states may differ with different symmetry of the non-aromatic ligands and as well as that, the lowest state or J_z. As presented in Table 2.5, in both [Tb(TPP)Crown]$^+$ and [Tb(TPP)Azacrown]$^+$, J_z was determined to be $|\pm6\rangle$ and the next substates are $|\pm5\rangle$. Nonetheless, in [Tb(TPP)Azacrown]$^+$, the energy states of substates were positioned at relatively higher compared to [Tb(TPP)Crown]$^+$. For instance, the next substate after $|\pm6\rangle$ was $|\pm5\rangle$, determined in the energy around 120 cm^{-1} for [Tb(TPP)Crown]$^+$ and approximately 140 cm^{-1} for its counterpart. This trend is still observed for the other substates where the energy levels in [Tb(TPP)Azacrown]$^+$ are comparatively higher. Furthermore, in [Tb(TPP)Azacrown]$^+$, the substates are more mixed at higher energy levels starting from around 180 cm^{-1} that it is more complicated to define which substate positioned in corresponding level. It can be inferred that less symmetrical second ligand in Tb-porphyrin caused the substates become more less stabilized and undergo mixing between each other at higher energy levels.

S.O states	Energy (cm^{-1})	g_z	L_z	S_z
1	0.00	17.98	2.99	2.99
2	0.11			
214	25962.06	26.21	7.11	2.99
215	25962.07			
216	25971.45	9.65	-1.16	2.99
217	25971.45			
508	48259.89	18.18	3.10	2.99
509	48259.89			
510	48269.40	17.72	2.87	2.99
511	48269.40			

Table 2.6 Low-Lying Spin Orbit of $[Tb(TPP)Crown]^+$ obtained from RASSCF/RASSI/single_aniso calculations

Computational approach at excited states was only performed on $[Tb(TPP)Crown]^+$ as the electronic interaction cannot be reproduced and the results are tabulated at Table 2.6. The lowest S.O states have L_z 2.99$\hbar$ and S.O states at energy around 25,962 cm^{-1} have L_z 7.11$\hbar$ with $\Delta L_z = 4\hbar$ and at 25,971 cm^{-1}, L_z is -1.16$\hbar$ ($\Delta L_z = -4\hbar$). On the other hand, at the higher S.O states energy, L_z becomes 3.10$\hbar$ at 48,259 cm^{-1} ($\Delta L_z = 0.1\hbar$) and 2.87$\hbar$ ($\Delta L_z = -0.1\hbar$) at S.O doublet states at 48,269 cm^{-1}. Those differences originate from $L_z(\pi)$ of Q band and B band. Thus, S.O states at around 25,960-25,970 cm^{-1} are associated with Q(0,0) band and those at 48,250-48,270 cm^{-1} are associated with B(0,0) band. ΔL_z of lower S.O states is on the opposite sign with the ΔL_z of higher S.O states on higher energy level, meaning that $L_z(\pi)$ are coupled ferromagnetically with L_z of 4f lanthanide or L_z(4f).

As well as that, half of the energy gap between lower doublet S.O states and higher doublet S.O states for both B and Q bands is denoted as Δ_{JL} where for B band Δ_{JL} was calculated to be 4.75 cm^{-1} and on the other hand, Δ_{JL} of Q band was 4.69 cm^{-1}. Even though Δ_{JL} for B band is less reproducible than for Q band, computational chemistry approach can be applied to provide deeper analysis for symmetrical non-aromatic ligand. Furthermore, compared to $[Tb(TPP)Cyclen]^+$, the S.O states energy levels in $[Tb(TPP)Crown]^+$ undergo stabilization with lower energy values which could be attributed to the presence of 12-crown-4 ether.

2.4 Conclusion

From this chapter, it can be concluded that different symmetry of cyclododecane ligands do not alter the pattern of electronic transition within lanthanide-porphyrin molecular system with the observed bands of Q(0,0), Q(1,0), B(0,0), and B(1,0). As well as that, the electronic interaction in the excited states between 4f electron of lanthanide and cyclic-18 π

electrons Δ_{JL} have been conducted by magnetic circular dichroism (MCD). The A-term pattern bands corresponding to Q(0,0), Q(1,0), and B(0,0) were observed in all compounds regardless the non-aromatic ligands and all A-term bands demonstrate temperature dependence except in the Y complexes. With simulation to $\mathcal{A}_1/\mathcal{D}_0$ ratios, L_z and Δ_{JL} were estimated in the table below.

Compound	B(0,0)		Q(0,0)		Q(1,0)	
	L_z ($\hbar$)	Δ_{JL} (cm^{-1})	L_z ($\hbar$)	Δ_{JL} (cm^{-1})	L_z ($\hbar$)	Δ_{JL} (cm^{-1})
[Y(TPP)Crown]Cl	0.54	-	3.44	-	2.35	-
[Y(TPP)Azarown]Cl	0.61	-	3.5	-	2.25	-
[Tb(TPP)Crown]Cl	0.63	0.81	3.61	5.24	2.83	3.63
[Tb(TPP)Azacrown]Cl	0.54	1.02	3.68	6.77	3.9	4.37
[Dy(TPP)Crown]Cl	0.84	-3.19	3.53	-0.39	2.26	-0.26
[Dy(TPP)Azacrown]Cl	0.28	-4.19	3.44	-3.24	1.03	-1.74

Table 2. The value of L_z and **J-L** interaction (Δ_{JL}) of all [Ln(TPP)Crown]Cl and [Ln(TPP)Azacrown]Cl.

2.5 Reference

1. F. Gendron, V.E. Fleischauer, T.J. Duignan, B.L. Scott, M.W. Loble, S.K. Cary, S.A. Kozimor, H. Bolvin, M.L. Neidig, J. Autschbach, *Phys. Chem. Chem. Phys.*, 2017, **19**, 17300-17313.
2. A.G.H. Wee, A.Y.L. Shu, E. Bunnenberg, C. Djerassi, *J. Org. Chem.*, 1984, **49**, 3327-3336.
3. S. Ghidnelli, S. Abbate, E. Santoro, S. Belviso, G. Longhi *J. Phys. Chem. B.*, 2021, **125**, 264-280.
4. Z. Gasyna, M.J. Stillman, *Inorg. Chem.*, 1990, **29**, 5101-5109.
5. T. Yoshimura, H. Toi, S. Inaba, H. Ogoshi, *Inorg. Chem.*, 1991, **30**, 4315-4321.
6. M.G.I. Galinato, E.P. Brocious, F. Paulat, S. Martin, J. Skodack, J.B. Harland, N. Lehnert, *Inorg. Chem.*, 2020, **59**, 2144-2162.
7. H.M. Rhoda, J. Akhigbe, J. Ogikubo, J.R. Sabin, C.J. Ziegler, C. Bruckner, V.N. Nemykin, *J. Phys. Chem. A.*, 2016, **120**, 5805-5815.
8. V. Andruschenko, D. Padula, E. Zhivotova, S. Yamamoto, P. Bour, *Chirality*, 2014, **26**, 655-662.

9. M.J.D. Champion, P. Farina, W. Levason, G. Reid, *Dalton Trans.*, 2013, **42**, 13179-13189.
10. E.L. Gavey, M.A. Hareri, J. Regier, L.D. Carlos, R.A.S. Ferreira, F.S. Razavi, J.M. Rawson, M. Pilkington, *J. Mater. Chem. C*, 2015, **3**, 7738-7747.
11. Y.S. Ding, T. Han, Y.Q. Hu, M. Xu, S. Yang, Y.Z. Zheng, *Inorg. Chem. Front.*, 2016, **3**, 798–807.
12. F. Gao, F.L. Yang, X. Feng, H. Xu, W. Sun, H. Liu, X.L. Li, *Dalton Trans.*, 2017, **46**, 1317–1323.
13. B.D. White, K.A. Arnold, R.L. Garrell, F.R. Fronczek, R.D. Gandour, G.W. Gokel, *J. Org. Chem.*, 1987, **52**, 1128-1133.
14. A. Santria, A. Fuyuhiro, T. Fukuda, N. Ishikawa, *Inorg. Chem.*, 2017, **56**, 10625-10632.
15. S. B. Piepho, P. N. Schatz, Group Theory in Spectroscopy: With Applications to Magnetic Circular Dichroism; Wiley: New York, 1983.
16. T. Ida, M. Ando, H. Toraya, *J. App. Crystallogr.*, 2000, **33**, 1311-1316.
17. A. Santria and N. Ishikawa, *Inorg. Chem.*, 2020, **59**, 14326-14336.
18. A. Santria and N. Ishikawa, *Inorg. Chem.*, 2021, **60**, 14418-14425.
19. K. Kizaki, A. Santria, N. Ishikawa, *Inorg. Chem.*, 2020, **60**, 2037-2044.
20. K. Kizaki, H. Ozawa, T. Kobayashi, R. Matsuoka, Y. Sakaguchi, A. Fuyuhiro, T. Fukuda, N. Ishikawa, *Chem. Commun.*, 2017, **53**, 6168-6171.
21. T. Fukuda, H. Ozawa, Y. Sakaguvhi, K. Kizaki, T. Kobayashi, A. Fuyuhiro, N. Ishikawa, *Chem. Eur. J.*, 2017, **23**, 16357-16363.

2.6 Supporting Information

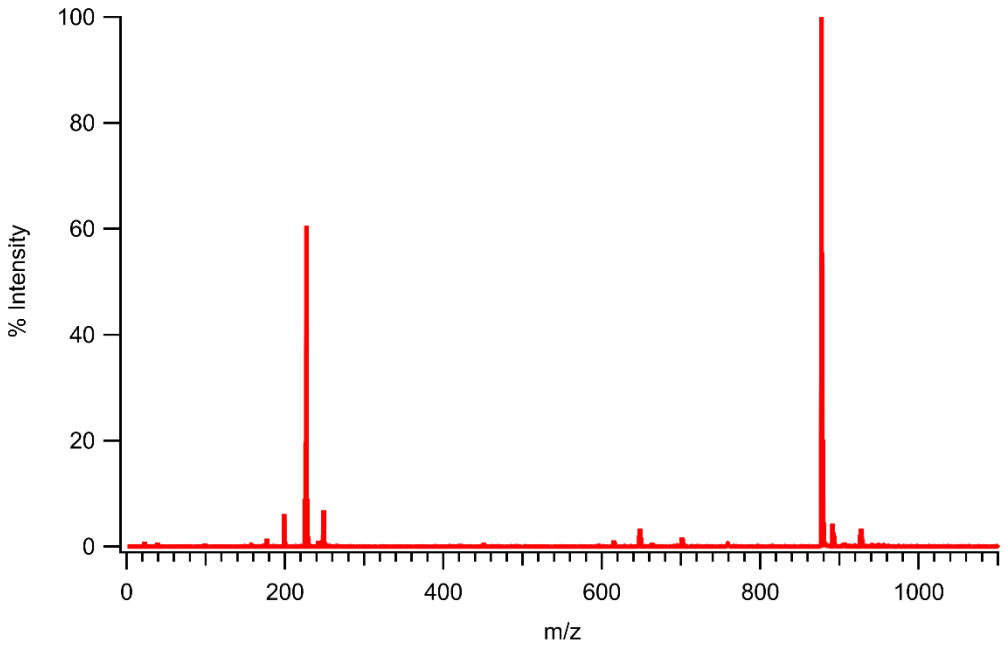

Figure S2-1 MALDI-TOF spectra of $[Y(TPP)Crown]^+$ with dithranol as matrix ($C_{14}H_{10}O_3$)at m/z equal 227.07.

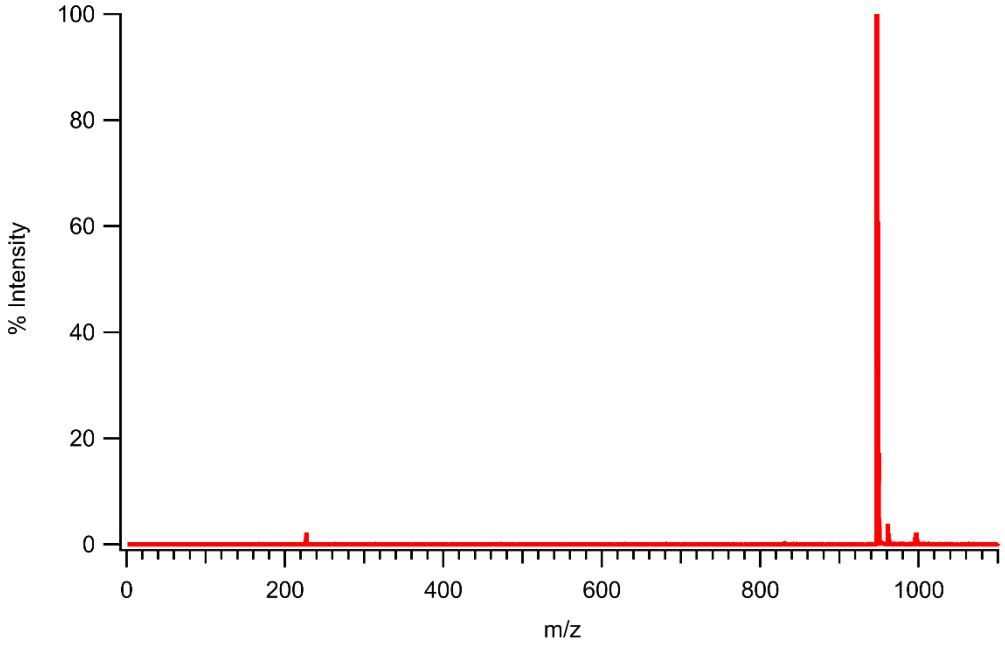

Figure S2-2 MALDI-TOF spectra of $[Tb(TPP)Crown]^+$ with dithranol as matrix ($C_{14}H_{10}O_3$) at m/z equal 227.06.

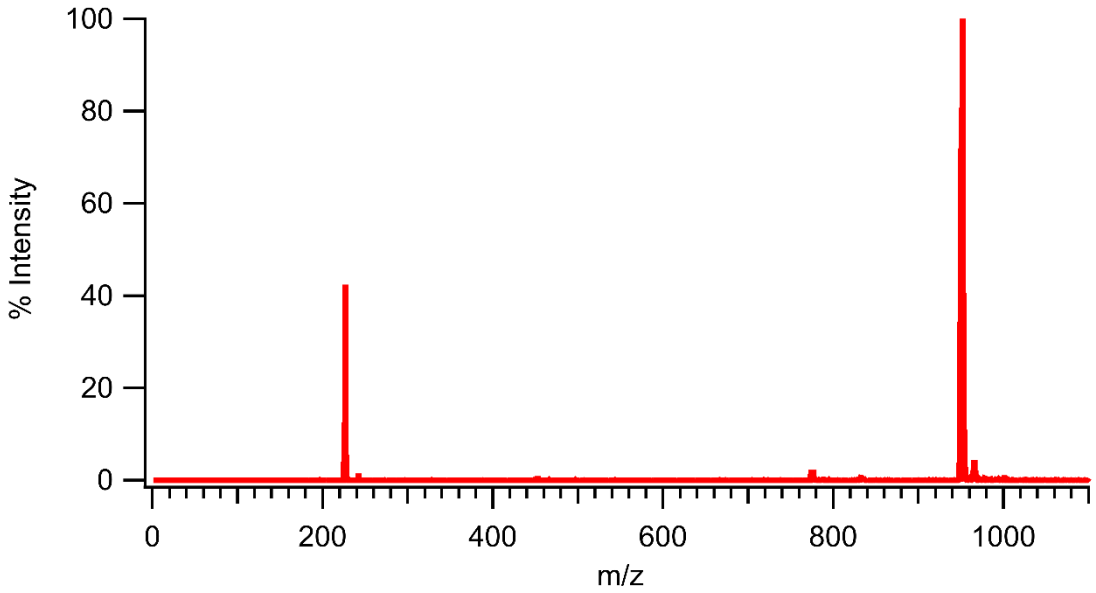

Figure S2-3 MALDI-TOF spectra of $[Dy(TPP)Crown]^+$ with dithranol as matrix ($C_{14}H_{10}O_3$)at m/z equal 227.08.

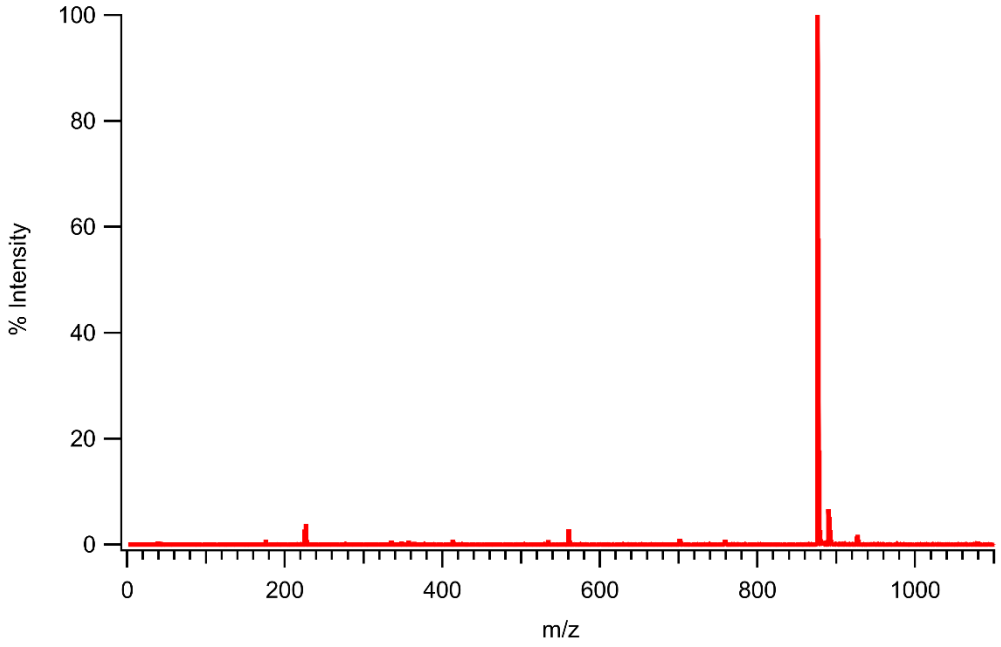

Figure S2-4 MALDI-TOF spectra of $[Y(TPP)Azacrown]^+$ with dithranol as matrix ($C_{14}H_{10}O_3$)at m/z equal 227.06.

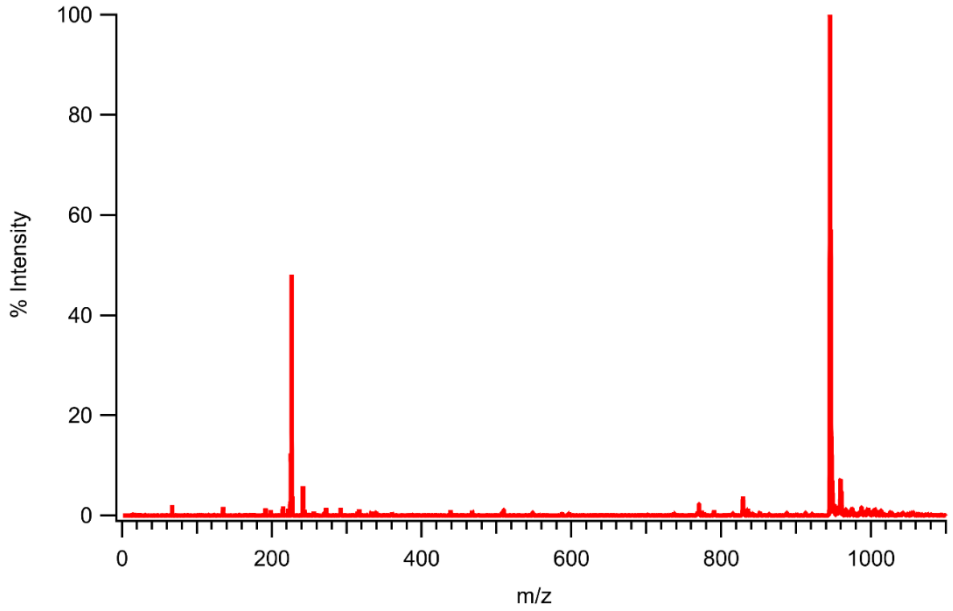

Figure S2-5 MALDI-TOF spectra of $[Tb(TPP)Azacrown]^+$ with dithranol as matrix ($C_{14}H_{10}O_3$)at m/z equal 227.06.

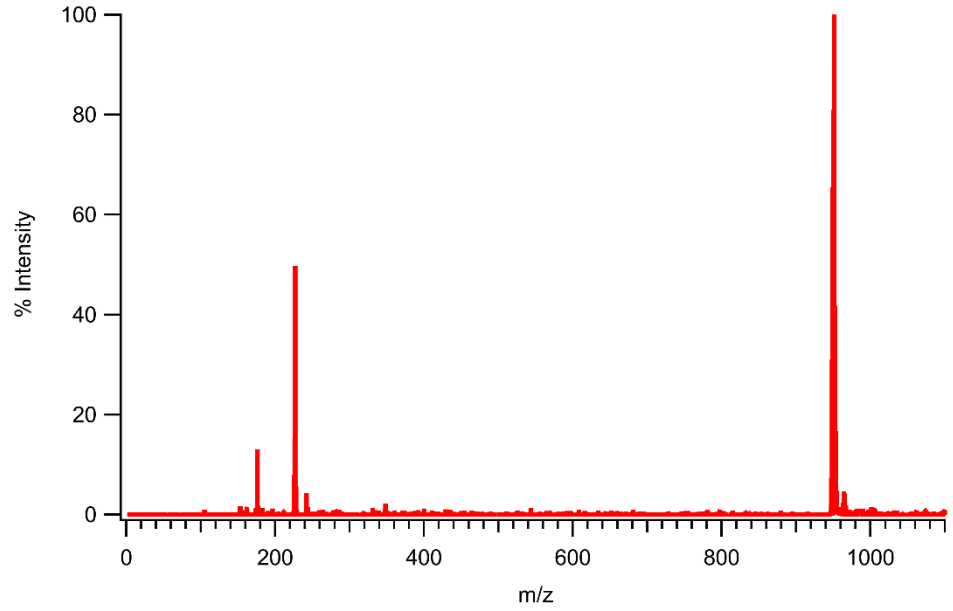

Figure S2-6 MALDI-TOF spectra of $[Dy(TPP)Azacrown]^+$ with dithranol as matrix ($C_{14}H_{10}O_3$)at m/z equal 227.07.

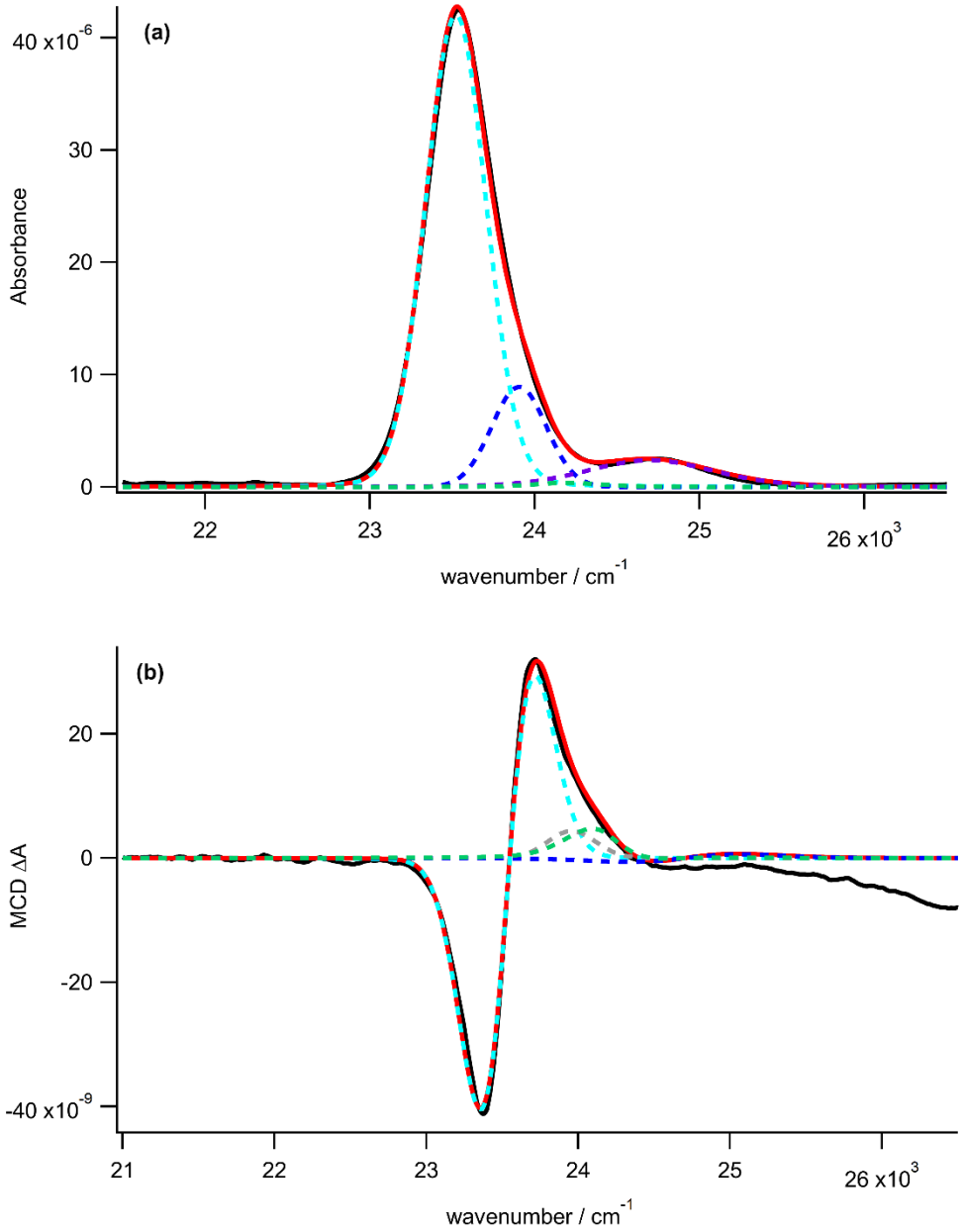

Figure S2-7 Band deconvolution of absorption (**a**) and MCD (**b**) of B(0,0) band spectra [Y(TPP)Crown]Cl at 100 K and 1 T. Experimental spectra is shown in black while simulated band is in red color. The components that give the simulated band are in dashed lines.

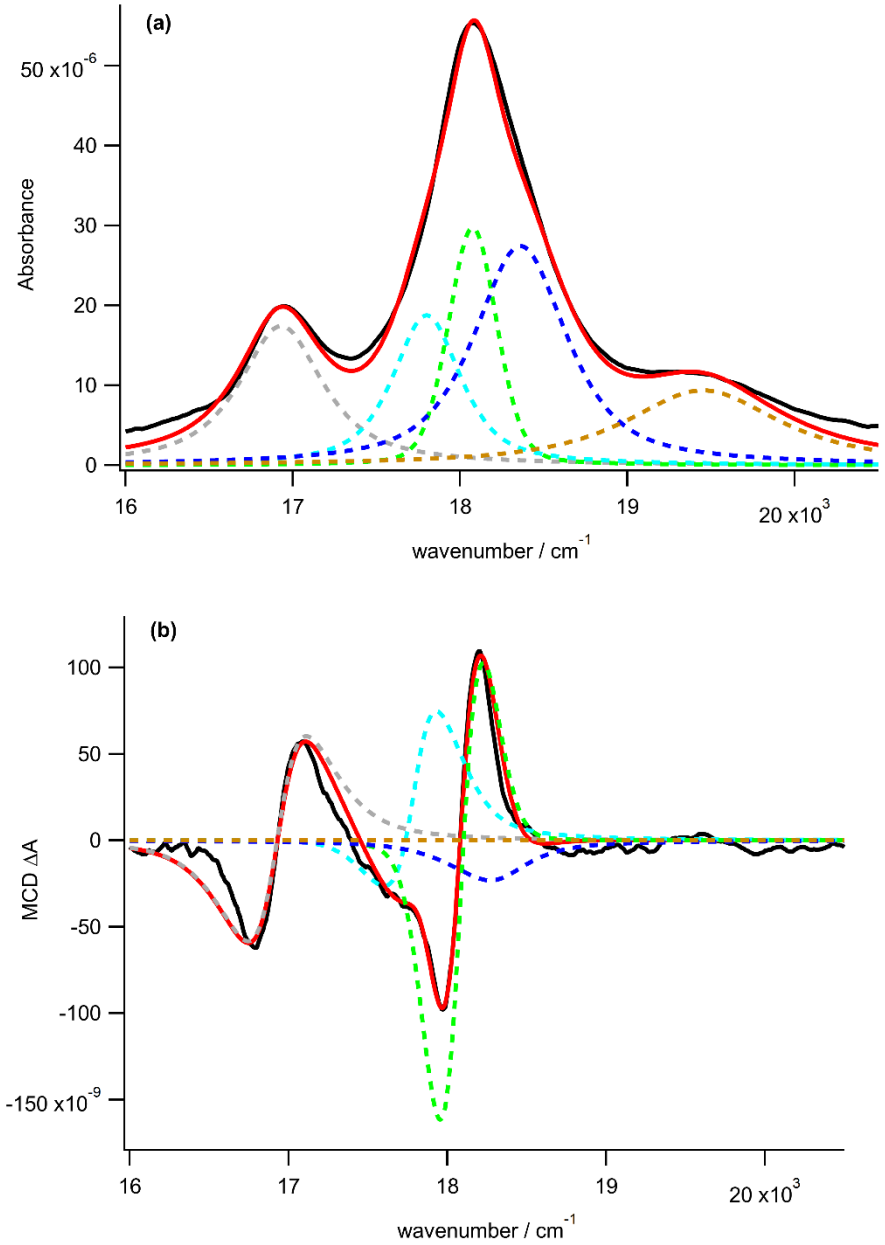

Figure S2-8 Band deconvolution of absorption (**a**) and MCD (**b**) of Q(0,0) and Q(1,0) band spectra [Y(TPP)Crown]Cl at 1.5 K and 1 T . Experimental spectra is shown in black while simulated band is in red color. The components that give the simulated band are in dashed lines.

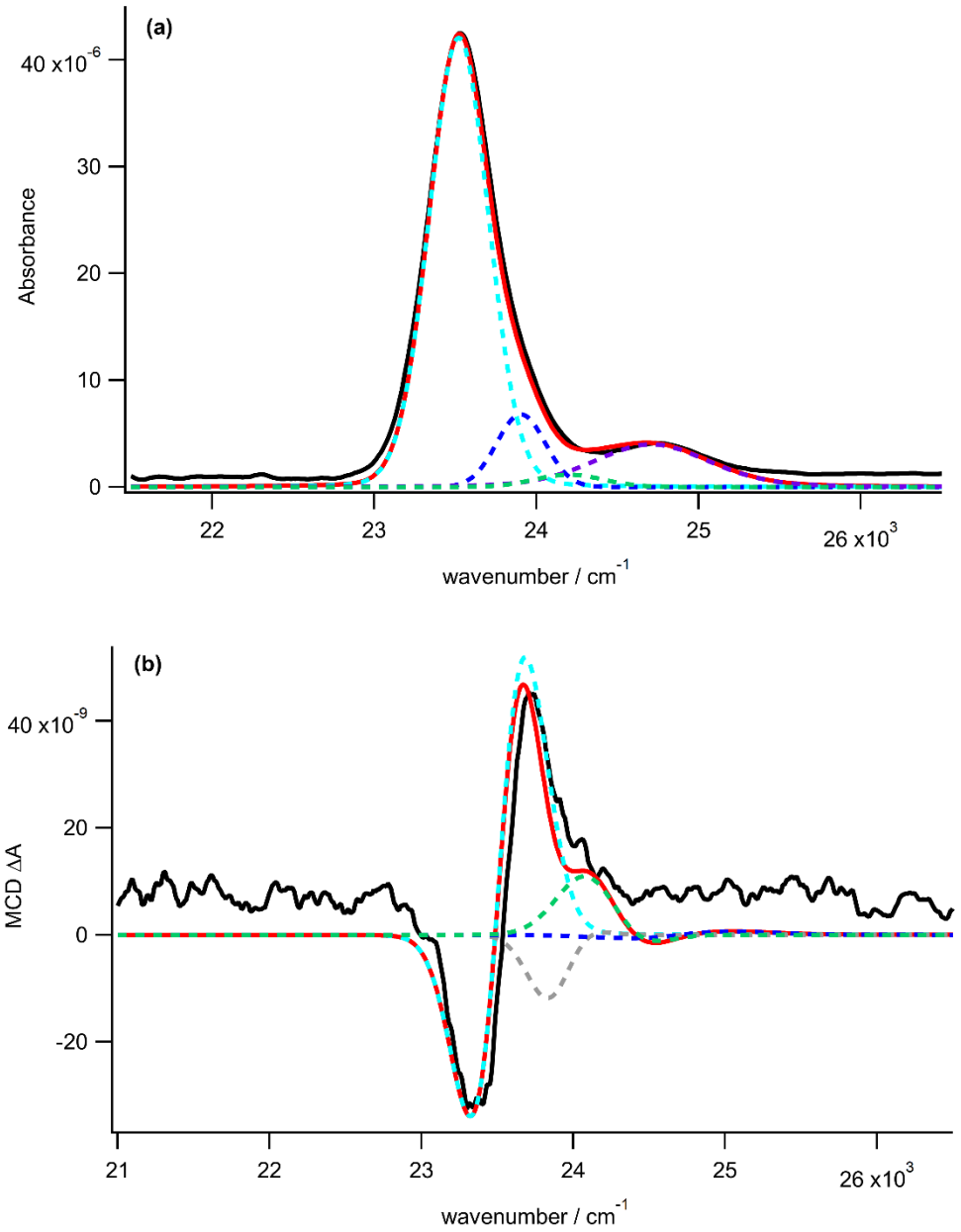

Figure S2-9 Band deconvolution of absorption (**a**) and MCD (**b**) of B(0,0) band spectra [Tb(TPP)Crown]Cl at 100 K and 1 T. Experimental spectra is shown in black while simulated band is in red color. The components that give the simulated band are in dashed lines.

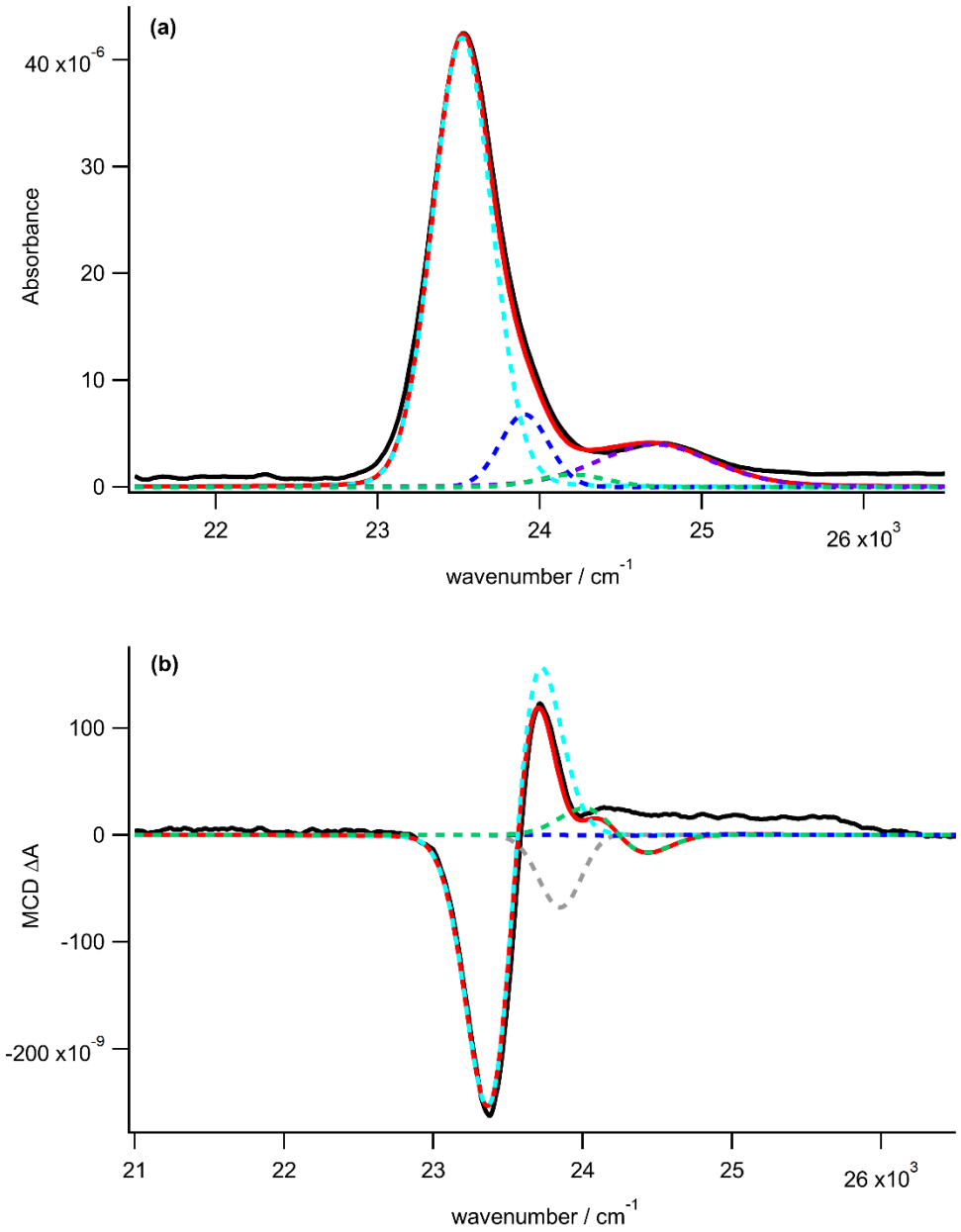

Figure S2-10 Band deconvolution of absorption (**a**) and MCD (**b**) of B(0,0) band spectra [Tb(TPP)Crown]Cl at 1.5 K and 1 T. Experimental spectra is shown in black while simulated band is in red color. The components that give the simulated band are in dashed lines.

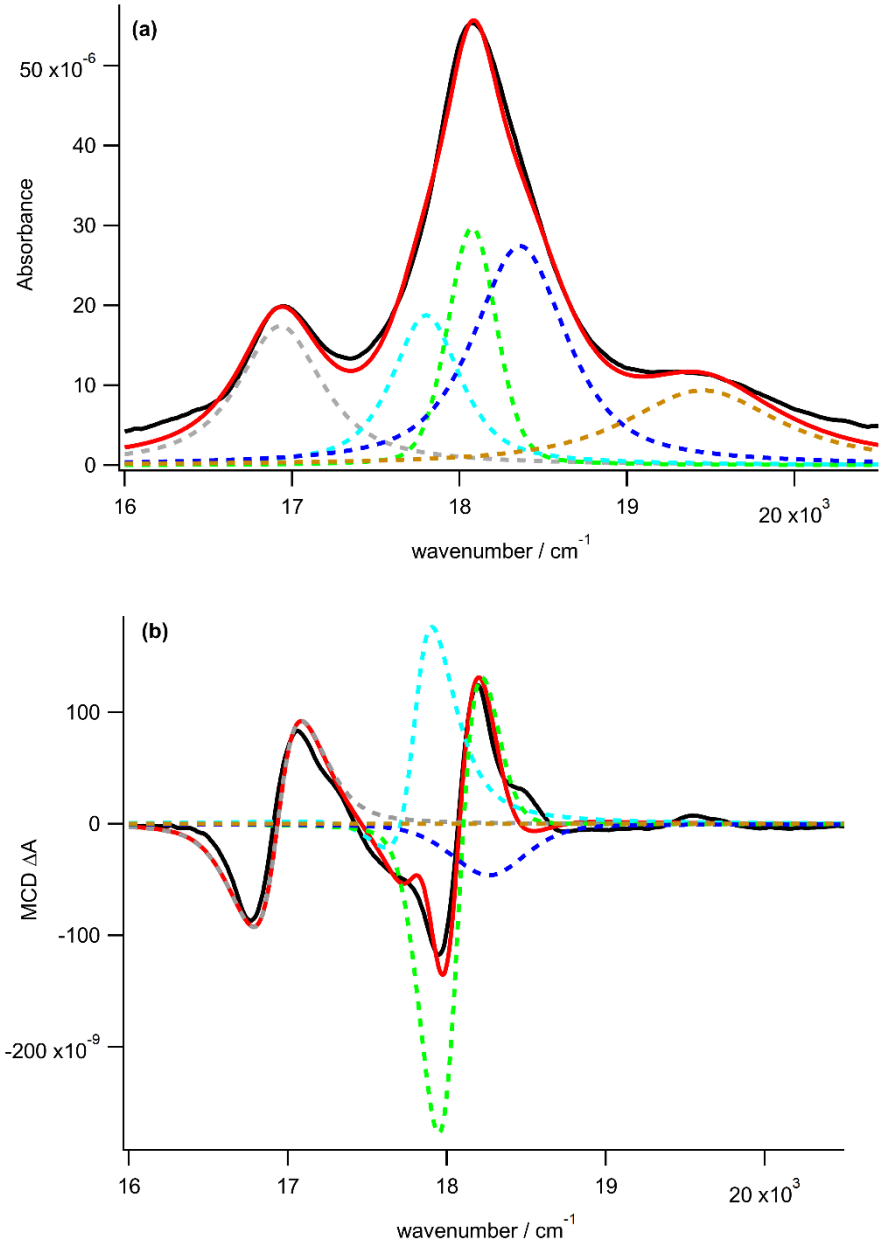

Figure S2-11 Band deconvolution of absorption (**a**) and MCD (**b**) of Q(0,0) and Q(1,0) band spectra [Tb(TPP)Crown]Cl at 100 K and 1 T. Experimental spectra is shown in black while simulated band is in red color. The components that give the simulated band are in dashed lines.

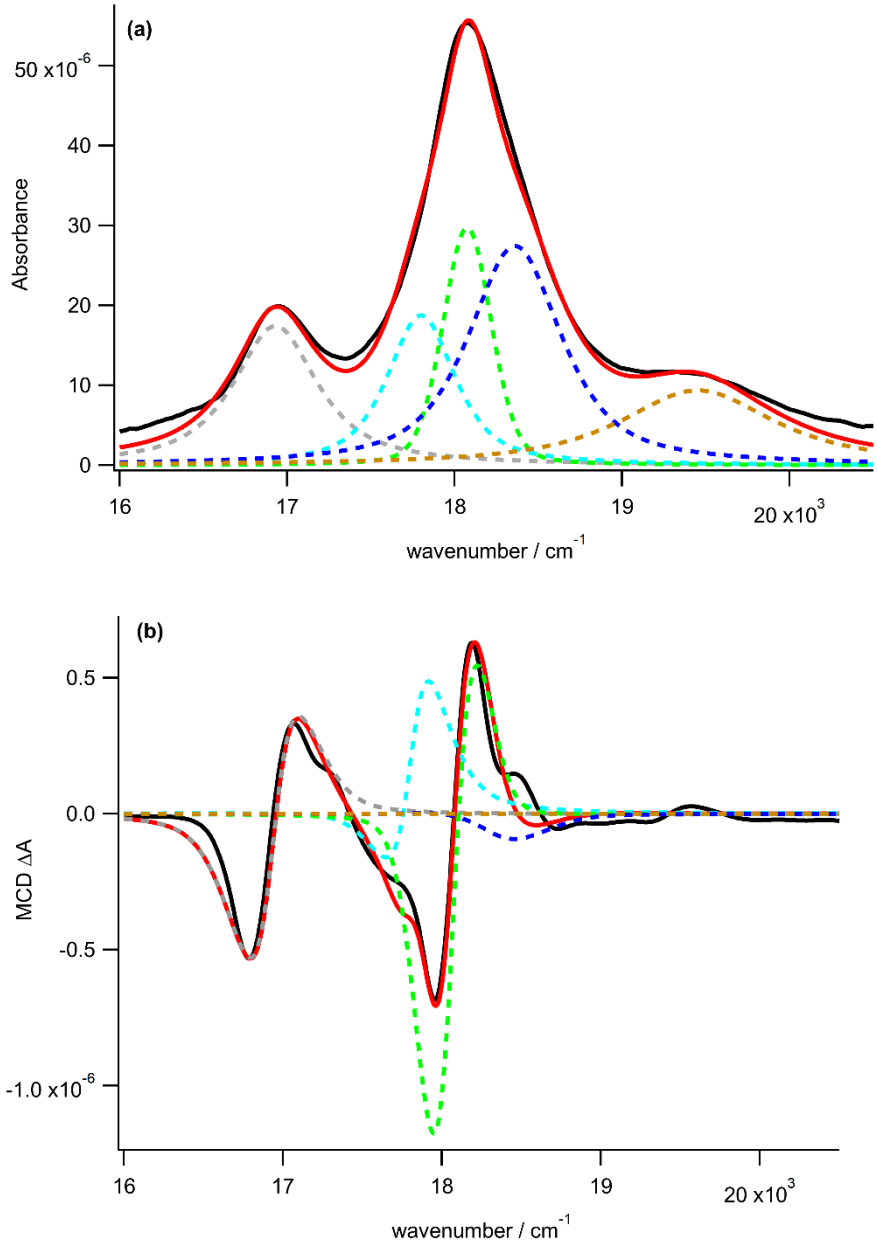

Figure S2-12 Band deconvolution of absorption (**a**) and MCD (**b**) of Q(0,0) and Q(1,0) band spectra [Tb(TPP)Crown]Cl at 1.5 K and 1 T. Experimental spectra is shown in black while simulated band is in red color. The components that give the simulated band are in dashed lines.

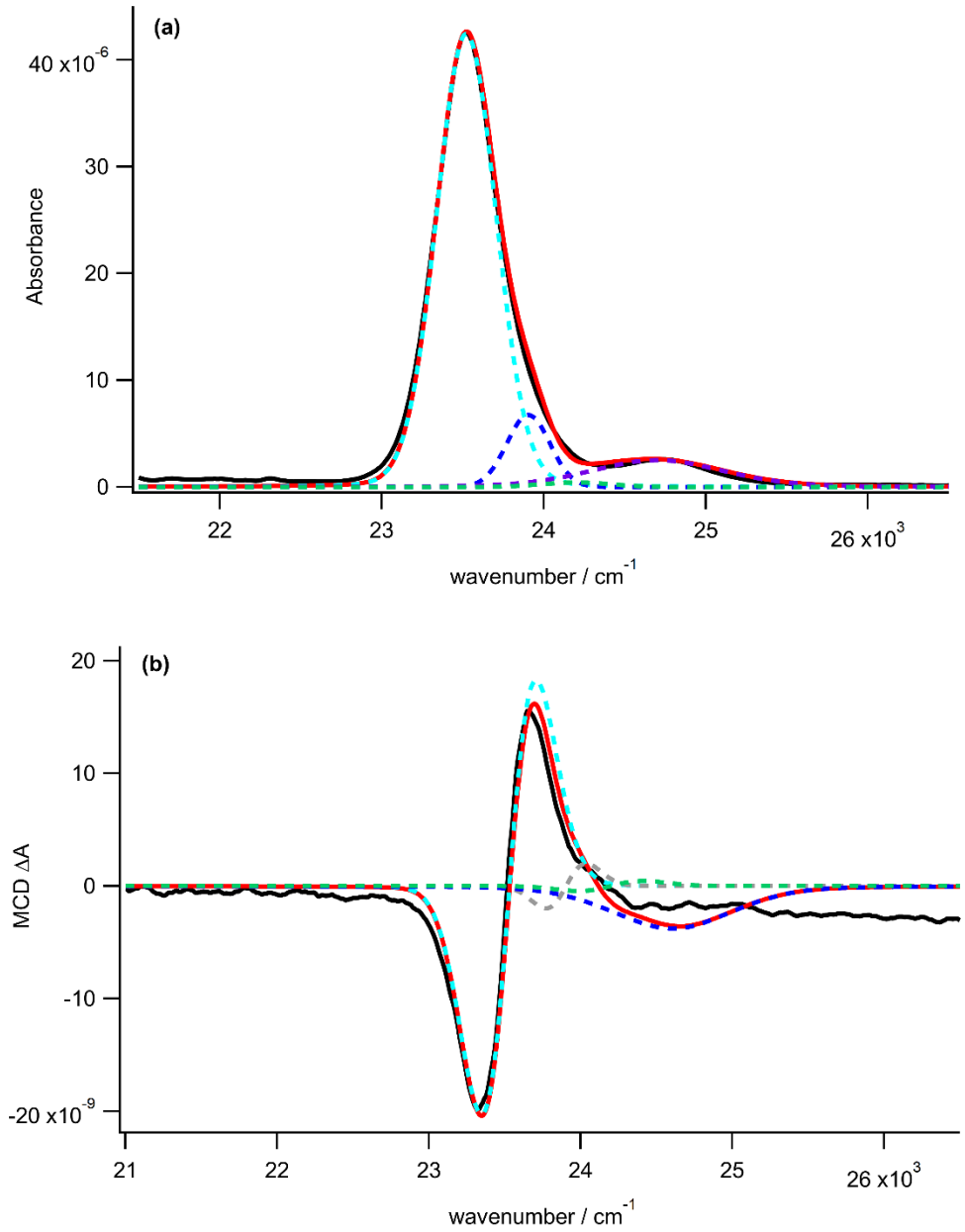

Figure S2-13 Band deconvolution of absorption (**a**) and MCD (**b**) of B(0,0) band spectra [Dy(TPP)Crown]Cl at 100 K and 1 T. Experimental spectra is shown in black while simulated band is in red color. The components that give the simulated band are in dashed lines.

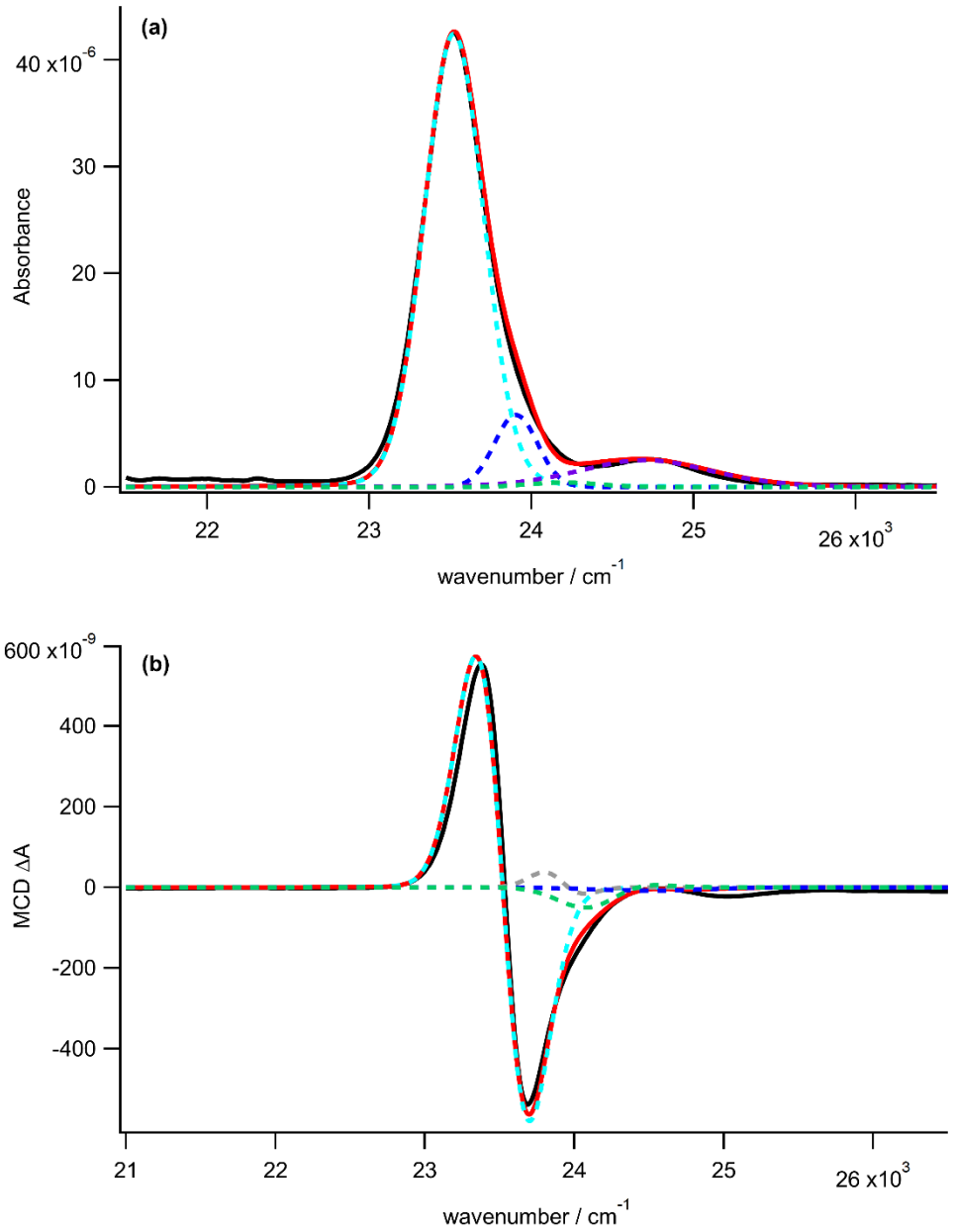

Figure S2-14 Band deconvolution of absorption (**a**) and MCD (**b**) of B(0,0) band spectra [Dy(TPP)Crown]Cl at 1.5 K and 1 T. Experimental spectra is shown in black while simulated band is in red color. The components that give the simulated band are in dashed lines.

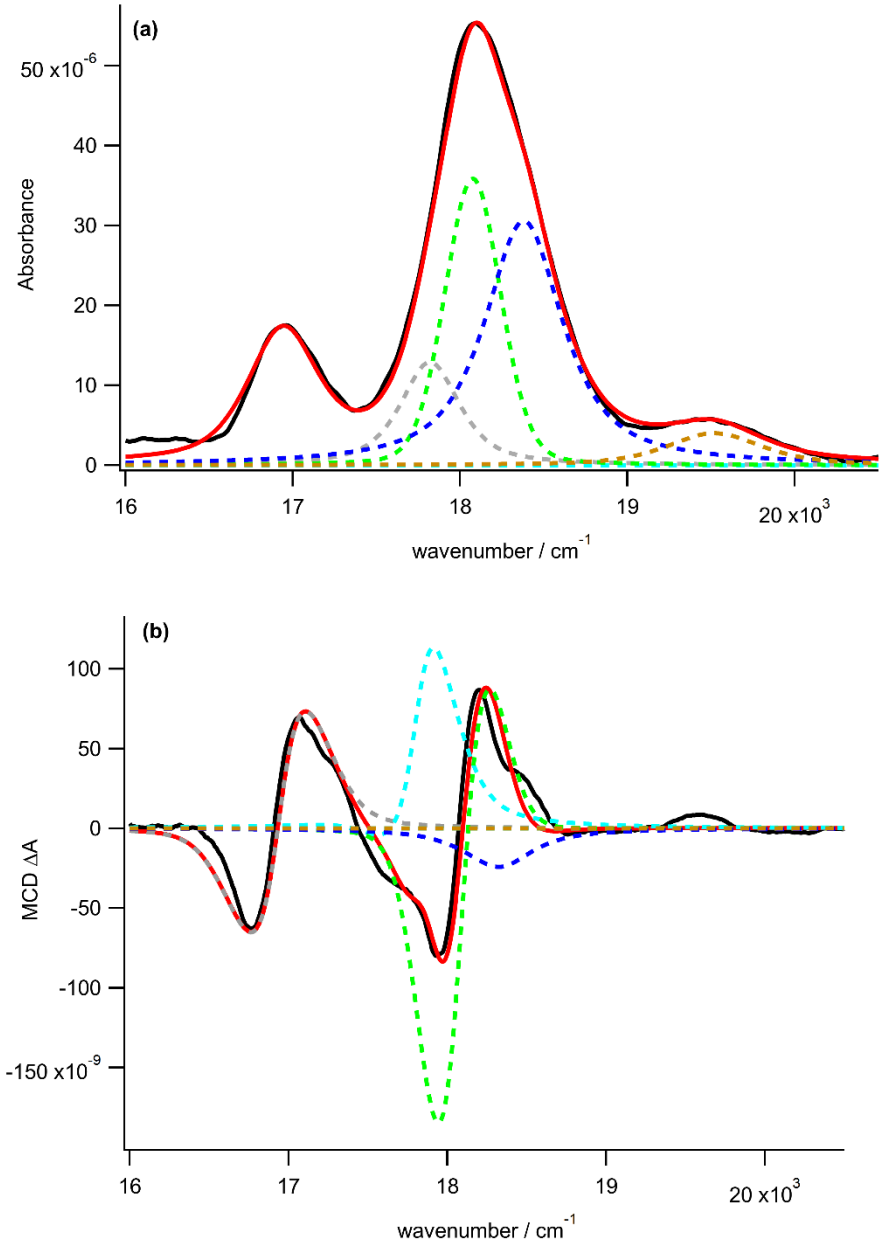

Figure S2-15 Band deconvolution of absorption (**a**) and MCD (**b**) of Q(0,0) and Q(1,0) band spectra [Dy(TPP)Crown]Cl at 100 K and 1.5 T. Experimental spectra is shown in black while simulated band is in red color. The components that give the simulated band are in dashed lines.

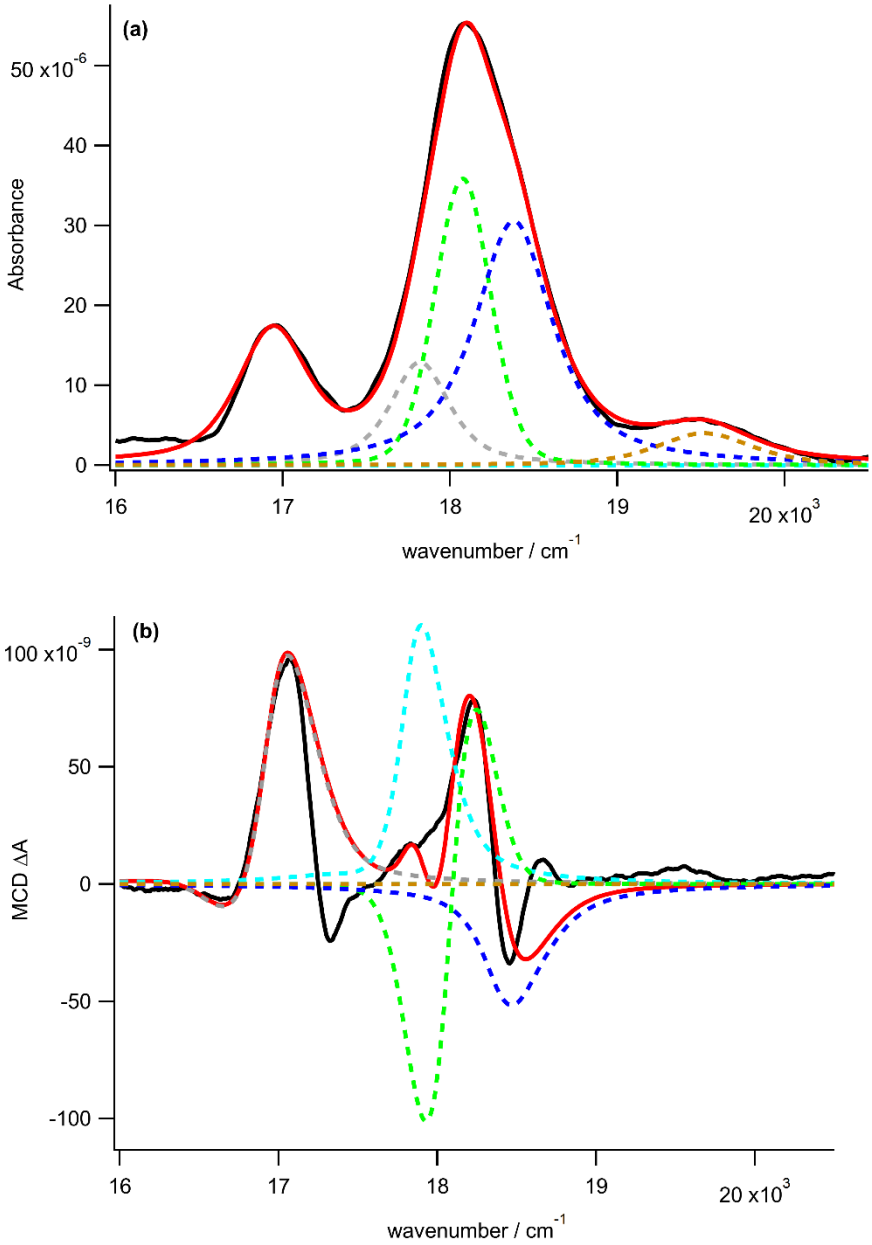

Figure S2-16 Band deconvolution of absorption (**a**) and MCD (**b**) of Q(0,0) and Q(1,0) band spectra [Dy(TPP)Crown]Cl at 1.5 K and 1 T. Experimental spectra is shown in black while simulated band is in red color. The components that give the simulated band are in dashed lines.

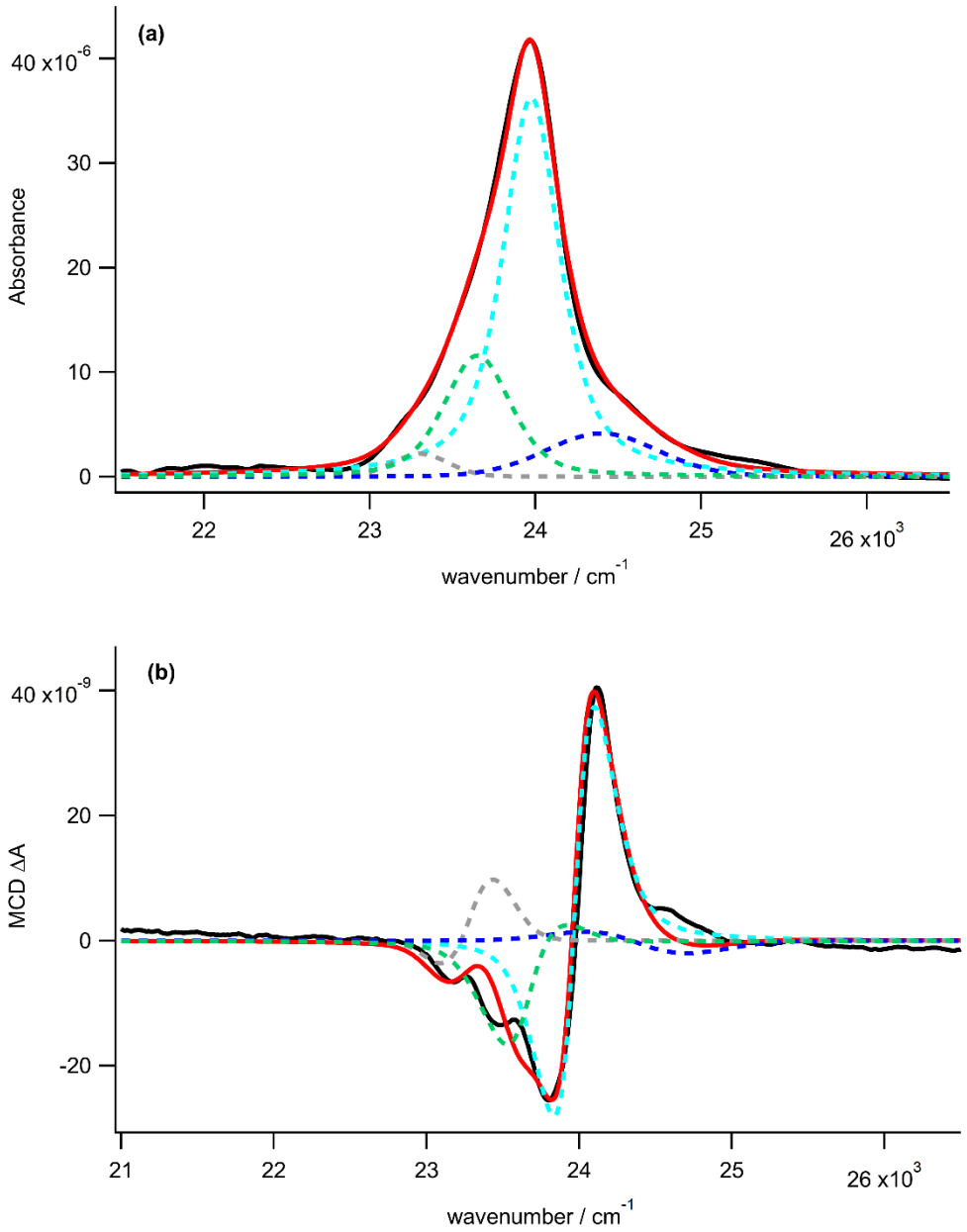

Figure S2-17 Band deconvolution of absorption (**a**) and MCD (**b**) of B(0,0) band spectra [Y(TPP)Azacrown]Cl at 1.5 K and 1 T. Experimental spectra is shown in black while simulated band is in red color. The components that give the simulated band are in dashed lines.

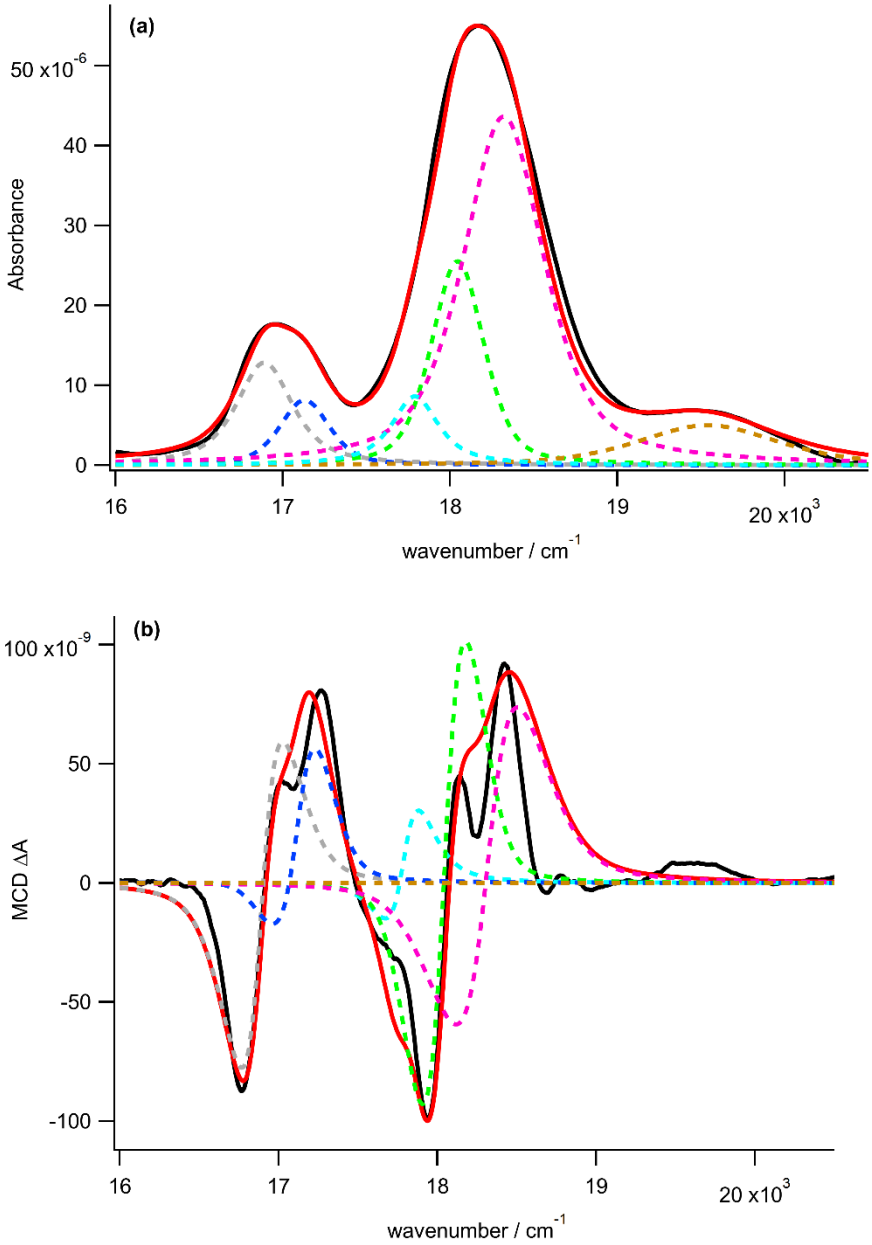

Figure S2-18 Band deconvolution of absorption (**a**) and MCD (**b**) of Q(0,0) and Q(1,0) band spectra [Y(TPP)Azacrown]Cl at 1.5 K and 1 T. Experimental spectra is shown in black while simulated band is in red color. The components that give the simulated band are in dashed lines.

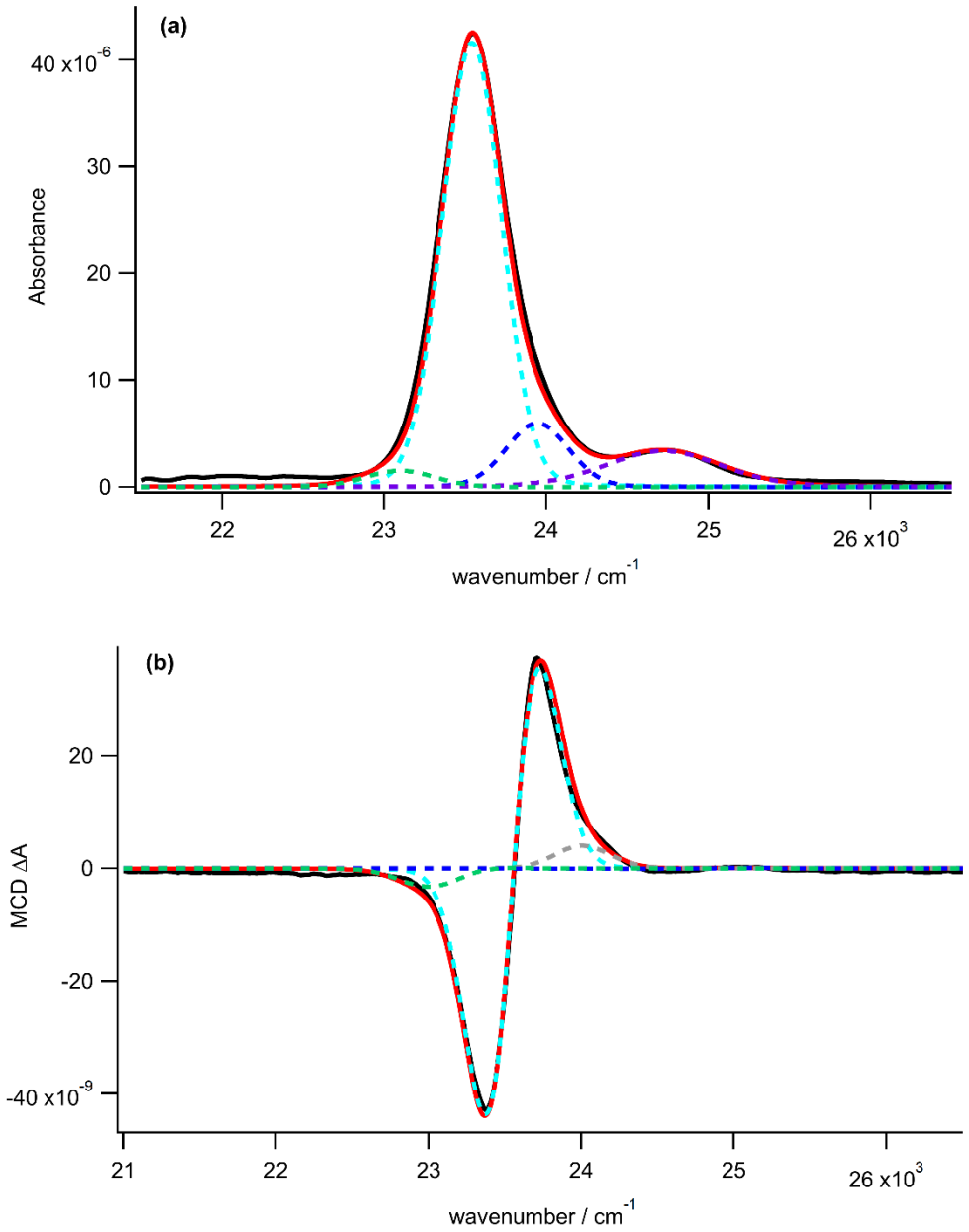

Figure S2-19 Band deconvolution of absorption (**a**) and MCD (**b**) of B(0,0) band spectra [Tb(TPP)Azacrown]Cl at 100 K and 1 T. Experimental spectra is shown in black while simulated band is in red color. The components that give the simulated band are in dashed lines.

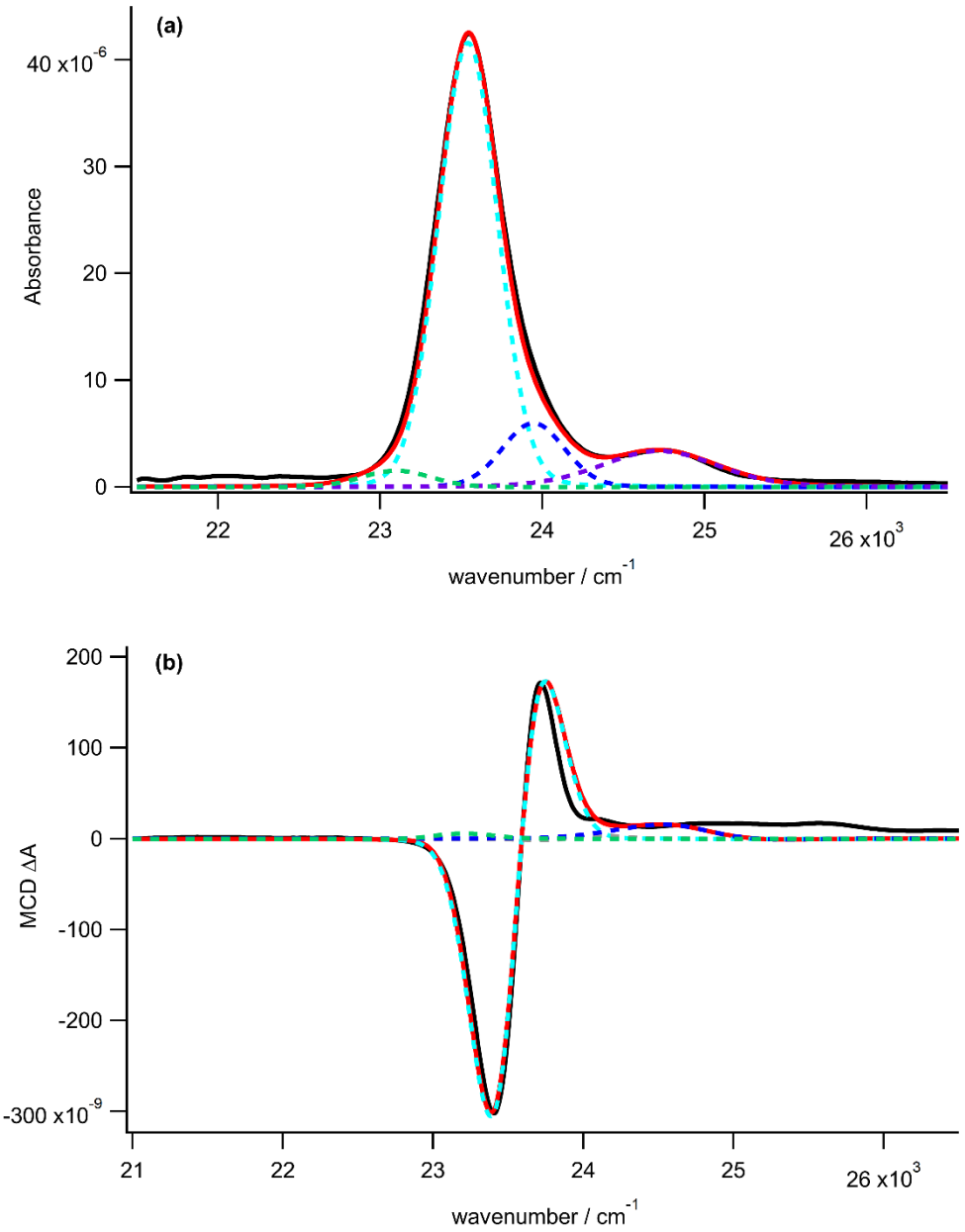

Figure S2-20 Band deconvolution of absorption (**a**) and MCD (**b**) of B(0,0) band spectra [Tb(TPP)Azacrown]Cl at 1.5 K and 1 T. Experimental spectra is shown in black while simulated band is in red color. The components that give the simulated band are in dashed lines.

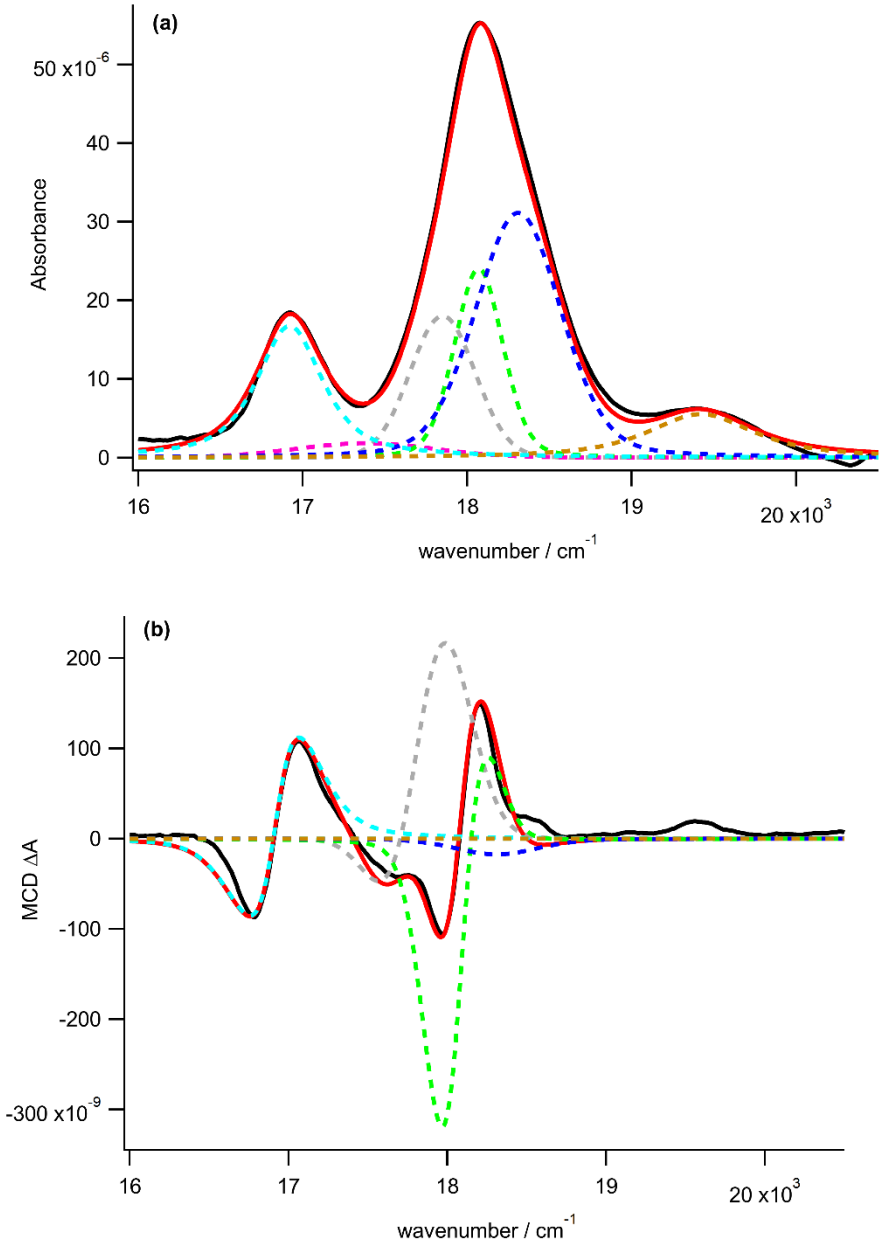

Figure S2-21 Band deconvolution of absorption (**a**) and MCD (**b**) of Q(0,0) and Q(1,0) band spectra [Tb(TPP)Azacrown]Cl at 100 K and 1 T. Experimental spectra is shown in black while simulated band is in red color. The components that give the simulated band are in dashed lines.

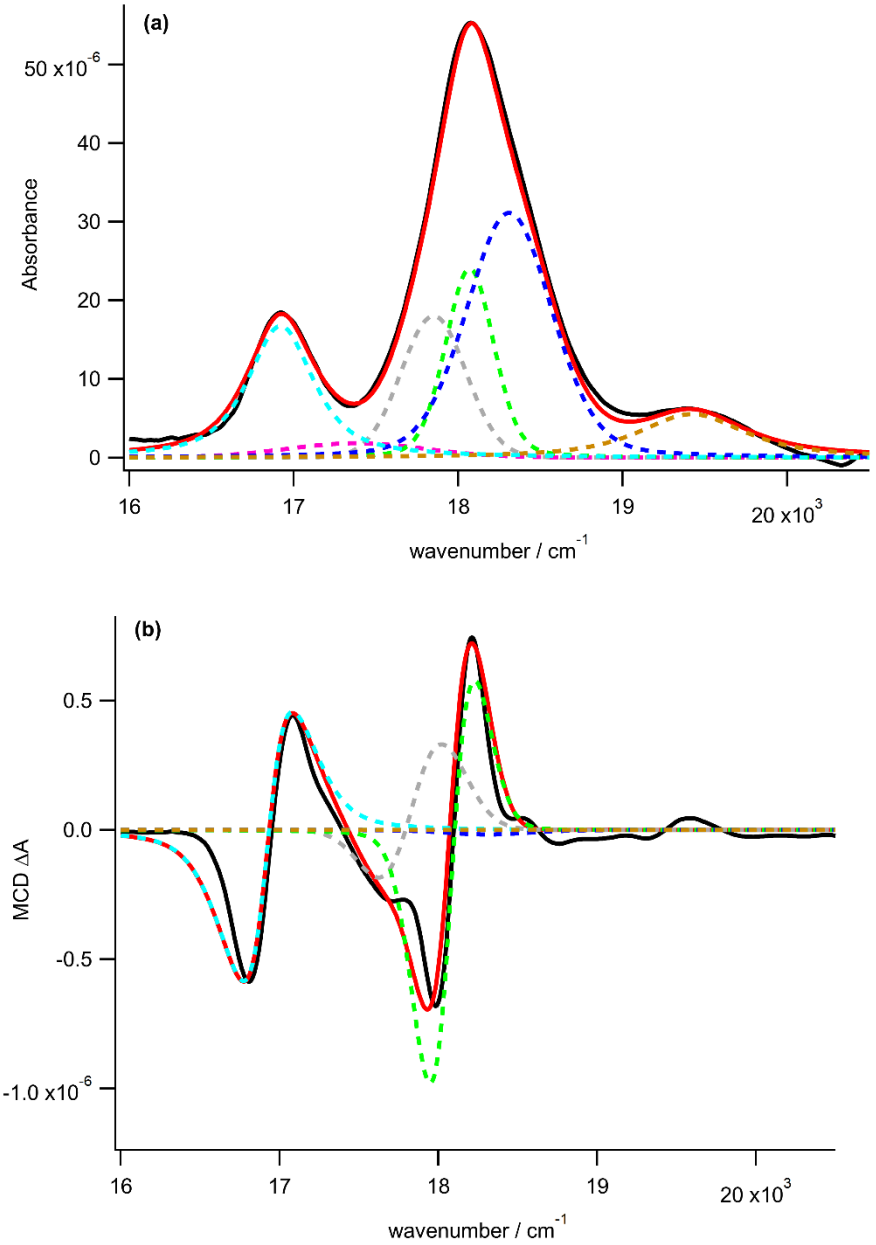

Figure S2-22 Band deconvolution of absorption (**a**) and MCD (**b**) of Q(0,0) and Q(1,0) band spectra [Tb(TPP)Azacrown]Cl at 1.5 K and 1 T. Experimental spectra is shown in black while simulated band is in red color. The components that give the simulated band are in dashed lines.

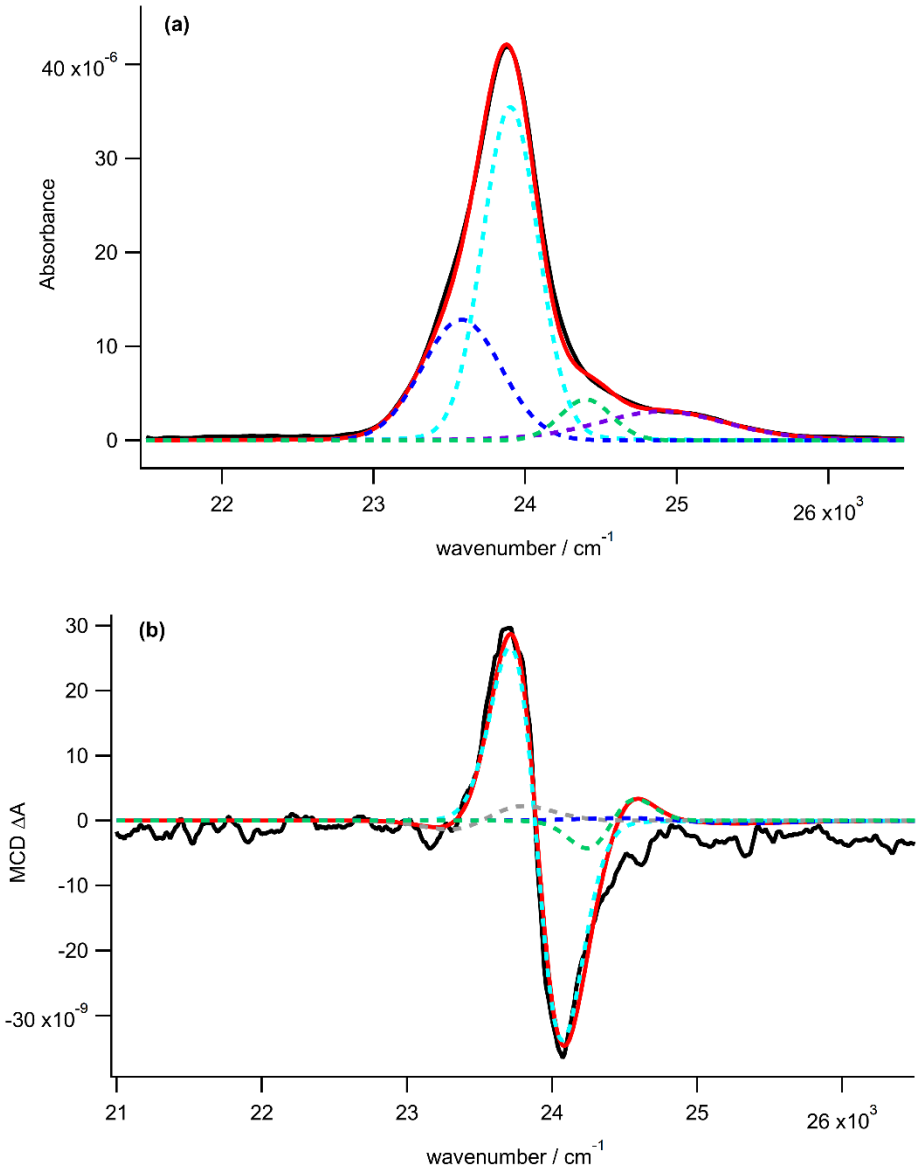

Figure S2-23 Band deconvolution of absorption (**a**) and MCD (**b**) of B(0,0) band spectra [Dy(TPP)Azacrown]Cl at 100 K and 1 T. Experimental spectra is shown in black while simulated band is in red color. The components that give the simulated band are in dashed lines.

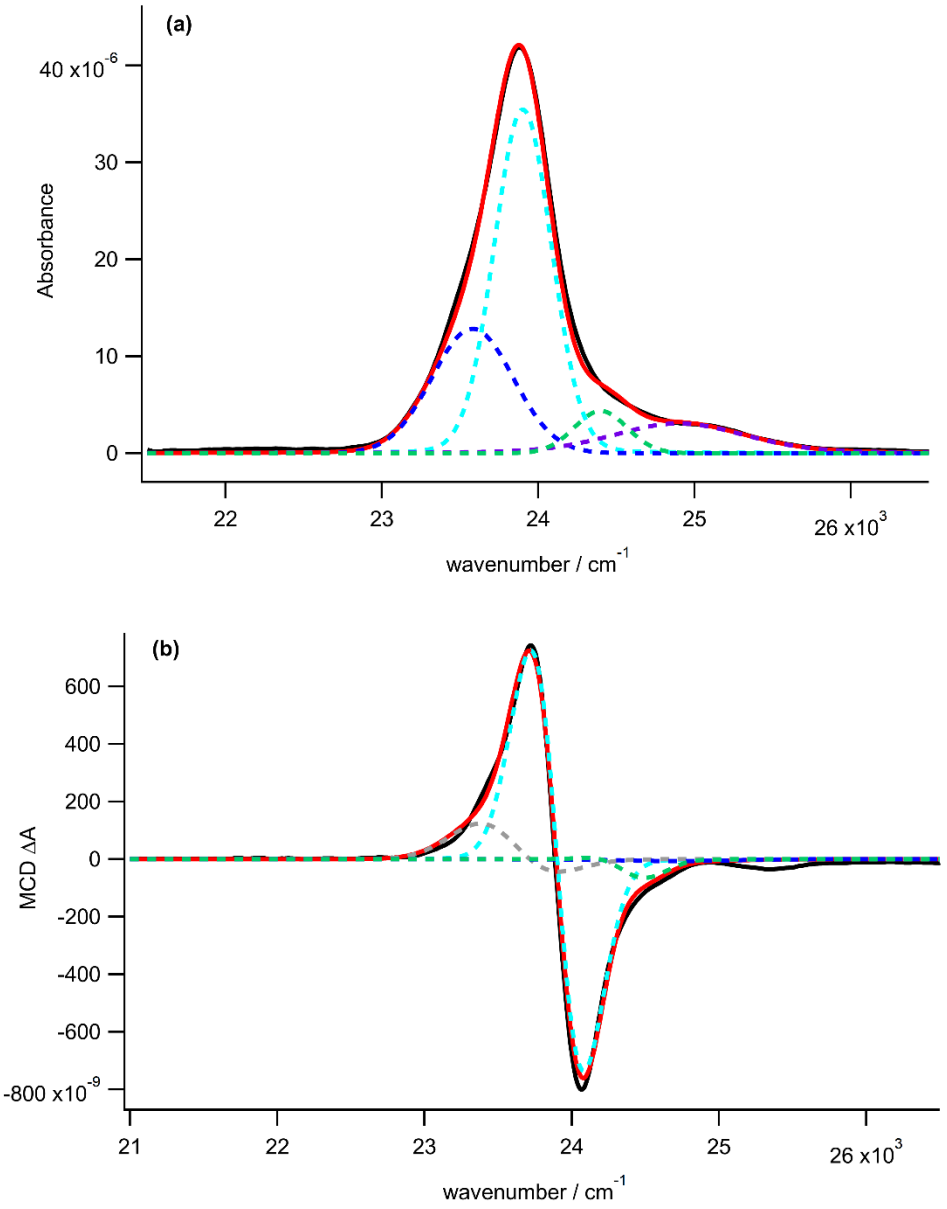

Figure S2-24 Band deconvolution of absorption (**a**) and MCD (**b**) of B(0,0) band spectra [Dy(TPP)Azacrown]Cl at 1.5 K and 1 T. Experimental spectra is shown in black while simulated band is in red color. The components that give the simulated band are in dashed lines.

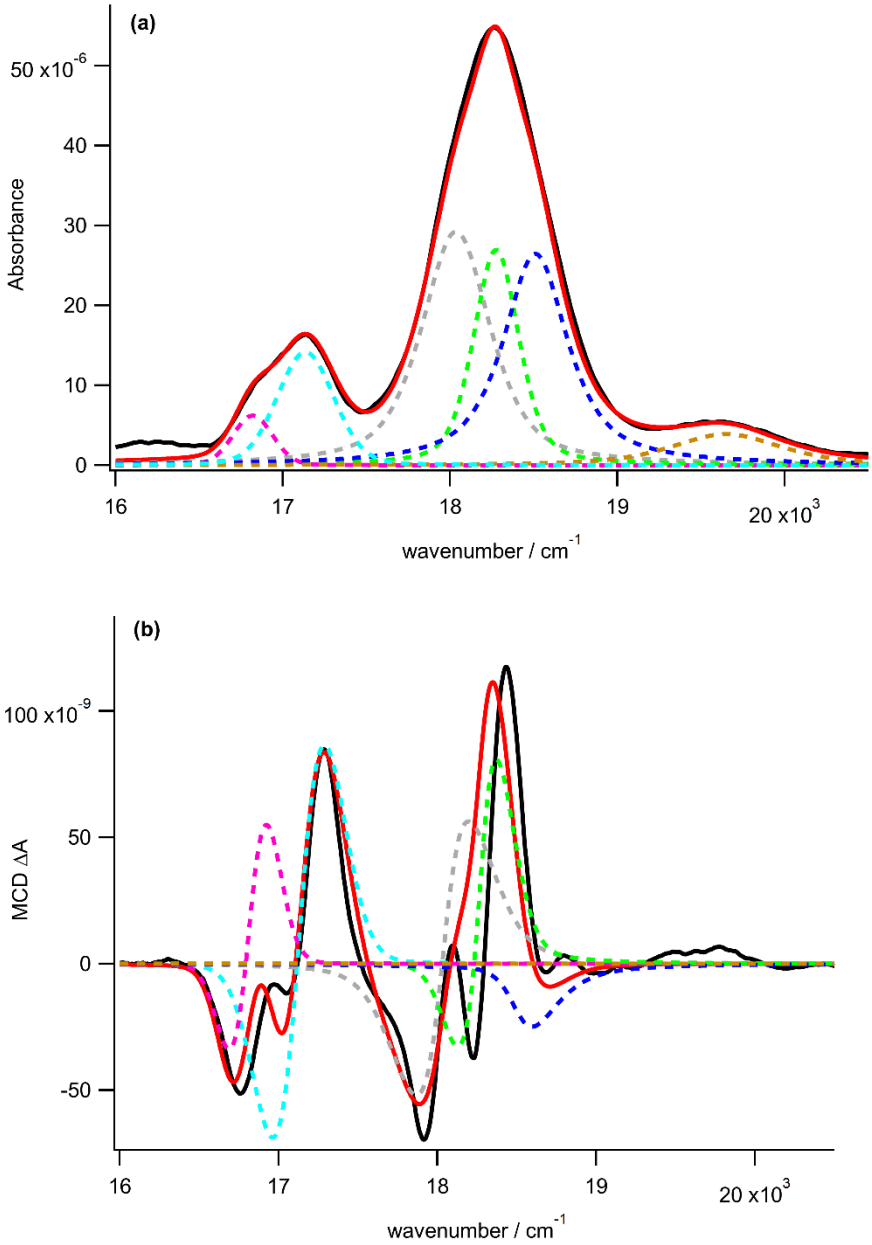

Figure S2-25 Band deconvolution of absorption (**a**) and MCD (**b**) of Q(0,0) and Q(1,0) band spectra [Dy(TPP)Azacrown]Cl at 100 K and 1 T. Experimental spectra is shown in black while simulated band is in red color. The components that give the simulated band are in dashed lines.

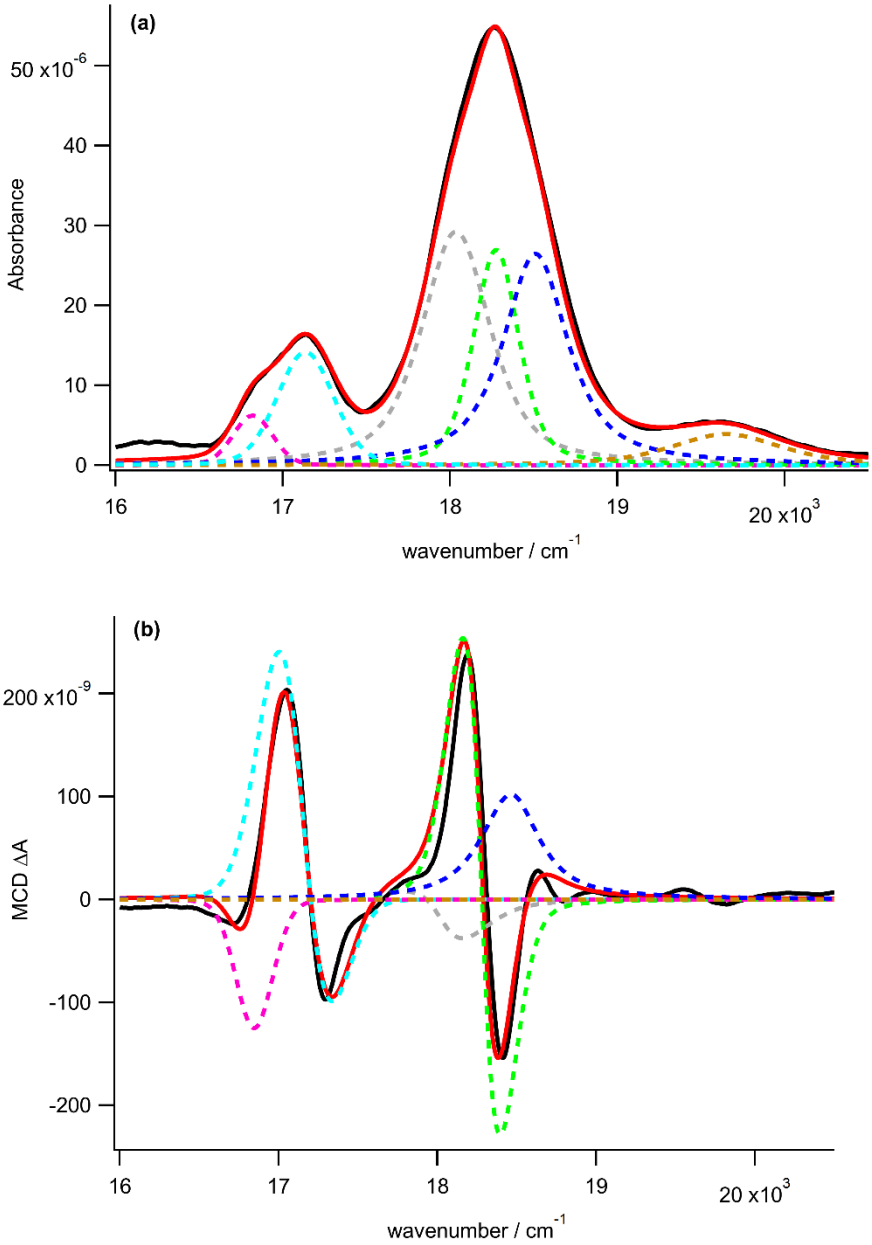

Figure S2-26 Band deconvolution of absorption (**a**) and MCD (**b**) of Q(0,0) and Q(1,0) band spectra [Dy(TPP)Azacrown]Cl at 1.5 K and 1 T. Experimental spectra is shown in black while simulated band is in red color. The components that give the simulated band are in dashed lines.

		Q band					B band			
		Band 1	Band 2	Band 3	Band 4	Band 5	Band 6	Band 7	Band 8	Band 9
$E_0\,(cm^{-1})^{\xi}$		16930	17800	18075	18360	19450	23522	23905	24200	24700
$\Gamma\,(cm^{-1})^{\xi}$		600	480	340	660	1100	431	390	500	910
η^{ξ}		0.89	0.76	0.31	0.78	0.89	0.08	0.00	0.50	0.30
D_0		0.62	0.51	0.47	1.03	0.62	21.56	4.02	0.26	2.78
Values obtained under 1 T										
T (K)		Band 1	Band 2	Band 3	Band 4	Band 5	Band 6	Band 7	Band 8	Band 9
100	$\mathcal{A}_1/\mathcal{D}_0$	3.26451	2.06186	2.32179	0.1946	0.00000	0.52240	0.05827	-3.90625	0.35997
	$\mathcal{B}_0/\mathcal{D}_0$	0.00048	0.00434	-0.00300	-0.00165	0.00000	-0.00037	0.00099	0.02148	0.00000
1.5	$\mathcal{A}_1/\mathcal{D}_0$	3.41342	2.06186	2.33863	0.19461	0.00000	0.54039	0.54039	-3.90625	0.35997
	$\mathcal{B}_0/\mathcal{D}_0$	0.00016	0.00389	-0.00383	-0.00097	0.00000	-0.00045	-0.00045	0.02148	0.00000
Values obtained at 1.5 K										
B (T)		Band 1	Band 2	Band 3	Band 4	Band 5	Band 6	Band 7	Band 8	Band 9
1	$\mathcal{A}_1/\mathcal{D}_0$	3.41342	2.06186	2.33863	0.19461	0.00000	0.54039	0.54039	-3.90625	0.35997
	$\mathcal{B}_0/\mathcal{D}_0$	0.00016	0.00389	-0.00383	-0.00097	0.00000	-0.00045	-0.00045	0.02148	0.00000
2	$\mathcal{A}_1/\mathcal{D}_0$	3.35761	2.06186	2.35734	0.19461	0.00000	0.543323	0.05827	-7.8125	0.28797
	$\mathcal{B}_0/\mathcal{D}_0$	0.00024	0.00437	-0.00321	0.00000	0.00000	-0.00037	0.00049	0.01738	0.00000
3	$\mathcal{A}_1/\mathcal{D}_0$	3.35761	2.06186	2.06186	0.19461	0.00000	0.54332	0.05827	-3.90625	0.43196
	$\mathcal{B}_0/\mathcal{D}_0$	0.00024	0.00437	0.00437	0.00000	0.00000	-0.00037	0.00074	0.02519	0.00000
4	$\mathcal{A}_1/\mathcal{D}_0$	3.35761	2.06186	2.34284	0.19461	0.00000	0.54332	0.05827	-3.90625	0.35997
	$\mathcal{B}_0/\mathcal{D}_0$	0.00080	0.00437	-0.00301	0.00000	0.00000	-0.00037	0.00074	0.02519	0.00000
5	$\mathcal{A}_1/\mathcal{D}_0$	3.35761	2.06186	2.34284	0.19461	0.00000	0.54332	0.05827	-3.90625	0.35997
	$\mathcal{B}_0/\mathcal{D}_0$	0.00080	0.00437	-0.00301	0.00000	0.00000	-0.00037	0.00099	0.02556	0.00000
6	$\mathcal{A}_1/\mathcal{D}_0$	3.35762	2.06186	2.34284	0.19461	0.00000	0.54332	0.05827	-3.90625	0.35997
	$\mathcal{B}_0/\mathcal{D}_0$	0.00080	0.00433	-0.00301	0.00000	0.00000	-0.00037	0.00099	0.02148	0.00000

Table S2-1. Parameters of B and Q bands determined by the band deconvolution of absorption and MCD spectra of [Y(TPP)Crown]Cl incorporated into PMMA.

		Q band						B band			
		Band 1	Band 2	Band 3	Band 4	Band 5	Band 6	Band 7	Band 8	Band 9	Band 10
$E_0\,(cm^{-1})^{\xi}$		16890	17130	17790	18045	18320	19540	23305	23650	23975	24400
$\Gamma\,(cm^{-1})^{\xi}$		400	350	335	370	575	990	400	477	410	800
η^{ξ}		0.79	0.55	0.89	0.51	0.71	0.60	0.10	0.50	0.78	0.13
D_0		0.29	0.15	0.17	0.48	1.38	0.26	1.05	7.64	23.02	4.00
Values obtained under 1 T											
T (K)		Band 1	Band 2	Band 3	Band 4	Band 5	Band 6	Band 7	Band 8	Band 9	Band 10
100	$\mathcal{A}_1/\mathcal{D}_0$	3.43126	2.06379	1.43374	2.15542	1.44822	0.00000	1.09227	0.55465	0.58564	-0.50000
	$\mathcal{B}_0/\mathcal{D}_0$	-0.00259	0.00884	0.00584	0.00000	0.00058	0.00000	0.00287	-0.00200	0.00037	-0.00025
1.5	$\mathcal{A}_1/\mathcal{D}_0$	3.49975	2.41429	1.43374	2.15542	1.43374	0.00000	1.76561	0.55465	0.60677	-0.5
	$\mathcal{B}_0/\mathcal{D}_0$	-0.00293	0.00816	0.00000	0.00055	0.00066	0.00000	0.00494	-0.00200	0.00038	-0.00025
Values obtained at 1.5 K											
B (T)		Band 1	Band 2	Band 3	Band 4	Band 5	Band 6	Band 7	Band 8	Band 9	Band 10
1	$\mathcal{A}_1/\mathcal{D}_0$	3.49975	2.41429	1.43374	2.15542	1.43374	0.00000	1.76561	0.55465	0.60677	-0.50000
	$\mathcal{B}_0/\mathcal{D}_0$	-0.00293	0.00816	0.00000	0.00055	0.00066	0.00000	0.00494	-0.00200	0.00038	-0.00025
2	$\mathcal{A}_1/\mathcal{D}_0$	3.49975	2.41429	1.43374	2.15542	1.43374	0.00000	1.43085	0.55465	0.60465	-0.50000
	$\mathcal{B}_0/\mathcal{D}_0$	-0.00293	0.00816	0.00000	0.00055	0.00066	0.00000	0.00430	-0.00200	0.00048	-0.00025
3	$\mathcal{A}_1/\mathcal{D}_0$	3.49975	2.41429	1.43374	2.15542	1.43374	0.00000	1.44424	0.55465	0.60465	-0.50000
	$\mathcal{B}_0/\mathcal{D}_0$	-0.00201	0.00816	0.00000	0.00055	0.00066	0.00000	0.00316	-0.00200	0.00036	-0.00025
4	$\mathcal{A}_1/\mathcal{D}_0$	3.49975	2.41429	1.43374	2.15542	1.43374	0.00000	1.20513	0.55465	0.60465	-0.50000
	$\mathcal{B}_0/\mathcal{D}_0$	-0.00201	0.00816	0.00000	0.00055	0.00066	0.00000	0.00287	-0.00200	0.00041	-0.00025
5	$\mathcal{A}_1/\mathcal{D}_0$	3.49975	2.41429	1.43374	2.15542	1.43374	0.00000	1.49742	0.55465	0.60465	-0.50000
	$\mathcal{B}_0/\mathcal{D}_0$	-0.00201	0.00748	0.00000	0.00055	0.00066	0.00000	0.00434	-0.00200	0.00043	-0.00025
6	$\mathcal{A}_1/\mathcal{D}_0$	3.49975	2.41429	2.15542	1.43374	1.43374	0.00000	1.28739	0.55465	0.60465	-0.50000
	$\mathcal{B}_0/\mathcal{D}_0$	-0.00201	0.00748	0.00031	0.00000	0.00066	0.00000	0.00191	-0.00200	0.00037	-0.00025

Table S2-2. Parameters of B and Q bands determined by the band deconvolution of absorption and MCD spectra of [Y(TPP)Azacrown]Cl incorporated into PMMA.

		Q band					B band			
		Band 1	Band 2	Band 3	Band 4	Band 5	Band 6	Band 7	Band 8	Band 9
$E_0\ (cm^{-1})^{\xi}$		16935	17810	18060	18330	19450	23522	23905	24200	24710
$\Gamma\ (cm^{-1})^{\xi}$		463	410	340	580	700	431	353	500	840
η^{ξ}		0.78	0.86	0.32	0.41	0.90	0.08	0.00	0.00	0.3
D_0		0.49	0.39	0.57	0.95	0.20	24.51	3.15	0.76	4.88
Values obtained under 1 T										
T (K)		Band 1	Band 2	Band 3	Band 4	Band 5	Band 6	Band 7	Band 8	Band 9
100	$\mathcal{A}_1/\mathcal{D}_0$	4.17493	4.12796	3.30086	0.22681	0.00000	0.66040	0.31723	-3.07275	0.20501
	$\mathcal{B}_0/\mathcal{D}_0$	0.00000	0.01565	-0.00763	-0.00311	0.00000	0.00075	-0.00317	0.01568	0.00000
1.5	$\mathcal{A}_1/\mathcal{D}_0$	19.33305	14.25014	13.23885	-1.0543	0.00000	3.14332	1.26895	-13.22751	0.20501
	$\mathcal{B}_0/\mathcal{D}_0$	-0.01511	0.02982	-0.03296	-0.00297	0.00000	-0.00403	-0.01972	0.01323	0.00000 0
Values obtained at 1.5 K										
B (T)		Band 1	Band 2	Band 3	Band 4	Band 5	Band 6	Band 7	Band 8	Band 9
1	$\mathcal{A}_1/\mathcal{D}_0$	19.33305	14.25014	13.23885	-1.0543	0.00000	3.14332	1.26895	-13.22751	0.20501
	$\mathcal{B}_0/\mathcal{D}_0$	-0.01511	0.02982	-0.03296	-0.00297	0.00000	-0.00403	-0.01972	0.01323	0.00000
2	$\mathcal{A}_1/\mathcal{D}_0$	12.33618	9.20003	8.52986	-1.05429	0.00000	1.96002	-0.11103	1.32275	-0.41002
	$\mathcal{B}_0/\mathcal{D}_0$	-0.00832	0.02983	-0.02419	-0.00297	0.00000	-0.00235	-0.00415	0.02622	0.00000
3	$\mathcal{A}_1/\mathcal{D}_0$	9.134167	7.89442	6.85377	-1.05429	0.00000	1.44031	-0.11103	-1.32275	-0.41002
	$\mathcal{B}_0/\mathcal{D}_0$	-0.00491	0.02858	-0.01995	-0.00297	0.00000	-0.00162	-0.00101	0.02411	0.00000
4	$\mathcal{A}_1/\mathcal{D}_0$	7.78777	5.36936	5.59515	-1.05429	0.00000	1.23627	-0.11103	-2.64550	-0.41002
	$\mathcal{B}_0/\mathcal{D}_0$	-0.00457	0.01848	-0.01427	-0.00297	0.00000	-0.00130	-0.00101	0.01719	0.00000
5	$\mathcal{A}_1/\mathcal{D}_0$	7.09438	5.36936	5.06911	-1.05429	0.00000	1.11384	-0.11103	-2.64550	-0.41002
	$\mathcal{B}_0/\mathcal{D}_0$	-0.00375	0.01776	-0.01469	-0.00125	0.00000	-0.00095	-0.00101	0.01719	0.00000
6	$\mathcal{A}_1/\mathcal{D}_0$	6.48245	5.36936	4.54305	-1.05429	0.00000	1.03223	-0.11103	-1.32275	-0.41002
	$\mathcal{B}_0/\mathcal{D}_0$	-0.00242	0.01776	-0.01469	-0.00125	0.00000	-0.00081	-0.00101	0.01362	0.00000

Table S2-3. Parameters of B and Q bands determined by the band deconvolution of absorption and MCD spectra of [Tb(TPP)Crown]Cl incorporated into PMMA.

		Q band						B band			
		Band 1	Band 2	Band 3	Band 4	Band 5	Band 6	Band 7	Band 8	Band 9	Band 10
$E_0\,(cm^{-1})^{\xi}$		16920	17380	17850	18070	18310	19420	23100	23542	23945	24720
$\Gamma\,(cm^{-1})^{\xi}$		474	1000	465	345	614	770	500	430	450	840
η^{ξ}		0.78	0.10	0.03	0.25	0.28	0.83	0.00	0.08	0.10	0.27
D_0		0.49	0.09	0.39	0.42	0.98	0.27	1.00	24.15	3.65	4.08
Values obtained under 1 T											
T (K)		Band 1	Band 2	Band 3	Band 4	Band 5	Band 6	Band 7	Band 8	Band 9	Band 10
100	$\mathcal{A}_1/\mathcal{D}_0$	4.58032	0.00000	4.51085	4.21337	0.00000	0.00000	0.50000	0.62048	0.09404	0.02452
	$\mathcal{B}_0/\mathcal{D}_0$	0.00238	0.00000	0.01693	-0.01639	-0.00119	0.00000	-0.00400	-0.00034	0.50000	0.00000
1.5	$\mathcal{A}_1/\mathcal{D}_0$	24.18027	0.00000	9.78821	17.10965	0.00000	0.00000	1.00000	3.68446	0.27375	-2.35715
	$\mathcal{B}_0/\mathcal{D}_0$	-0.01136	0.00000	0.01440	-0.02833	-0.00119	0.00000	0.00700	-0.00556	1.00000	0.00785
Values obtained at 1.5 K											
B (T)		Band 1	Band 2	Band 3	Band 4	Band 5	Band 6	Band 7	Band 8	Band 9	Band 10
1	$\mathcal{A}_1/\mathcal{D}_0$	24.18027	0.00000	9.78821	17.10965	0.00000	0.00000	1.00000	3.68446	0.27375	-2.35715
	$\mathcal{B}_0/\mathcal{D}_0$	-0.01136	0.00000	0.01440	-0.02833	-0.00119	0.00000	0.00700	-0.00556	1.00000	0.00785
2	$\mathcal{A}_1/\mathcal{D}_0$	14.59789	0.00000	7.26315	10.99485	0.00000	0.00000	0.00000	2.20465	0.18459	-0.39531
	$\mathcal{B}_0/\mathcal{D}_0$	0.004715335	0.00000	0.01440	-0.01888	-0.00184	0.00000	-0.00600	-0.00271	0.00000	0.00245
3	$\mathcal{A}_1/\mathcal{D}_0$	10.93451	0.00000	5.77642	8.65523	0.00000	0.00000	0.00000	1.66635	0.20345	-0.39531
	$\mathcal{B}_0/\mathcal{D}_0$	-0.00228	0.00000	0.01440	-0.01725	-0.00184	0.00000	-0.00600	-0.00193	0.00000	0.00245
4	$\mathcal{A}_1/\mathcal{D}_0$	9.19401	0.00000	5.37525	7.48263	0.00000	0.00000	0.00000	1.40454	0.21899	-0.39531
	$\mathcal{B}_0/\mathcal{D}_0$	-0.00061	0.00000	0.01440	-0.01661	-0.00119	0.00000	-0.00600	-0.00151	0.00000	0.00245
5	$\mathcal{A}_1/\mathcal{D}_0$	8.12400	0.00000	5.08262	6.84545	0.00000	0.00000	0.00000	1.25295	0.16425	-0.39531
	$\mathcal{B}_0/\mathcal{D}_0$	0.00069	0.00000	0.01440	-0.01661	-0.00119	0.00000	-0.00600	-0.00118	0.00000	0.00245
6	$\mathcal{A}_1/\mathcal{D}_0$	7.42056	0.00000	4.83012	6.41835	0.00000	0.00000	0.00000	1.15609	0.13687	-0.39531
	$\mathcal{B}_0/\mathcal{D}_0$	0.00131	0.00000	0.01440	-0.01661	-0.00119	0.00000	-0.00600	-0.00103	0.00000	0.00245

Table S2-4. Parameters of B and Q bands determined by the band deconvolution of absorption and MCD spectra of [Tb(TPP)Azacrown]Cl incorporated into PMMA.

		Q band					B band			
		Band 1	Band 2	Band 3	Band 4	Band 5	Band 6	Band 7	Band 8	Band 9
$E_0\,(cm^{-1})^{\xi}$		16940	17820	18075	18380	19520	23522	23905	24200	24700
$\Gamma\,(cm^{-1})^{\xi}$		492	420	393	555	670	431	313	500	960
η^{ξ}		0.622	0.76	0.22	0.86	0.67	0.08	0.00	0.00	0.30
$\mathcal{D}_0$		0.45	0.33	0.69	1.07	0.16	22.51	2.52	0.26	3.19
Values obtained under 1 T										
T (K)		Band 1	Band 2	Band 3	Band 4	Band 5	Band 6	Band 7	Band 8	Band 9
100	$\mathcal{A}_1/\mathcal{D}_0$	3.48136	2.65953	2.23240	0.10506	0.00000	0.29685	0.13878	0.78125	0.31369
	$\mathcal{B}_0/\mathcal{D}_0$	0.00078	0.01335	-0.00464	-0.00162	0.00000	-0.00008	0.00000	0.00000	-0.00314
1.5	$\mathcal{A}_1/\mathcal{D}_0$	2.33216	1.99032	1.47701	-0.40669	0.00000	-8.88516	-1.76705	38.28125	1.50575
	$\mathcal{B}_0/\mathcal{D}_0$	0.00894	0.01489	-0.00127	-0.00316	0.00000	-0.00027	0.00564	-0.19375	-0.00627
Values obtained at 1.5 K										
B (T)		Band 1	Band 2	Band 3	Band 4	Band 5	Band 6	Band 7	Band 8	Band 9
1	$\mathcal{A}_1/\mathcal{D}_0$	2.33216	1.99031	1.47701	-0.40669	0.00000	-8.88516	-1.76705	38.28125	1.50575
	$\mathcal{B}_0/\mathcal{D}_0$	0.00894	0.01183	-0.00117	-0.00316	0.00000	-0.00027	0.00564	-0.19375	-0.00627
2	$\mathcal{A}_1/\mathcal{D}_0$	2.91004	2.32836	1.84483	0.29289	0.00000	-4.23276	-0.97145	31.25000	1.50575
	$\mathcal{B}_0/\mathcal{D}_0$	0.00551	0.01335	-0.00222	-0.00111	0.00000	0.00022	-0.00075	-0.10156	-0.00627
3	$\mathcal{A}_1/\mathcal{D}_0$	3.13301	2.17965	1.98731	0.29289	0.00000	-2.58865	-0.49064	19.53125	1.50575
	$\mathcal{B}_0/\mathcal{D}_0$	0.00372	0.01335	-0.00265	-0.00112	0.00000	-0.00008	-0.00075	-0.06250	-0.00627
4	$\mathcal{A}_1/\mathcal{D}_0$	3.236581	2.63255	2.06046	0.29289	0.00000	-1.81296	-0.57493	16.40625	1.50575
	$\mathcal{B}_0/\mathcal{D}_0$	0.003728	0.01395	-0.00391	-0.00111	0.00000	-0.00008	-0.00075	-0.01953	-0.00627
5	$\mathcal{A}_1/\mathcal{D}_0$	3.27301	2.48385	2.08872	0.29289	0.00000	-1.30729	-0.33703	15.625	1.50575
	$\mathcal{B}_0/\mathcal{D}_0$	0.00275	0.01335	-0.00392	-0.00111	0.00000	-0.000003	-0.00075	-0.015625	-0.00627
6	$\mathcal{A}_1/\mathcal{D}_0$	3.33468	2.48385	2.11017	0.29289	0.00000	-0.99065	-0.13877	11.71875	1.56848
	$\mathcal{B}_0/\mathcal{D}_0$	0.00227	0.01228	-0.00392	-0.00111	0.00000	-0.00003	-0.00075	-0.01172	-0.00627

Table S2-5. Parameters of B and Q bands determined by the band deconvolution of absorption and MCD spectra of [Dy(TPP)Crown]Cl incorporated into PMMA.

		Q band						B band			
		Band 1	Band 2	Band 3	Band 4	Band 5	Band 6	Band 7	Band 8	Band 9	Band 10
$E_0\,(cm^{-1})^{\xi}$		16820	17135	18035	18275	18510	19650	23580	23902	24400	24900
$\Gamma\,(cm^{-1})^{\xi}$		280	400	485	320	460	780	613	431	400	1000
η^{ξ}		0.10	0.19	0.69	0.52	0.85	0.68	0.00	0.08	0.00	0.30
$\mathcal{D}_0$		0.08	0.29	0.87	0.49	0.80	0.19	11.52	23.20	2.55	4.98
Values obtained under 1 T											
T (K)		Band 1	Band 2	Band 3	Band 4	Band 5	Band 6	Band 7	Band 8	Band 9	Band 10
100	$\mathcal{A}_1/\mathcal{D}_0$	3.00521	2.95580	1.47102	0.83642	-0.24924	0.00000	0.21320	0.03500	0.01262	-0.20089
	$\mathcal{B}_0/\mathcal{D}_0$	0.00128	0.00339	-0.00059	0.00366	-0.00036	0.00000	-0.00038	0.00028	-0.00038	0.00000
1.5	$\mathcal{A}_1/\mathcal{D}_0$	1.31009	-6.51392	-0.28604	-4.33780	-0.30353	0.00000	-1.77543	-12.68273	-3.53496	0.96428
	$\mathcal{B}_0/\mathcal{D}_0$	-0.02752	0.01379	-0.00265	0.00152	0.00791	0.00000	0.02592	-0.00940	-0.02570	-0.00402
Values obtained at 1.5 K											
B (T)		Band 1	Band 2	Band 3	Band 4	Band 5	Band 6	Band 7	Band 8	Band 9	Band 10
1	$\mathcal{A}_1/\mathcal{D}_0$	1.31009	-6.51392	-0.28604	-4.33780	-0.30353	0.00000	-1.77543	-12.68273	-3.53496	0.96428
	$\mathcal{B}_0/\mathcal{D}_0$	-0.02752	0.01379	-0.00265	0.00152	0.00791	0.00000	0.02592	-0.00940	-0.02570	-0.00402
2	$\mathcal{A}_1/\mathcal{D}_0$	0.00000	-1.69781	0.45767	-1.70857	-0.52911	0.00000	-1.32789	-6.44670	-0.86410	0.96428
	$\mathcal{B}_0/\mathcal{D}_0$	-0.02402	0.01312	-0.00250	-0.00056	0.00572	0.00000	0.01003	-0.00300	-0.01283	-0.00402
3	$\mathcal{A}_1/\mathcal{D}_0$	1.44938	0.00359	0.68650	-0.81554	0.01816	0.00000	-0.59414	-4.21795	-0.47133	0.96428
	$\mathcal{B}_0/\mathcal{D}_0$	-0.01061	0.00874	-0.00300	0.00138	0.00479	0.00000	0.00712	-0.00246	-0.00851	-0.00402
4	$\mathcal{A}_1/\mathcal{D}_0$	2.73907	0.84170	0.86957	-0.35467	0.01816	0.00000	-0.21320	-3.10455	-0.39277	0.96428
	$\mathcal{B}_0/\mathcal{D}_0$	-0.00141	0.00554	-0.00253	0.00025	0.00574	0.00000	0.00314	-0.00128	-0.00715	-0.00402
5	$\mathcal{A}_1/\mathcal{D}_0$	2.95470	1.35757	1.16430	-0.07646	-0.18165	0.00000	-0.36747	-2.43808	-0.39277	0.96428
	$\mathcal{B}_0/\mathcal{D}_0$	-0.00183	0.00527	-0.00238	-0.00049	0.00561	0.00000	0.00122	-0.00055	-0.00715	-0.00402
6	$\mathcal{A}_1/\mathcal{D}_0$	2.95470	1.68305	1.37300	0.12663	-0.26741	0.00000	-0.43531	-1.95197	0.39277	0.96428
	$\mathcal{B}_0/\mathcal{D}_0$	-0.00156	0.00544	-0.00127	-0.00193	0.00564	0.00000	-0.00132	0.00054	-0.00543	-0.00402

Table S2-6. Parameters of B and Q bands determined by the band deconvolution of absorption and MCD spectra of [Dy(TPP)Azacrown]Cl incorporated into PMMA.

[Y(TPP)Crown]$^+$						
From	To	Oscillator Strength	Einstein Coefficient (sec^{-1})			Total A (sec^{-1})
			A_x	A_y	A_z	
1	2	2.79×10^{-4}	2.01×10^{2}	1.26×10^{5}	2.11×10^{2}	1.26×10^{5}
1	3	2.50×10^{-4}	1.12×10^{5}	9.88×10^{1}	6.73×10^{2}	1.13×10^{5}
1	4	5.45	3.76×10^{8}	7.78×10^{9}	5.35×10^{-1}	8.16×10^{9}
1	5	5.45	7.80×10^{9}	3.77×10^{8}	4.53×10^{2}	8.18×10^{9}
2	4	4.91×10^{-4}	1.02×10^{5}	5.34×10^{2}	4.71×10^{4}	1.49×10^{5}
2	5	4.69×10^{-4}	1.21×10^{2}	1.26×10^{5}	1.73×10^{4}	1.43×10^{5}
3	4	5.14×10^{-4}	7.06	1.39×10^{5}	1.72×10^{4}	1.56×10^{5}
3	5	4.92×10^{-4}	1.04×10^{5}	3.53×10^{1}	4.64×10^{4}	1.50×10^{5}

Table S2-7. Dipole transition strengths for [Y(TPP)Crown]$^+$ obtained from RASSCF/RASSI/single_aniso calculations.

[Y(TPP)Azacrown]$^+$						
From	To	Oscillator Strength	Einstein Coefficient (sec^{-1})			Total A (sec^{-1})
			A_x	A_y	A_z	
1	2	2.24×10^{-3}	4.20×10^{5}	5.91×10^{5}	3.43	1.01×10^{6}
1	3	7.59×10^{-4}	8.03×10^{1}	3.44×10^{5}	4.11	3.44×10^{5}
1	4	5.44	4.78×10^{9}	3.28×10^{9}	4.05×10^{4}	8.07×10^{9}
1	5	5.44	3.30×10^{9}	4.79×10^{9}	1.61×10^{3}	8.09×10^{9}
2	4	4.61×10^{-3}	1.07×10^{6}	1.87×10^{5}	1.18×10^{5}	1.37×10^{6}
2	5	3.12×10^{-3}	7.18×10^{5}	2.07×10^{5}	8.66×10^{3}	9.34×10^{5}
3	4	1.07×10^{-3}	6.46×10^{4}	2.37×10^{5}	1.47×10^{4}	3.17×10^{5}
3	5	1.58×10^{-3}	5.34×10^{4}	3.81×10^{5}	3.74×10^{4}	4.72×10^{5}

Table S2-8. Dipole transition strengths for [Y(TPP)Azacrown]$^+$ obtained from RASSCF/RASSI/single_aniso calculations.

[Tb(TPP)Crown]$^{+}$						
From	To	Oscillator Strength	Einstein Coefficient (sec^{-1})			Total A (sec^{-1})
			A_x	A_y	A_z	
1	214	3.68×10^{-3}	1.36×10^{6}	2.94×10^{5}	1.33×10^{-9}	1.65×10^{6}
1	215	3.68×10^{-3}	2.94×10^{5}	1.36×10^{6}	5.01×10^{-9}	1.65×10^{6}
1	216	3.53×10^{-3}	2.55×10^{5}	1.33×10^{6}	7.20×10^{-9}	1.59×10^{6}
1	217	3.53×10^{-3}	1.33×10^{6}	2.55×10^{5}	5.61×10^{-9}	1.59×10^{6}
1	508	2.92	2.40×10^{9}	2.13×10^{-9}	1.83×10^{-7}	4.53×10^{9}
1	509	2.92	2.13×10^{9}	2.40×10^{-9}	7.96×10^{-9}	4.53×10^{9}
1	510	2.79	9.45×10^{7}	4.24×10^{-9}	7.60×10^{-8}	4.34×10^{9}
1	511	2.79	4.24×10^{9}	9.46×10^{7}	3.86×10^{-9}	4.34×10^{9}

Table S2-9. Dipole transition strengths for [Tb(TPP)Crown]$^{+}$ obtained from RASSCF/RASSI/single_aniso calculations.

Chapter 3

Investigation of J-L Interaction in Excited States of lanthanide-porphyrin with Schiff-base Ligand by Using Magnetic Circular Dichroism

3.1 Introduction

The use of spectroscopy analysis to study electronic structures in porphyrin research has been expanding not limited to symmetrical porphyrin, but also to asymmetrical porphyrin and different axial ligation in metalated-porphyrin. The study by Nemykin and Hadt[1], symmetries of porphyrin were studied using *meso*(Ferrocenyl)-Porphyrins showed that tuned-symmetry due to the existence of the *meso*-substituents did not change spectra pattern where B and Q band absorbtion was still detected. Moreover, the ferrocenyl substituents also has contribution in HOMO-LUMO electronic transition where HOMO orbitals became predominantly iron-centered molecular orbitals. In other report[2,3], asymmetric porphyrins were studied with N-confused porphyrin or inverted porphyrin and MCD spectroscopy was proven to be able to distinguish the compound from normal porphyrin where MCD did not exhibit any A-term spectra corresponding to B-band spectra as in normal porphyrin and B-term profile was detected due to the mixing of excited states. By Fathi-Rasekh et al.[4], MCD instrument was used to examine Ru-tetraphenylporphyrin which was axially substituted with 2-isocyanoazulene and 6-isocyanoazulene. It was concluded that spectra profile indicated the appearance of B and Q band absorbtion with small difference. However, complex with 6-isocyanoazulene possessed more stabilized molecular orbital compared to its counterpart. According to the research report by Ma et al.[5], lanthanide-porphyrin heteroleptic could maintain the square-antiprismatic structure when lanthanide-porphyrin had a Schiff-base ligand on its axial position with 2 N atoms and 2 O atoms of the ligand binding lanthanide ion, yielding a sandwich-like structure. However, no MCD analysis was performed in that report.

Schiff-base ligands are prepared by condensation reaction between 1,2-diammines with salicylaldehydes or salicylaldehyde derivatives. As a tetradentate ligand, Schiff-base ligands are able to coordinate metals via immine nitrogen and hydroxyl group. One of the ligands is Salen which is widely known due to its facile synthesis and it resembles to

porphyrin[6]. Salen-metal complexes have been long studied due to the fast reaction between the ligand and metals. According to single-crystal x-ray diffraction, the hydroxyl functional groups deprotonated to bind metal and therefore complexes could be easily yielded[7-9]. Such results were also observed in lanthanide metals and it is worth noting that Salen-lanthanide complexes exhibit magnetic and optical properties which make Salen-lanthanides possible to be more widely functionalized[10-13].

In this chapter, **J–L** interaction in [Ln(TPP)Salen]Cl with Ln = Tb, Dy, and Y is going to investigated. Theoretically, Salen is expected to lead the molecular system to have smaller symmetry relatively compared to cyclododecane ligands. The distortion is not only brought by the presence of two phenyl rings but also by two hydroxyl and amine groups on the tetradentate site. Salen is also chosen due to its facile preparation and therefore more efficient to investigate for introducing less asymmetric organic moiety for the purpose of this research.

3.2 Experimental Methods

3.2.1 Materials and Synthesis

Salen ligand was synthesized with reaction between salicyladehyde and ethylenediamine[6] with 2 mL of salicylaldehyde was dissolved in 10 mL in ethanol. Separately, 1 mL of ethylenediammine was dissolved in 10 mL of ethanol. Salicylaldehyde in ethanol was added into ethylenediammine in ethanol by droplets with vigorous stirring. After approximately 10 minutes, yellow powder of salen appeared in the solution and the mixture was filtered in order to isolate the compound. This powder was later dried overnight and analyzed with proton nuclear magnetic resonance (H-NMR), mass spectroscopy, and elemental analysis.

The salen complexes were synthesized by referring to previous publication[14] with replacing cyclen with salen accompanied with KOH to make the bonding between salen and lanthanide-porphyrin easier. All complexes were named as [Y(TPP)Salen]Cl, [Tb(TPP)Salen]Cl, and [Dy(TPP)Salen]Cl. For the instrumental analysis, ^{1}H-NMR spectra of the complexes were measured in deuterated chloroform, $CDCl_3$, solution at 25 °C with tetramethylsylane (TMS) or $(CH_3)_4Si$, as an internal standard by using a JEOL Lambda-500 NMR spectrometer. Absorption spectra were measured by using a Thermo Scientific Evolution 220 UV-Visible spectrophotometer. For elemental analysis (C, H, and N), the analysis was done with a Yanaco CHN Corder MT-5 and MT-6 Elemental Analyzer.

Mass spectra were measured using a Kratos PC Axima CFR V.2.3.5 (Shimadzu Corporation) operated in reflectron mode. For room temperature MCD, MCD measurements were performed at 298 K for solution samples under permanent magnet of 1.6 T while for VT-VH-MCD analysis, samples were incorporated into PMMA films and measurements were performed at varying temperatures from 100 to 1.5 K and with magnetic field range of 0−6 T using a JASCO J-720W spectrodichrometer equipped with an Oxford Instruments SM4000 Spectromag cryostat.

For salen, the formation of salen was confirmed by ^{1}H-NMR with δ 13.17 ppm (s 2H hydroxyl), 8.35 ppm (s 2H –N=CH), 3.93 ppm (s 4H ethylene bridge) and in the unit (m/z), the cation peak was found to be 267.87. The purity of the obtained ligand was confirmed by elemental analysis (found percentage C: 71.62 H: 5.96 N: 10.44, calculated C: 71.59 H: 6.10 N: 10.42). The cationic peaks were found to be m/z equal 1046.63, 116.93, and 1119.04 that are respectively corresponding to $[Y(TPP)SalenK_2]^+$, $[Tb(TPP)SalenK_2]^+$, and $[Dy(TPP)SalenK_2]^+$. Elemental analysis of C, H, and N gave experimental results in percentage as C:67.20, H: 5.64, N: 9.48 (calcd. C: 67.21, H: 5.56, N: 9.64) for [Y(TPP)Salen]Cl. For [Tb(TPP)Salen]Cl, C: 48.34, H: 4.28, N: 6.32 (calculated C: 48.33, H: 4.38, N: 6.34). For [Dy(TPP)Salen]Cl, C: 50.12, H: 4.61, N: 6.50 (calculated C: 50.17, H: 4.77, N: 6.45).

3.2.2 Principles of MCD Measurements

The absorption and MCD spectra were measured at different temperatures and magnetic field and analysed quantitatively as $\mathcal{A}_1/\mathcal{D}_0$ ratio where $\mathcal{A}_1$ denotes the A-term intensity and $\mathcal{D}_0$ corresponds to the oscillator strength of the band. The $\mathcal{A}_1/\mathcal{D}_0$ values were obtained by fitting of the spectra shape to the following equation[15]

$$\frac{\Delta A}{E} = \gamma \mu_{Bohr} B \left[\mathcal{A}_1 \left(\frac{-\delta f(E)}{\delta E} \right) + \left(\mathcal{B}_0 + \frac{\mathcal{C}_0}{k_B T} \right) f(E) \right]$$

$$\frac{A}{E} = \gamma D_0 f(E)$$

Here, ΔA is the difference between absorbance of left and right circularly polarized light, lcp and rcp, in a magnetic field, E is energy in cm^{-1}, B is the magnetic field in tesla (T), μ_{Bohr} is Bohr magneton (magnetic moment), γ = 326.5cl (c = concentration in mol/L, l is path length which in this case is thickness of sample film in cm), $\mathcal{A}_1$ is MCD A-term, $\mathcal{B}_0$ is MCD B-term, $\mathcal{C}_0$ is MCD C-term, $\mathcal{D}_0$ is oscillator strength, and $f(E)$ is the band shape function[16].

However, the temperature and the magnetic field of $\boldsymbol{\mathcal{A}_1/\mathcal{D}_0}$ ratio can be explained using theoretical model that previously has been explained in other works[17-21]. In PMMA matrix, sample is expected same absorbance spectra as in dichloromethane solvent. Zeeman energy of **J** and **L** have a component of θ because the z axis of the molecule in the matrix is assumed to be randomly distributed in the range from 0 to 90° and the relations can be stated with $g_J\mu_B J_z B\cos\theta$ and $g_J\mu_B L_z B\cos\theta$ respectively. Here, θ is the angle between the direction of the magnetic field B and the z axis. The transition moments from ground states to the π–π* excited states at θ = 0 are represented by the equations below.

$$\left|\langle\alpha|\hat{m}_{\pm1}|\alpha\ \mp\rangle\right|^2 = \left|\langle\alpha\ \pm|\hat{m}_{\pm1}|\alpha\rangle\right|^2 \equiv M^2$$

$$\left|\langle\alpha|\hat{m}_{\pm1}|\alpha\ \pm\rangle\right|^2 = \left|\langle\alpha\ \mp|\hat{m}_{\pm1}|\alpha\rangle\right|^2 \equiv 0$$

$$\hat{m}_{\pm1} = \mp\left(\frac{1}{\sqrt{2}}\right)\left(\hat{m}_x \pm i\hat{m}_y\right)$$

with α is either + or -, $\hat{m}_{\pm1}$ is the transition moment operator defined by Piepho and Schatz[15]. The spatially averaged $\mathcal{D}_0$ related with M is formulated below.

$$\mathcal{D}_0 = \left(\frac{1}{3}\right)\mathcal{D}_0\,(\theta = 0) = \left(\frac{2}{3}\right)M^2$$

When $\theta \neq 0$ the equation will be

$$|\langle\alpha|\hat{m}_{-1}|\alpha\ \mp\rangle_\theta|^2 = |\langle\alpha\,|\hat{m}_{+1}|\alpha\ \mp\rangle_\theta|^2 = \frac{(M^2(1\ \pm\cos\theta)^2)}{4}$$

Also, there is a transition from $|\alpha\rangle$ to $|\alpha,\pm\rangle$ whose energy is shifted by Zeeman term and by interaction between **J** and **L** denoted as $\Delta_{\mathbf{JL}}$. These can be represented as

$$\mu_{Bohr}B\langle\alpha\lambda|L_z|\alpha\lambda\rangle\cos\theta + \delta_{\alpha\lambda}\Delta_{JL}$$

where α and λ are either $+$ or $-$ and

$$\delta_{\alpha\lambda} = \begin{cases}+1, & \text{for } \alpha \neq \lambda\\ -1, & \text{for } \alpha = \lambda\end{cases}$$

By including the thermal population to the ground states, $\mathcal{A}_1(\theta)$ thus will be written as following

$$\mathcal{A}_1(\theta) = \sum_{\alpha=-,+}\{\sum_{\lambda=-,+}\left(\langle\alpha\lambda|L_z|\alpha\lambda\rangle\cos\theta + \frac{\delta_{\alpha\lambda}\Delta_{JL}}{\mu_{Bohr}B}\right)\times(|\langle\alpha|\hat{m}_{-1}|\alpha\lambda\rangle|^2 - |\langle\alpha\,|\hat{m}_{+1}|\alpha\lambda\rangle|^2)\cos\theta\}\times\frac{\exp\left(\frac{-g_J\mu_{Bohr}\langle\alpha|J_z|\alpha\rangle B\cos\theta}{k_BT}\right)}{\sum_{\alpha=-,+}exp\left(\frac{-g_J\mu_{Bohr}\langle\alpha|J_z|\alpha\rangle B\cos\theta}{k_BT}\right)}$$

Both **J** and **L** have components along z-axis which each is symbolized as J_z and L_z. There are six states which are assumed to be diagonal in $\hat{J}_z$ and $\hat{L}_z$ and are non-zero matrix elements for the angular momentum operators are

$$\langle -|\hat{J}_z|-\rangle = \langle -+|\hat{J}_z|-+\rangle = \langle --|\hat{J}_z|--\rangle = -|J_z|$$
$$\langle +|\hat{J}_z|+\rangle = \langle ++|\hat{J}_z|++\rangle = \langle +-|\hat{J}_z|+-\rangle = +|J_z|$$
$$\langle ++|\hat{L}_z|++\rangle = \langle -+|\hat{L}_z|-+\rangle = +|L_z|$$
$$\langle +-|\hat{L}_z|+-\rangle = \langle --|\hat{L}_z|--\rangle = -|L_z|$$

3.2.3 Computational Chemistry Calculations

The calculations were conducted using Open Molcas v 19.11 program package with the molecular structure was optimized using Gaussian09 software. The basis set ANO-RCC-VTZP was used for the metals and the other basis set ANO-RCC-MB was applied on the other atoms. The calculations also used state averaged RASSCF (restricted active space self-consistent field) wave functions and employed RASSI (restricted active space state interaction) and single_aniso calculation to get oscillator strength and spin-orbit (S.O) coupling states.

3.3 Results and Discussion

3.3.1 Analysis of [Y(TPP)Salen]Cl

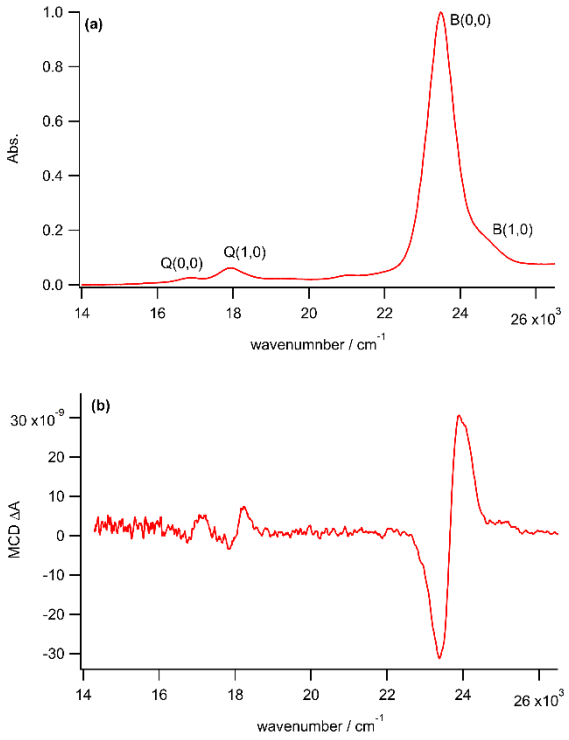

Figure 3.1 UV-vis spectra (a) and room-temperature MCD spectra under 1.6 T permanent magnet (b) of [Y(TPP)Salen]Cl in CH_2Cl_2.

As well as in the study of cyclododecane complexes in Chapter 2, analysis of [Y(TPP)Salen]Cl is necessary in investigation of lanthanide-porphyrin with salen ligand since due to its diamagnetic character, Y therefore is used as a reference in order to determine the L_z of lanthanide-porphyrin with different second ligand. The MCD spectra are plotted as ΔA MCD against wavenumber with ΔA MCD is the difference between absorbance of left circular polarized light (A_{lcp}) and right circular polarized light (A_{rcp}). A_{lcp} corresponds to the excitation to higher energy state ($+|L_z|$) and A_{rcp} corresponds to the excitation to lower energy state ($-|L_z|$) with L_z is the z-axis component of the angular momentum.

As shown in Figure 3.1(a), at room temperature, [Y(TPP)Salen]Cl indicated four bands as Q(0,0), Q(1,0), B(0,0), and B(1,0). However, contrast to [Y(TPP)Crown]Cl and [Y(TPP)Azacrown]Cl, the B(1,0) band is almost unobservable by UV-Vis spectrophotometer. In Figure 3.1(b), under 1.6 T magnetic field, the MCD spectra yielded the positive A-term bands were detected, attributed to Q(0,0), Q(1,0), and B(0,0) bands and B(1,0) did not yield any band in the MCD spectra. Specifically, in B(0,0) band that was

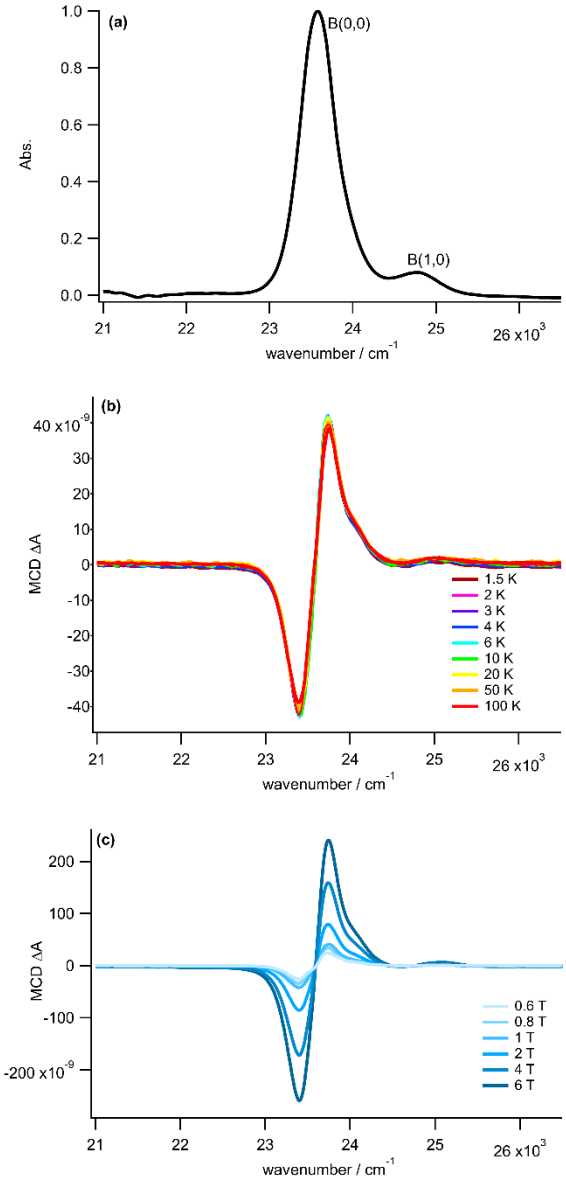

Figure 3.2 a) Absorption, (b) temperature-dependent MCD spectra measured at temperatures of 1.5-100 K under a magnetic field of 1 T, and (c) magnetic field-dependent MCD spectra measured at temperatures of 1.5 K of B band in [Y(TPP)Salen]Cl in PMMA film.

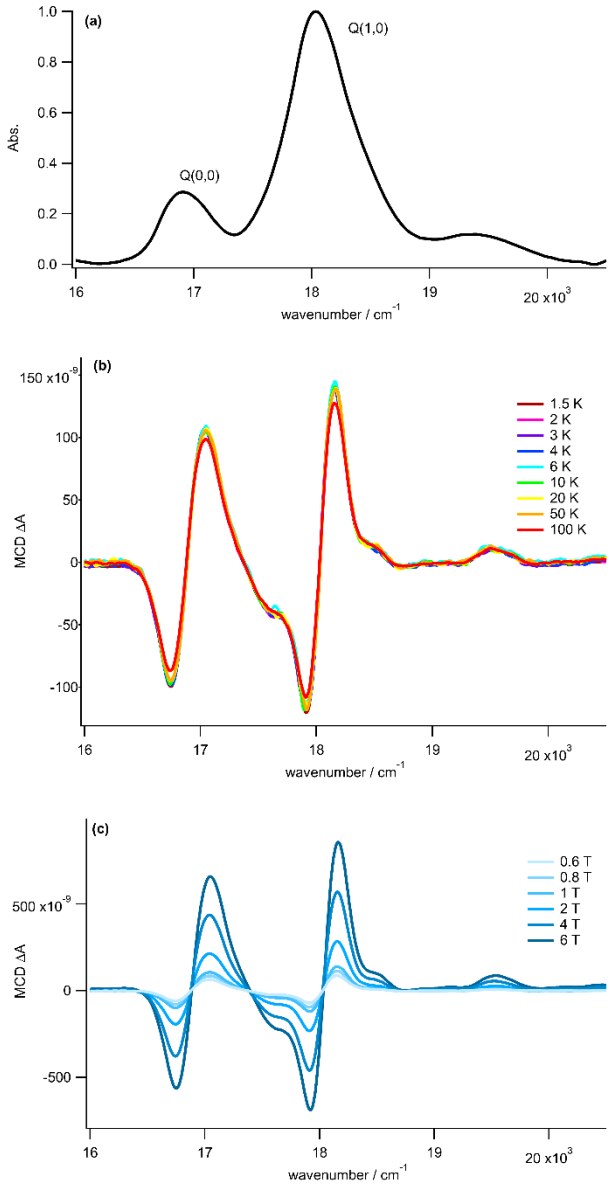

Figure 3.3 a) Absorption, (b) temperature-dependent MCD spectra measured at temperatures of 1.5-100 K under a magnetic field of 1 T, and (c) magnetic field-dependent MCD spectra measured at temperatures of 1.5 K of Q(0,0) and Q(1,0) bands in [Y(TPP)Salen]Cl in PMMA film.

detected between 22,000-26,000 cm^{-1} has an anomaly compared to that of cyclododecane complexes. Here, on the positive lobe, there are two peaks observed instead of only one, creating broken lobe. Even so, the presence of positive A-term pattern in MCD spectra of both Q and B bands at room temperature indicates that replacement of the second ligand with less did not change the degeneracy of excited states of porphyrin and this degeneracy is maintained.

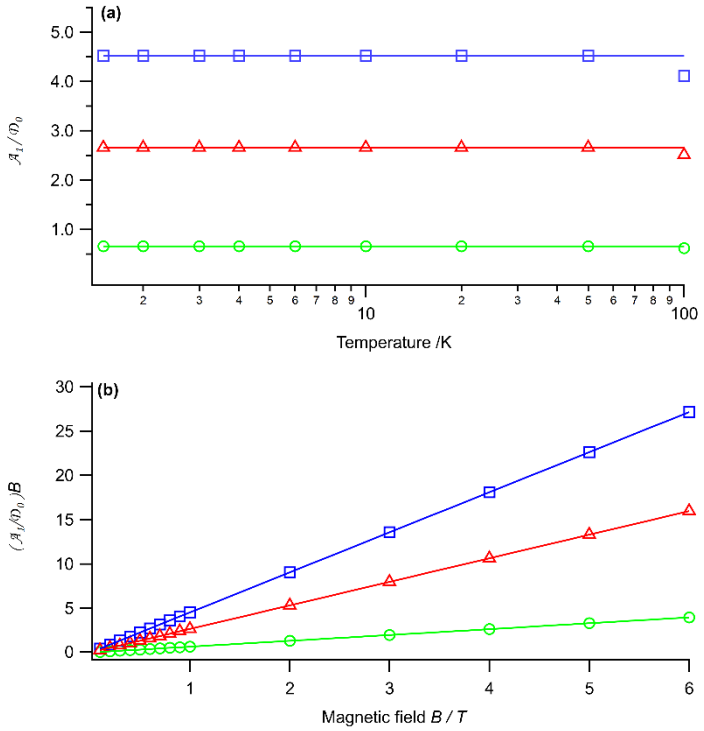

Figure 3.4 Experimental values (squares, triangles, and circles) and calculated value (straight line) of $\mathcal{A}_1/\mathcal{D}_0$ of [Y(TPP)Salen]Cl for B(0,0) in green, Q(1,0) in red, and Q(0,0) in blue under 1 T of magnetic field with varied temperature (a) and under varied magnetic field at 1.5 K.

From Figure 3.2 and Figure 3.3, VT-VH-MCD measurement demonstrated several differences compared to room temperature-MCD. In particular, in Figure 3.2(a), for B band, B(0,0) showed narrower shape between 23,000-24,500 cm^{-1} and as well as that, B(1,0) is more obviously detected between 24,500-26,000 cm^{-1}. Furthermore, B(0,0) band did not yield a distorted band as displayed in Figure 3.2(b) for temperature-dependence measurement and Figure 3.2(c) for magnetic field-dependence MCD measurement. At all temperatures from 100 K until 1.5 K, B(0,0) indicated positive A-term band with constant ΔA intensities. When the temperature was set at 1.5 K, ΔA intensity demonstrated changes with tuned magnetic field *B*. For Q(0,0) and Q(1,0) bands, temperature independence of positive A-term pattern corresponding with Q(0,0) and Q(1,0) bands was measured and is shown in Figure 3.3(b). As well as that, applied magnetic field caused ΔA intensity was varied with different field magnitudes (Figure 3.3(c)). Thus, it can be inferred that the diamagnetic character of Y was maintained with different non-aromatic ligand.

Band deconvolution gave $\mathcal{A}_1/\mathcal{D}_0$ values for all bands and they were plotted versus temperature and magnetic field as shown in Figure 3.4. For temperature dependence (Figure 3.4(a)), all bands had constant $\mathcal{A}_1/\mathcal{D}_0$ ratios which were the indication of temperature independence of [Y(TPP)Salen]Cl and thus its diamagnetic character. Under different field in Figure 3.4(b), $\mathcal{A}_1/\mathcal{D}_0$ demonstrated linear dependence with the applied magnetic field from 0.1 T to 6 T. With least-square fitting to $\mathcal{A}_1/\mathcal{D}_0$ ratios, the angular momentum denoted as L_z for each band could be determined. For B(0,0), L_z was estimated to be $0.66\hbar$ while for Q(0,0) and Q(1,0), L_z values were determined to be $4.53\hbar$ and $2.66\hbar$. The results are tabulated below in Table 3.1.

Compound	**Lz ($\hbar$)**			
	B band	**Q(0,0) band**	**Q(1,0) band**	
[Y(TPP)Salen]Cl	0.66	4.53	2.66	***a***
[Y(TPP)Crown]Cl	0.54	3.44	2.35	***a***
[Y(TPP)Azacrown]Cl	0.61	3.5	2.25	***a***
[Y(TPP)cyclen]Cl	0.66	3.59	2.61	***b***

Table 3.1 The value of L_z interaction (Δ_{JL}) of Y complexes with ***a*** is the reported work and ***b*** is cited from reference.

By comparing to L_z values of the cyclododecane complexes, it can be concluded that more asymmetric ligand did not change L_z of B band. However, L_z increased for Q(0,0) in [Y(TPP)Salen]Cl with difference approximately $1.1\hbar$ while on the other hand, L_z of Q(1,0) remained relatively constant.

3.3.2 Analysis of [Tb(TPP)Salen]Cl

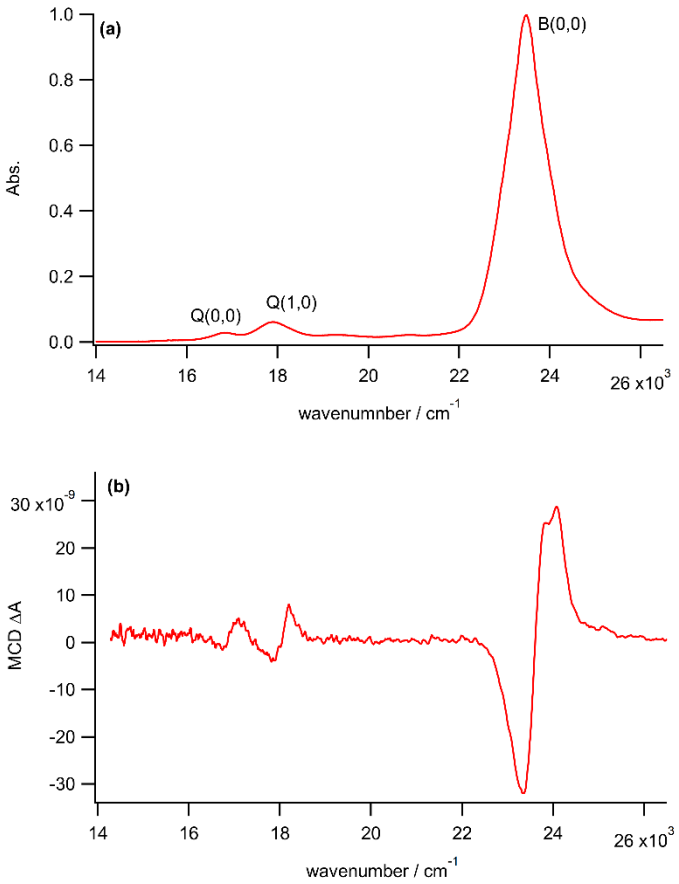

Figure 3.5 UV-vis spectra (a) and room-temperature MCD spectra under 1.6 T permanent magnet (b) of [Tb(TPP)Salen]Cl in CH_2Cl_2.

Based from the cyclododecane complexes, Tb has interesting characters due to its magnetic anisotropic character. In this section, the study of **J–L** interaction is expanded into Tb-porphyrin with salen ligand in order to examine how more distorted ligand affect the interaction within the ferromagnetic molecular system. From Figure 3.5(a), the UV-Vis spectra of [Tb(TPP)Salen]Cl yielded only Q(0,0), Q(1,0), and B(0,0) bands without any appearance of a shoulder of B(1,0) band. This is contrast to the UV-Vis spectra of [Y(TPP)Salen]Cl where four bands appeared. Furthermore, referring to Figure 3.5(b), three positive A-term bands were detected in room-temperature MCD analysis which each is attributed to Q(0,0), Q(1,0), and B(0,0) bands. In [Tb(TPP)Salen]Cl, broken positive A-term MCD band associated with B(0,0) band was observed as previously also observed in [Y(TPP)Salen]Cl. The present of three positive A-term in MCD spectra which each is

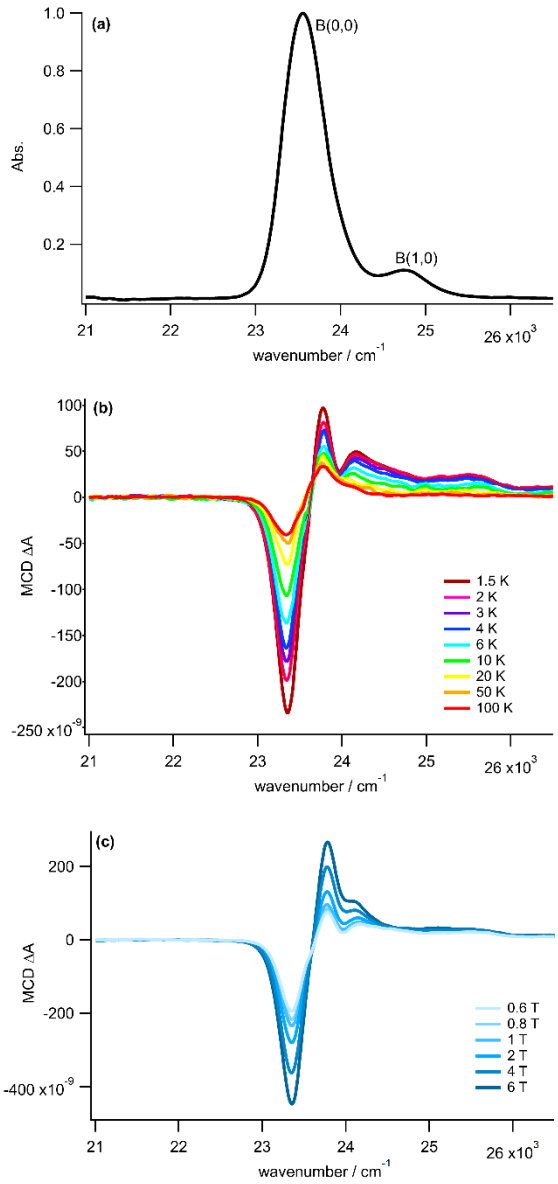

Figure 3.6 a) Absorption, (b) temperature-dependent MCD spectra measured at temperatures of 1.5-100 K under a magnetic field of 1 T, and (c) magnetic field-dependent MCD spectra measured at temperatures of 1.5 K of B band in [Tb(TPP)Salen]Cl in PMMA film.

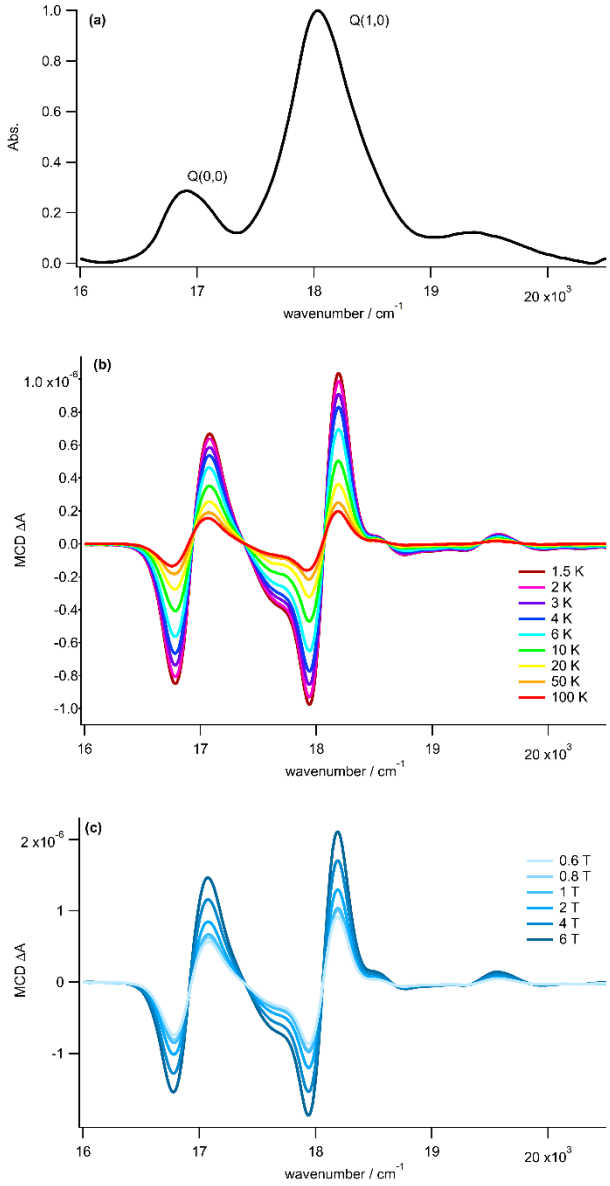

Figure 3.7 a) Absorption, (b) temperature-dependent MCD spectra measured at temperatures of 1.5-100 K under a magnetic field of 1 T, and (c) magnetic field-dependent MCD spectra measured at temperatures of 1.5 K of Q bands in [Tb(TPP)Salen]Cl in PMMA film.

assigned to the Q(0,0), Q(1,0), and B(0,0) bands indicates that salen did not change the degeneracy of the excited states within Tb-porphyrin.

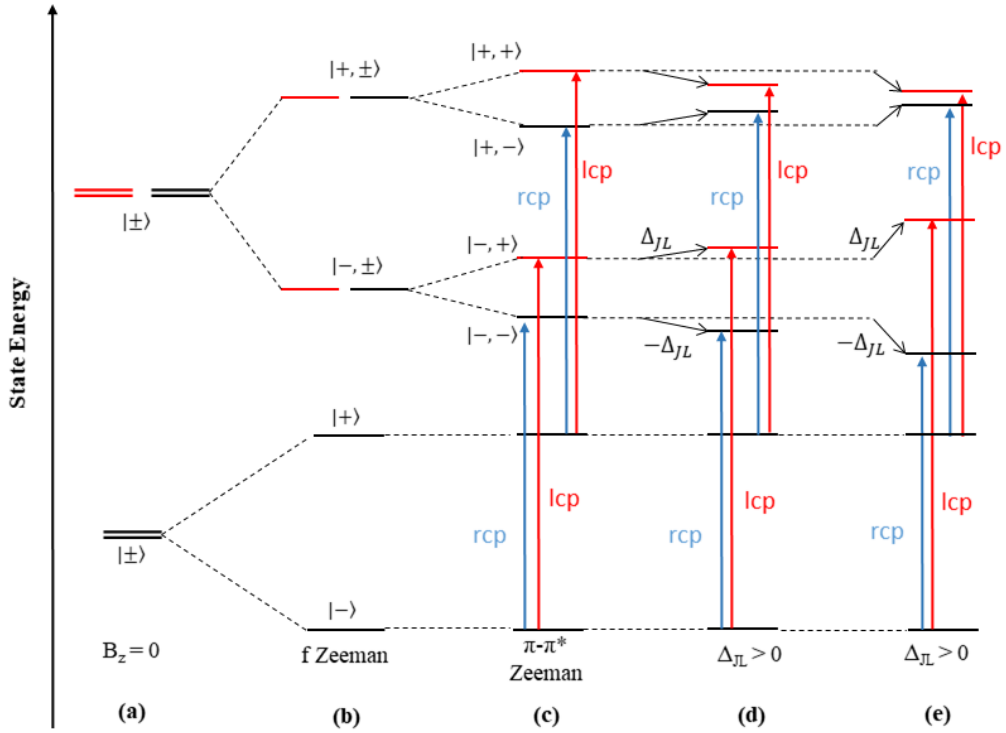

Figure 3.8 Schematic energy of the ground and the excited states of [Tb(TPP)Salen]Cl

Several distinguishing aspects were observed in VT-VH-MCD measurement and the results are presented in Figure 3.6 for B band and Figure 3.7 for Q bands. In Figure 3.6(a), the spectral shape of B band in PMMA was different than the spectral shape in solution where B(0,0) was narrower and B(1,0) shoulder was detected in the range between 24,500-26,000 cm^{-1}. Moreover, in Figure 3.6(b), positive A-term profile corresponding with B(0,0) was observed and a shoulder that was more intense as the temperature was lowered. However, the shoulder did not corresponding with B(1,0) band and it was not observed in [Tb(TPP)Crown]Cl and [Tb(TPP)Azacrown]Cl. Here, in general the ΔA MCD intensity of positive A-term is no longer constant as in [Y(TPP)Salen]Cl complex but demonstrates increase as the temperature was decreased and at the lowest temperature, ΔA MCD reached approximate 9.2×10^{-8}. The positive A-term pattern of B band in Figure 3.6(b) and Figure 3.6(c) was also dominated by the negative lobe, making the pattern to be non-symmetrical. For Q bands, VT-VH-MCD spectra are shown in Figure 3.7. In PMMA matrix, Q(0,0) and Q(1,0) bands were observed and two positive A-term MCD patterns attributed to each band

was also recorded. As well as B band, positive A-term MCD signals showed temperature dependence with increase of ΔA MCD as the temperature was lowered from 100 K to 1.5 K. The phenomenon of temperature dependence of [Tb(TPP)Salen]Cl without reversal

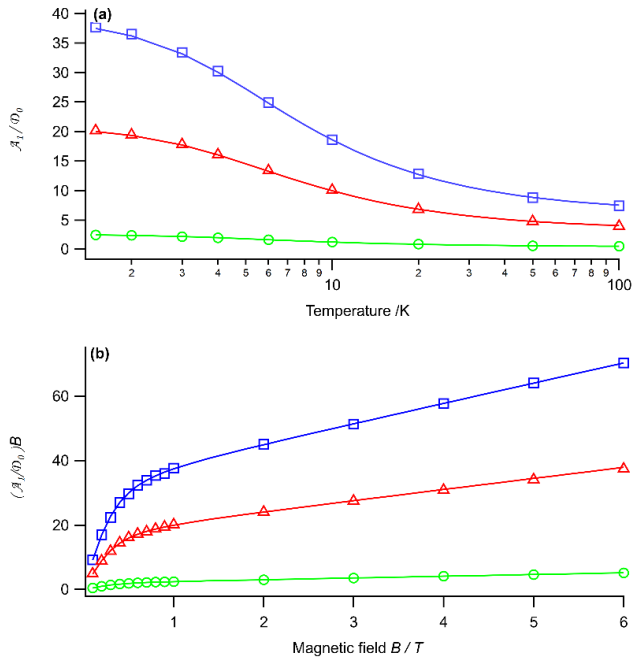

Figure 3.9 Experimental values (squares, triangles, and circles) and calculated value (straight line) of $\mathcal{A}_1/\mathcal{D}_0$ of [Tb(TPP)Salen]Cl for B(0,0) in green, Q(1,0) in red, and Q(0,0) in blue under 1 T of magnetic field with varied temperature (a) and under varied magnetic field at 1.5 K.

confirmed the ferromagnetic nature of Tb complexes and such phenomenon was also observed before[17,19,20]. From general observation, ΔA MCD intensity of [Tb(TPP)Salen]Cl is higher than that of [Tb(TPP)Crown]Cl or [Tb(TPP)Azacrown]Cl and thus, the electronic interaction in [Tb(TPP)Salen]Cl is expected to be bigger than the other Tb complexes.

As in the case of complexes with cyclododecane ligands, the **J–L** interaction by using Figure 3.8. Here, there are doubly degenerate ground state denoted as $|J_z\rangle = |\pm\rangle$ and 4-fold degenerate π-π* excited state belong to porphyrin, symbolized as $|J_z, L_z\rangle = |\pm, \pm\rangle$ (Figure 3.8(a)). Under applied magnetic field along the z-axis, the ground state and the excited state are split and specifically π-π* excited state lost its degeneracy by L_z (Figure 3.8(b) and Figure 3.8(c)). It should be noted that the J_z of the 4f system is unchanged and the $|-\rangle \rightarrow |-, \pm\rangle$ and $|+\rangle \rightarrow |+, \pm\rangle$ will occur and specifically, the $|-\rangle \rightarrow |-, -\rangle$ transition occurs because of lcp and the $|-\rangle \rightarrow |-, +\rangle$ transition occurs due to rcp. The letter transition

gains more contribution as temperature is lowered because the $|-\rangle$ of J_z has larger thermal population. In ferromagnetic system, the energy difference between $|-,+\rangle$ and $|-,-\rangle$ becomes larger because $|-,-\rangle$ stabilizes while $|-,+\rangle$ destabilizes and hence causes a larger A-term strength for the $|-\rangle \rightarrow |-,\pm\rangle$ transition and smaller for the other one. At lower temperature range, the $|-\rangle \rightarrow |-,\pm\rangle$ transition becomes more dominant leading to increase of the magnitude of A-term. However, based on the comparison of the MCD spectra, the $|-\rangle \rightarrow |-,\pm\rangle$ transition of [Tb(TPP)Salen]Cl (Figure 3.8(e)) is predicted to be more significant than that of [Tb(TPP)Crown]Cl (Figure 3.9(d)). Based on that prediction also, $\mathcal{A}_1/\mathcal{D}_0$ ratios are expected to increase at lower temperatures.

From Figure 3.9, $\mathcal{A}_1/\mathcal{D}_0$ ratios at various temperature of both B and Q bands are not constant as in the case of [Y(TPP)Salen]Cl. Those ratios tend to increase during temperature lowering from 100 K to 1.5 K (Figure 3.9(a)). In Figure 3.9(b), the linear relation between $(\mathcal{A}_1/\mathcal{D}_0)B$ and magnetic field B is not detected, meaning that $(\mathcal{A}_1/\mathcal{D}_0)$ ratios are not constant under different magnetic field B. The determination of Δ_{JL} was carried out with L_z as a parameter to be determined and J_z is equal ±6 according to computational chemistry calculation by assuming analogous structure between [Tb(TPP)Salen]Cl and [Tb(TPP)Cyclen]Cl[14]. Simulation result of $\mathcal{A}_1/\mathcal{D}_0$ from VT-VH-MCD is also showed in Figure 3.9 and L_z of Q(0,0), Q(1,0), and B(0,0) bands were estimated to be $6.26\hbar$, $3.45\hbar$, and $0.53\hbar$. As well as that, Δ_{JL} values were found to be equal 9.31 cm^{-1}, 5.77 cm^{-1}, and 0.66 cm^{-1} associated with Q(0,0), Q(1,0), B(0,0) band respectively.

Compound	B(0,0)		Q(0,0)		Q(1,0)		Note
	L_z	Δ_{JL}	L_z	Δ_{JL}	L_z	Δ_{JL}	
[Tb(TPP)Salen]Cl	0.53	0.66	6.26	9.31	3.45	5.77	***a***
[Tb(TPP)Crown]Cl	0.63	0.81	3.61	5.24	2.83	3.63	***a***
[Tb(TPP)Azacrown]Cl	0.54	1.02	3.68	6.77	3.9	4.37	***a***
[Tb(TPP)Cyclen]Cl	0.64	-1.01	3.86	4.42	2.62	5.01	***b***

Table 3.2 The value of **J-L** interaction (Δ_{JL}) of complexes with ***a*** is the reported work and ***b*** is taken from reference 17.

From the Table 3.2 above, the values of L_z of [Tb(TPP)Salen]Cl on B band region is unchanged compared to that of complexes with 12-crown-4 ether, 1-aza-12-crown-4 ether, or cyclen. Moreover, Δ_{JL} in this region is also the

smallest among the other Tb complexes. For Q band region, L_z of Q(0,0) band is reported to be larger than that of Q(0,0) in [Y(TPP)Salen]Cl where in [Y(TPP)Salen]Cl, L_z of Q(0,0) band is $4.53\hbar$. However, there is increase of Δ_{JL} with magnitude as much as 9.31 cm^{-1} and this value is noted to be the highest compared all Tb with cyclododecane moieties. In other words, second ligand with smaller symmetry leads to higher electronic interaction compared to second ligands with more ordered structure.

3.3.3 Analysis of [Dy(TPP)Salen]Cl

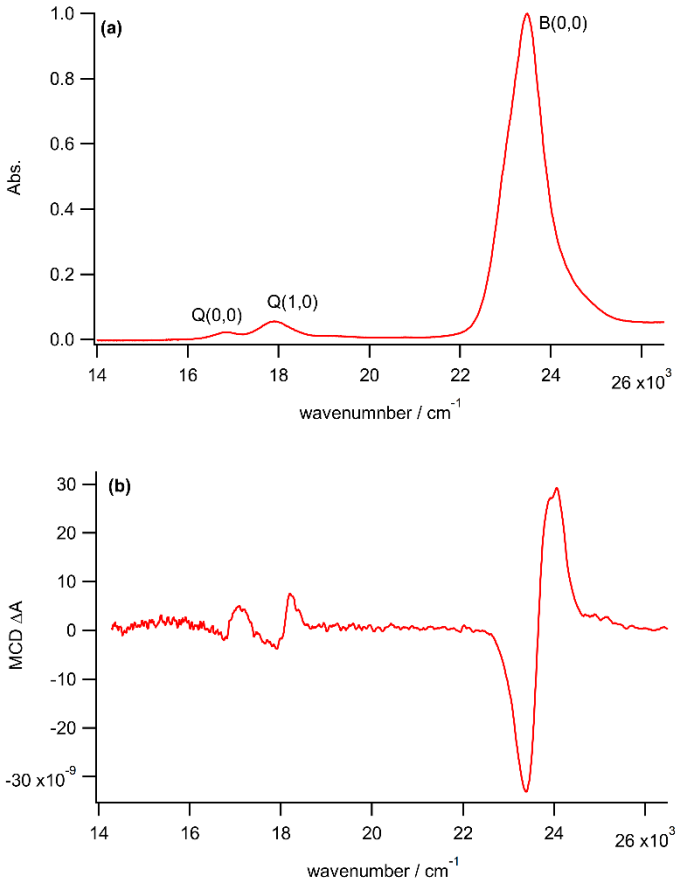

Figure 3.10 UV-vis spectra (a) and room-temperature MCD spectra under 1.6 T permanent magnet (b) of [Dy(TPP)Salen]Cl in CH_2Cl_2.

From the discussion in Chapter 2, Dy complexes have interesting features especially regarding how the MCD spectral shape changed only by replacing the non-aromatic ligand with different symmetry or different atoms on the tetradentate site. Thus, it is important how non-cyclododecane results different electronic interaction in a Dy-porphyrin molecular system.

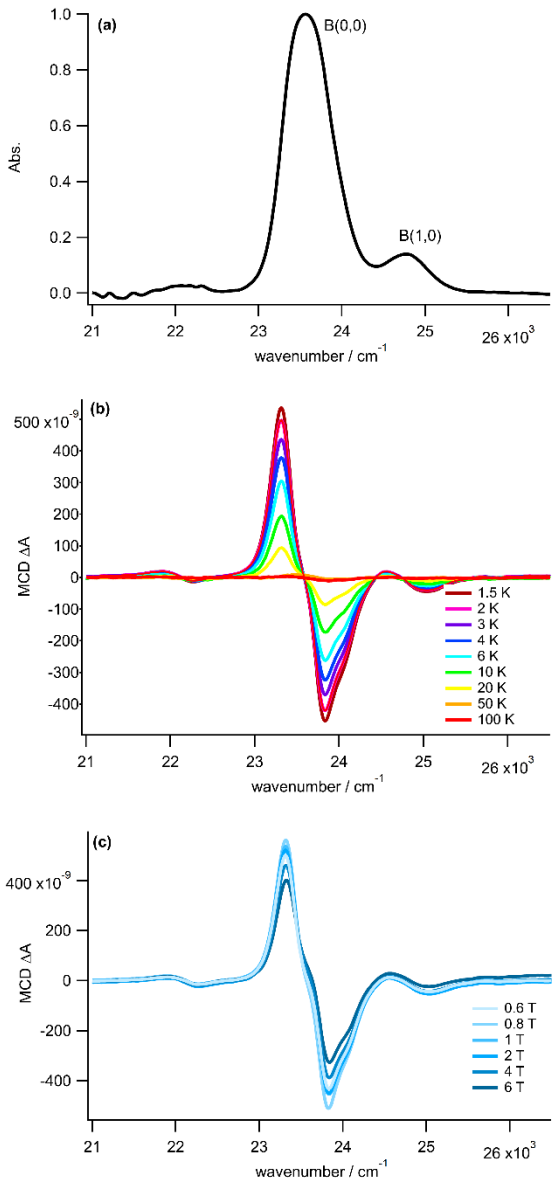

Figure 3.11 a) Absorption, (b) temperature-dependent MCD spectra measured at temperatures of 1.5-100 K under a magnetic field of 1 T, and (c) magnetic field-dependent MCD spectra measured at temperatures of 1.5 K of B band in [Dy(TPP)Salen]Cl in PMMA film.

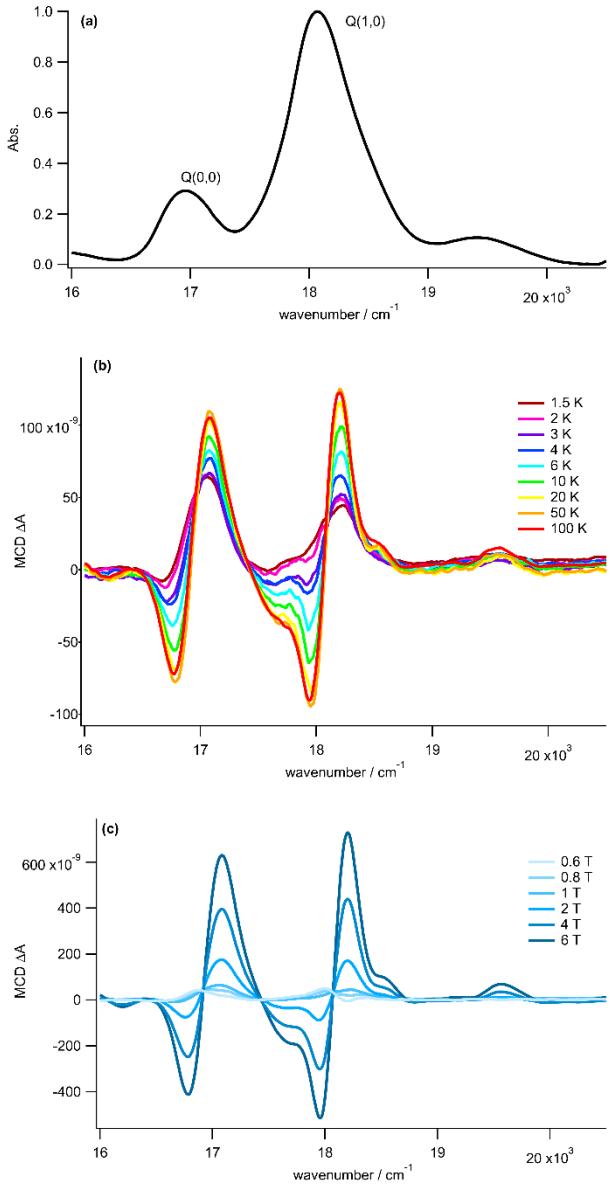

Figure 3.12 a) Absorption, (b) temperature-dependent MCD spectra measured at temperatures of 1.5-100 K under a magnetic field of 1 T, and (c) magnetic field-dependent MCD spectra measured at temperatures of 1.5 K of B band in [Dy(TPP)Salen]Cl in PMMA film.

As presented in Figure 3.10(a), UV-Vis spectra of [Dy(TPP)Salen]Cl has similar profile as [Tb(TPP)Salen]Cl where B(1,0) shoulder was not observed. This is contrast to [Dy(TPP)Crown]Cl and [Dy(TPP)Azacrown]Cl where in the two complexes, absorption band of B(1,0) was detected. In MCD measurement at room temperature (Figure 3.10(b)), three positive A-term associated with Q(0,0), Q(1,0), and B(0,0) respectively appeared. As well as [Y(TPP)Salen]Cl and [Tb(TPP)Salen]Cl, the positive lobe of A-term spectral shape in B-band region indicates split peak. By considering [Y(TPP)Salen]Cl and [Tb(TPP)Salen]Cl, the split peak that is observed also in [Dy(TPP)Salen]Cl may correspond to the widened B(0,0) spectral shape from UV-Vis spectrometry. From Figure 3.10, it can be concluded that non-aromatic ligand with reduced symmetry than cyclododecanes did not cause reversal of positive A-term into negative A-term at room temperature.

[Dy(TPP)Salen]Cl was incorporated into PMMA film and subjected for VT-VH-MCD measurement for B band region as shown in Figure 3.11 and for Q bands region given in Figure 3.12. In Figure 3.11(a), the spectral shape of B band in PMMA is different from B band in solution where B(1,0) band was detected. Nonetheless, B(1,0) band does not correspond to any spectra measured by MCD. From Figure 3.11(b) B band shape is almost a straight line at 100 K and 50 K, making it to be complicated to decide whether the spectral shape to be positive or negative A-term. At 20 K, the spectral shape became clearer to observe with negative A-term was detected and the intensity denoted as ΔA MCD became higher as the temperature was lowered down to 1.5 K. In Figure 3.11(c), negative A-term pattern was observed under various applied magnetic field without reversal to positive A-term or vice versa. In Q band region i.e. Q(0,0) and Q(1,0) bands, at 100 K, two positive A-term which each attributed to Q(0,0) and Q(1,0) bands. When the temperature was diminished, ΔA MCD reduced because the intensity of positive A-term profile became lower. It is worth noting that even though ΔA MCD intensity of positive A-term of Q bands diminished, it did not undergo reversal becoming negative A-term. Starting from 4 K (dark blue color), the negative lobes of Q(0,0) and Q(1,0) bands began to disappear and completely perished at 1.5 K. On the other hand, in Figure 3.12(c), even though under 6 T of magnetic field Q(0,0) and Q(1,0) positive A-term pattern was detected, this pattern was inversed to negative A-term pattern with small ΔA MCD intensity when the field was smaller than 1 T.

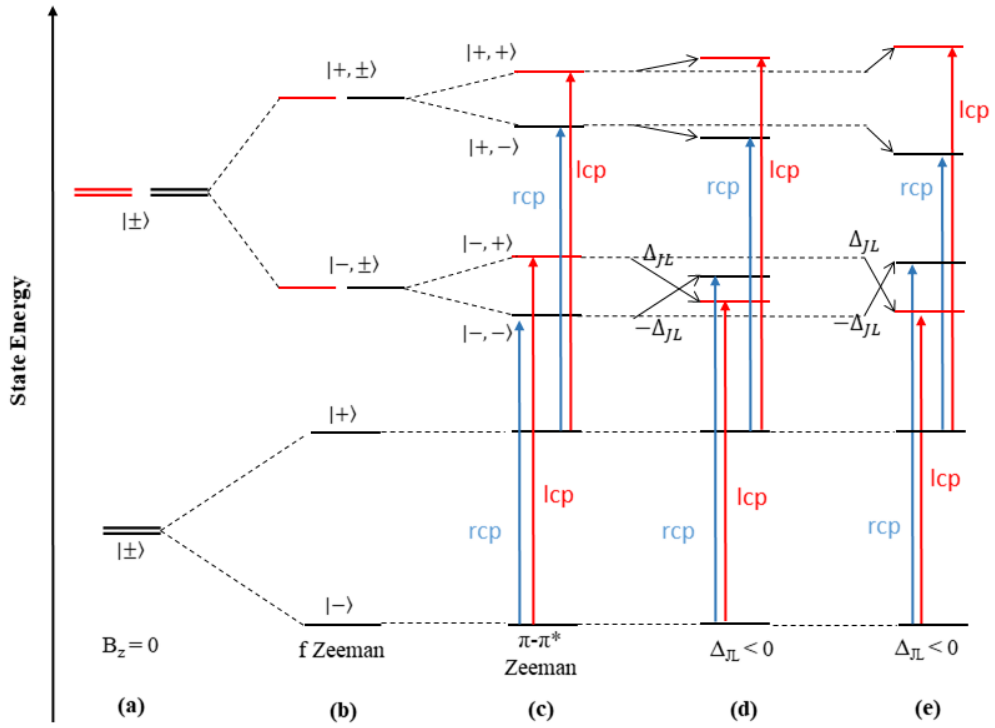

Figure 3.13 Schematic energy of the ground and the excited states of [Dy(TPP)Salen]Cl

From previous explanation, negative A-term MCD spectral shape was observed in [Dy(TPP)Salen]Cl, proving that antiferromagnetic nature of Dy-porphyrin was not changed with different non-aromatic ligand from cyclododecane to salen. The antiferromagnetic nature of Dy was also reported in other work before[18,21]. Referring to the results of [Tb(TPP)Salen]Cl, Δ_{JL} of [Dy(TPP)Salen]Cl is predicted to be higher than that of [Dy(TPP)Crown]Cl. Using Figure 3.13, the doubly degenerate ground state J_z and fourfold degenerate π–π* can be stated as $|J_z\rangle = |\pm\rangle$ and $|J_z, L_z\rangle = |\pm, \pm\rangle$ respectively (Figure 3.13 (a)). The degeneracy was split by the introduction of external magnetic field caused the degeneracy to be lifted (Figure 3.13(b)). Simultaneously, the degeneracy of π–π* excited states are split as much as L_z (Figure 3.13(c)). The $|-\rangle \rightarrow |-,\pm\rangle$ and $|+\rangle \rightarrow |+,\pm\rangle$ transitions will occur because J_z is constant during π–π* excitation. Particularly, $|-\rangle \rightarrow |-,-\rangle$ transition occurred because of lcp and $|-\rangle \rightarrow |-,+\rangle$ transition occurred by rcp. However, at lower temperature, $|-\rangle$ has more population than $|+\rangle$ and thus $|-\rangle \rightarrow |-,\pm\rangle$ transition is more likely than $|+\rangle \rightarrow |-,\pm\rangle$. The interaction between **J** and **L** in excited states is antiferromagnetic. Because stabilization occurs in the states where J_z and L_z have the same sign and destabilization occurs in those with opposite sign, therefore the energy difference between $|-,+\rangle$ and $|-,-\rangle$ becomes smaller and causes more significant negative

A-term magnitude as the $|-\rangle \rightarrow |-,\pm\rangle$ transition has bigger contribution. If the hypothesis is true, then more major contribution of rcp than lcp will be more significant in the case of [Dy(TPP)Salen]Cl (Figure 3.13(e)) than in [Dy(TPP)Azacrown]Cl (Figure 3.13(d)), indicated by greater Δ_{JL} in [Dy(TPP)Salen]Cl.

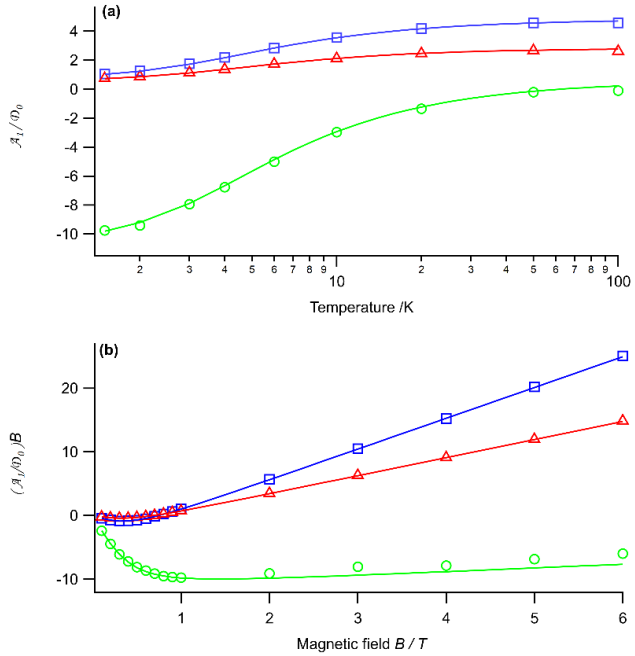

Figure 3.14 Experimental values (squares, triangles, and circles) and calculated value (straight line) of $\mathcal{A}_1/\mathcal{D}_0$ of [Dy(TPP)Salen]Cl for B(0,0) in green, Q(1,0) in red, and Q(0,0) in blue under 1 T of magnetic field with varied temperature (a) and under varied magnetic field at 1.5 K.

All $\mathcal{A}_1/\mathcal{D}_0$ ratios of B and Q bands are plotted in Figure 3.14 above. At different temperature, $\mathcal{A}_1/\mathcal{D}_0$ ratios of B band tend to decrease with $\mathcal{A}_1/\mathcal{D}_0$ value close to zero at 100 K. However, for Q(0,0) and Q(1,0) bands, $\mathcal{A}_1/\mathcal{D}_0$ ratios are positive when temperature was lowered down to 1.5 K. This results are consistent with MCD spectra of Q bands shown in Figure 3.12(b) where reversal from positive A-term into negative A-term did not occur. In Figure 3.14(b), under varied magnetic field B, $(\mathcal{A}_1/\mathcal{D}_0)B$ values show no direct dependence on the applied field, contrast to [Y(TPP)Salen]Cl. For B band (green dots), $(\mathcal{A}_1/\mathcal{D}_0)B$ are negative and diminishing with steep trend from 6 to 1 T and then increase when the field is smaller than 1 T. For Q(0,0) and Q(1,0) bands, the diminishing tendency is also observed from 6 T to 1 T with $(\mathcal{A}_1/\mathcal{D}_0)B$ are positive but the value start to become negative under

0.7 T. It also can be said that the trend of $\mathcal{A}_1/\mathcal{D}_0$ at varied temperature MCD has similar profile as [Dy(TPP)Crown]Cl as already explained in the previous chapter.

The determination of Δ_{JL} was carried out with L_z as a parameter and J_z equal ±11/2 by least-square fitting to $\mathcal{A}_1/\mathcal{D}_0$ ratios gained from the VT-VH-MCD measurement. The results are presented in Figure 3.14 as straight lines. From the calculation, the values of L_z and Δ_{JL} of [Dy(TPP)Salen]Cl can be tabulated in the table below.

Compound	B(0,0)		Q(0,0)		Q(1,0)		Note
	L_z	Δ_{JL}	L_z	Δ_{JL}	L_z	Δ_{JL}	
[Dy(TPP)Salen]Cl	0.59	-3.50	4.85	-1.29	2.85	-0.71	***a***
[Dy(TPP)Crown]Cl	0.84	-3.19	3.53	-0.39	2.26	-0.26	***a***
[Dy(TPP)Azacrown]Cl	0.75	-4.66	3.82	-3.58	1.32	-1.96	***a***
[Dy(TPP)Cyclen]Cl	0.88	-5.99	3.71	-3.40	2.38	-2.61	***b***

Table 3.3 The value of **J-L** interaction (Δ_{JL}) of complexes with ***a*** is the reported work and ***b*** is extracted from reference 18.

Based on Table 3.3, L_z of B band is practically unchanged with different non-aromatic ligands in Dy-porphyrinoid molecular systems. For Q(0,0) and Q(1,0) bands, L_z are unchanged relative to that of [Y(TPP)Salen]Cl where L_z was reported to be 4.55$\hbar$ and 2.66$\hbar$ respectively. However, in this work, Δ_{JL} of B(0,0) band is in between that of [Dy(TPP)Crown]Cl and [Dy(TPP)Azacrown]Cl. Such results were also obtained for both of Q(0,0) and Q(1,0) bands in which Δ_{JL} of [Dy(TPP)Salen]Cl is greater than that of [Dy(TPP)Crown]Cl but smaller than that of [Dy(TPP)Azacrown]Cl.

3.4 Computational Chemistry Analysis

As well as in the case of the complexes with cyclododecane moieties i.e. 12-crown-4 ether and 1-aza-12-crown-4 ether, *ab-initio* calculation was also conducted to investigate different L_z can be gained from theoretical approach. As well as that, because **J–L** interaction in $[Tb(TPP)Salen]^+$ and $[Dy(TPP)Salen]^+$ cannot be reproduced with calculation, thus *ab-initio* calculation was performed aimed to analyze electronic states energy levels within $[Tb(TPP)Salen]^+$ and $[Dy(TPP)Salen]^+$ since some differences have been noticed depending on the different symmetry between 12-crown-4 ether and 1-aza-12-crown-4 ether in the previous chapter.

[Y(Por)Salen]$^+$				
S.O state	Energy (cm^{-1})	g_z	L_z	S_z
1	0.00	-	-	-
2	26915.88	7.50	3.75	0.00
3	26998.63			
4	45979.99	0.36	0.18	0.00
5	47011.68			
[Y(TPP)Azacrown]$^+$				
S.O state	Energy (cm^{-1})	g_z	L_z	S_z
1	0.00	-	-	-
2	26030.76	8.07	4.03	0.00
3	26063.59			
4	47151.07	0.37	0.19	0.00
5	47212.79			

Table 3. Angular Momenta from RASSCF/RASSI/single_aniso calculations for [Y(TPP)Azacrown]$^+$ and [Y(Por)Salen]$^+$

According to the table above, there are 5 spin-orbit (S.O) states observed in [Y(Por)Salen]$^+$ as well as [Y(TPP)Azacrown]$^+$ and these states are assumed to be composed of one singlet and two doublet states. However, due to more distorted symmetry in salen, S.O state 2 and S.O state 3 became less degenerate with energy difference around 83 cm^{-1} and this noticeable energy difference is more prominent in S.O state 4 and S.O state 5 where energy difference was about 33 cm^{-1} and consequently, there 9 transitions occurring in [Y(Por)Salen]$^+$. The transition from S.O state 1 to the lowest doublet states is associated with the Q band and B band is generated from the transition from the lowest state to the highest doublet state. In adition to that, the lowest doublet states are determined at a relatively higher energy level than [Y(TPP)Azacrown]$^+$ yet the highest doublet states are calculated to be around the similar energy levels as in [Y(TPP)Azacrown]$^+$. Nonetheless, it can be said that less symmetrical non-aromatic ligand does not have significant effect on the S.O states and it reduced the magnetic tensor to 7.50, slightly lower than that of [Y(TPP)Azacrown]$^+$. The calculation was also able to estimate the L_z of B(0,0) band and Q(0,0) band where L_z of B(0,0) was predicted to be $0.18\hbar$ while that of Q(0,0) was equal $3.75\hbar$. L_z of B(0,0) band was calculated to be constant with different second ligands symmetries and contrast to that, L_z of Q(0,0) band was fairly reduced in comparison with that of the cyclododecane ligands and these results are consistent with the experimental results.

[Tb(TPP)Azacrown]$^+$		[Tb(TPP)Salen]$^+$	
Energy (cm^{-1})	*States*	*Energy (cm^{-1})*	*States*
0.000	$0.98\|\pm6\rangle$	0.000	$0.98\|\pm6\rangle$
0.058	$0.98\|\pm6\rangle$	0.056	$0.98\|\pm6\rangle$
144.860	$0.77\|\pm5\rangle$	177.693	$0.39\|\pm5\rangle$ $0.33\|\pm2\rangle$ $0.16\|\pm0\rangle$
146.052	$0.78\|\pm5\rangle$	185.715	$0.65\|\pm5\rangle$ $0.12\|\pm2\rangle$
185.998	$0.28\|\pm4\rangle$ $0.24\|\pm3\rangle$ $0.20\|0\rangle$	188.479	$0.13\|\pm3\rangle$ $0.72\|\pm1\rangle$
197.469	$0.20\|\pm5\rangle$ $0.31\|\pm3\rangle$ $0.21\|\pm1\rangle$	203.956	$0.39\|\pm5\rangle$ $0.38\|0\rangle$
205.889	$0.57\|\pm2\rangle$ $0.19\|0\rangle$	249.289	$0.20\|\pm4\rangle$ $0.14\|\pm3\rangle$ $0.35\|\pm2\rangle$ $0.22\|\pm1\rangle$
220.344	$0.18\|\pm3\rangle$ $0.54\|\pm1\rangle$	260.009	$0.20\|\pm5\rangle$ $0.38\|\pm3\rangle$ $0.28\|\pm2\rangle$
248.459	$0.71\|\pm4\rangle$ $0.21\|\pm3\rangle$	266.980	$0.12\|\pm5\rangle$ $0.28\|\pm4\rangle$ $0.39\|\pm3\rangle$ $0.12\|\pm1\rangle$
283.594	$0.36\|\pm4\rangle$ $0.42\|0\rangle$	292.007	$0.48\|\pm4\rangle$ $0.39\|\pm1\rangle$
296.282	$0.43\|\pm3\rangle$ $0.18\|\pm2\rangle$ $0.31\|\pm1\rangle$	305.213	$0.41\|\pm4\rangle$ $0.13\|\pm3\rangle$ $0.21\|\pm2\rangle$ $0.22\|0\rangle$
313.474	$0.29\|\pm3\rangle$ $0.34\|\pm2\rangle$ $0.18\|\pm1\rangle$	442.923	$0.17\|\pm4\rangle$ $0.26\|\pm3\rangle$ $0.35\|\pm2\rangle$ $0.13\|0\rangle$
317.366	$0.44\|\pm3\rangle$ $0.40\|\pm2\rangle$	445.492	$0.18\|\pm4\rangle$ $0.35\|\pm3\rangle$ $0.15\|\pm2\rangle$ $0.30\|\pm1\rangle$

Table 3. Energy level of the multiplet states in [Tb(TPP)Azacrown]$^+$ and [Tb(TPP)Salen]$^+$

In the case of [Tb(TPP)Salen]$^+$ complex, the **J–L** interaction still cannot reproduced with the present computational chemistry method. However, the electronic states of Tb(III) in this particular case can be determined with *ab-initio* calculation with purpose to analyze how more symmetry distortion of the non-aromatic ligand influence states energy levels as such phenomenon is already seen in Tb(III)-porphyrin when 12-crown-4 ether was replaced with 1-aza-12-crown-4 ether. The results of the calculation are presented in Table 3. According to the results, the lowest substates was calculated to be J_z equal $|\pm6\rangle$ which is similar as in [Tb(TPP)Crown]$^+$ and [Tb(TPP)Azacrown]$^+$. Hence, more distorted non-aromatic ligand is proven not to alter the value of J_z of Tb(III). Moreover, in

[Tb(TPP)Salen]$^+$ the second lowest states was value $|\pm5\rangle$ as in [Tb(TPP)Azacrown]$^+$ but the percentage was much smaller (approximately 39%) while that of [Tb(TPP)Azacrown]$^+$ was around 77%. Furthermore, this substate was located at higher energy level (ca. 177 cm^{-1}), meaning that smaller symmetry led to higher axiality indicated by bigger energy separation between the lowest states and the secondary-lowest states. As well as that, substates mixing is more prominent in the molecular system that contained distorted symmetries than the regular one, making the substates composition become more complicated.

3.5 Conclusion

From this chapter, it can be concluded that salen-type ligand can be synthesized as a second ligand for Ln-porphyrinoid complexes with Ln is Y, Tb, or Dy. The determination of the angular momentum L_z and the **J–L** interaction denoted as Δ_{JL} was also conducted with VT-VH-MCD for all complexes and the results are tabulated below.

Compound	**B(0,0)**		**Q(0,0)**		**Q(1,0)**	
	L_z **(ħ)**	Δ_{JL} **(cm^{-1})**	L_z **(ħ)**	Δ_{JL} **(cm^{-1})**	L_z **(ħ)**	Δ_{JL} **(cm^{-1})**
[Y(TPP)Salen]Cl	0.66	-	4.53	-	2.66	-
[Tb(TPP)Salen]Cl	0.53	0.66	6.26	9.31	3.45	5.77
[Dy(TPP)Salen]Cl	0.59	-3.50	4.85	-1.29	2.85	-0.71

Table 3.4 The value of L_z and **J-L** interaction (Δ_{JL}) of all [Ln(TPP)Salen]Cl complexes.

3.6 References

1. V.N. Nemykin, R.G. Hadt, *J. Phys. Chem. A.*, 2010, **114**, 12062-12066.
2. S. Sripothongnak, C.J. Ziegler, M.R. Dahlby, V.N. Nemykin, *Inorg. Chem.*, 2011, **50**, 6902-6909.
3. C.J. Ziegler, N.R. Erickson, M.R. Dahlby, V.N. Nemykin, *J. Phys. Chem. A.*, 2013, **117**, 11499-11508.
4. M. Fathi-Rasekh, G.T. Rohde, M.D. Hart, T. Nakakita, Y.V. Zatsikha, R.R. Valiev, M.V. Barybin, V.N. Nemykin, *Inorg. Chem.*, 2019, **58**, 9316-9325.
5. Q. Ma, S. Zeng, X. Feng, W. Cao, H. Wang, J. Dou, J. Jiang, *Eur. J. Inorg. Chem.*, 2016, **26**, 4194-4198.
6. P.G. Cozzi, *Chem. Soc. Rev.*, 2004, **33**, 410-421.
7. M. Pasquali, F. Marchetti, C. Floriani, M. Cesari, *Inorg. Chem.*, 1980, **19**, 1198-1202.

8. J.A. Bonadies, W.M. Butler, V.L. Pecoraro, C.J. Carraro, *Inorg. Chem.*, 1987, **26**, 1218-1222.
9. S.J. Coles, M.B. Hursthouse, D.G. Kelly, A.J. Toner, N.M. Walker, *J. Chem. Soc., Dalton Trans.*, 1998, **24**, 3489-3494.
10. X. Yang, R.A. Jones, *J. Am. Chem. Soc.*, 2005, **127**, 7686-7687.
11. X. Yang, R.A. Jones, W.K. Wong, *Chem. Comm.*, 2008, 3266-3268.
12. C.E. Burrow, T.J. Burchell, P.H. Lin, F. Habib, W. Wernsdorfer, R. Clerac, M. Murugesu, *Inorg. Chem.*, 2009, **48**, 8051-8053.
13. F. Pointillart, K. Bernot, R. Sessoli, D. Gatteschi, *Inorg. Chem.*, 2010, **49**, 4355-4361.
14. A. Santria, A. Fuyuhiro, T. Fukuda, N. Ishikawa, *Inorg. Chem.*, 2017, **56**, 10625-10632.
15. S. B. Piepho, P. N. Schatz, Group Theory in Spectroscopy: With Applications to Magnetic Circular Dichroism; Wiley: New York, 1983.
16. T. Ida, M. Ando, H. Toraya, *J. App. Crystallogr.*, 2000, **33**, 1311-1316.
17. A. Santria and N. Ishikawa, *Inorg. Chem.*, 2020, **59**, 14326-14336.
18. A. Santria and N. Ishikawa, *Inorg. Chem.*, 2021, **60**, 14418-14425.
19. K. Kizaki, A. Santria, N. Ishikawa, *Inorg. Chem.*, 2020, **60**, 2037-2044.
20. K. Kizaki, H. Ozawa, T. Kobayashi, R. Matsuoka, Y. Sakaguchi, A. Fuyuhiro, T. Fukuda, N. Ishikawa, *Chem. Commun.*, 2017, **53**, 6168-6171.
21. T. Fukuda, H. Ozawa, Y. Sakaguchi, K. Kizaki, T. Kobayashi, A. Fuyuhiro, T. Fukuda, N. Ishikawa, *Chem. Commun.*, 2017, **23**, 16357 – 16363.

3.7 Supplementary Information

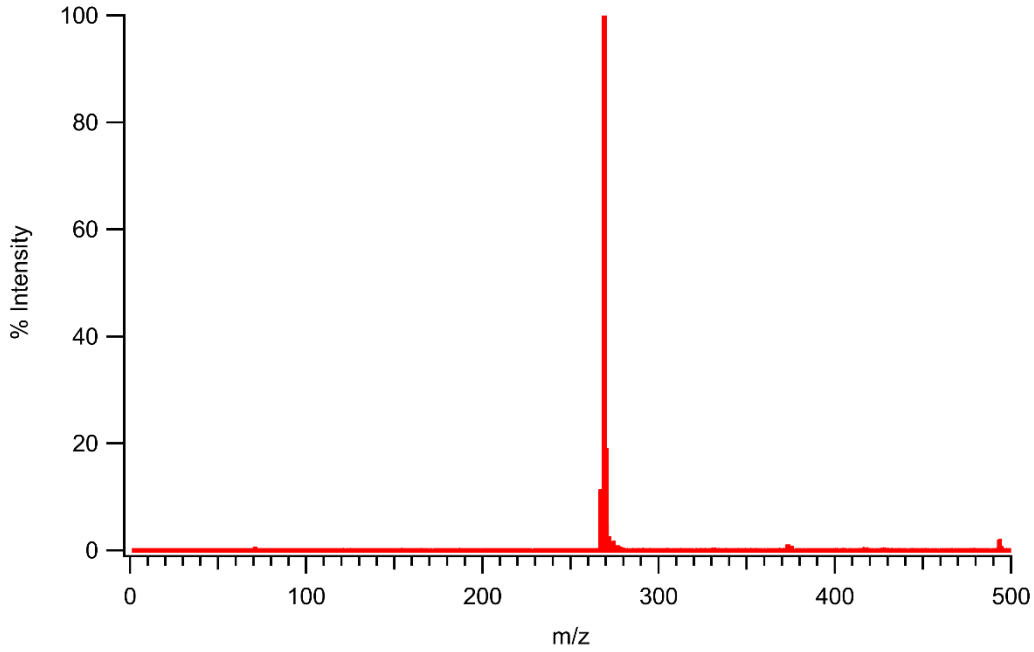

Figure S3-1 MALDI-TOF spectra of salen-H^+

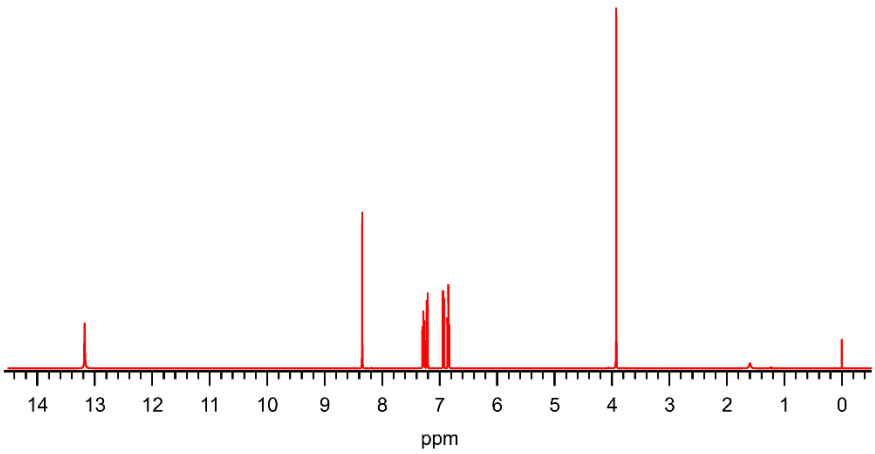

Figure S3-2 ^{1}H-NMR spectra of salen in $CDCl_3$ at room temperature

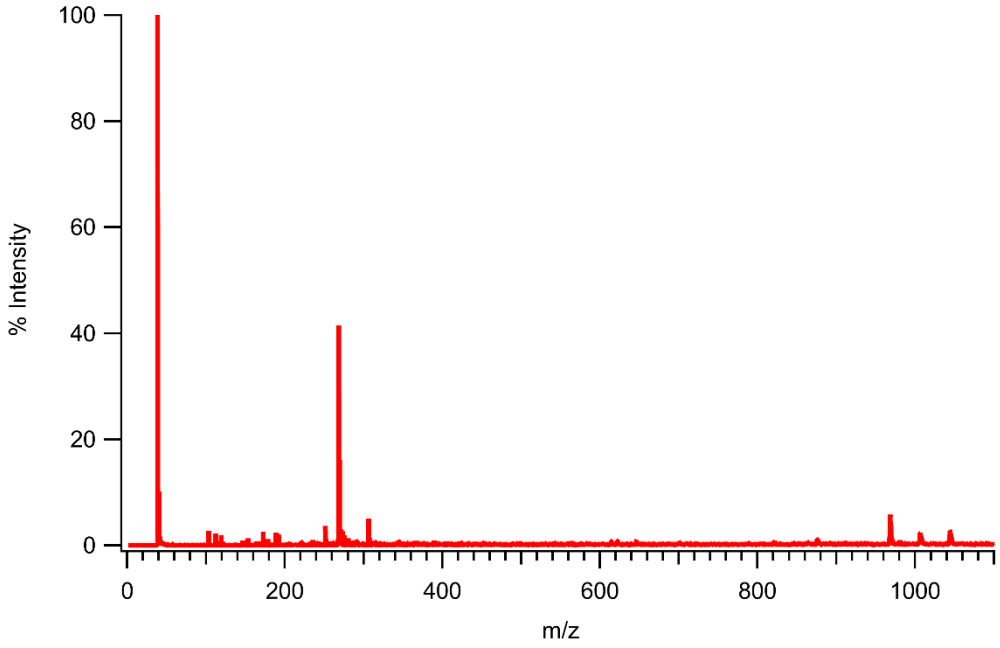

Figure S3-3 MALDI-TOF spectra of $[Y(TPP)SalenK_2]^+$ with peak at m/z equal 269 is associated with salen-H^+ and at m/z equal 39 is attributed to K^+.

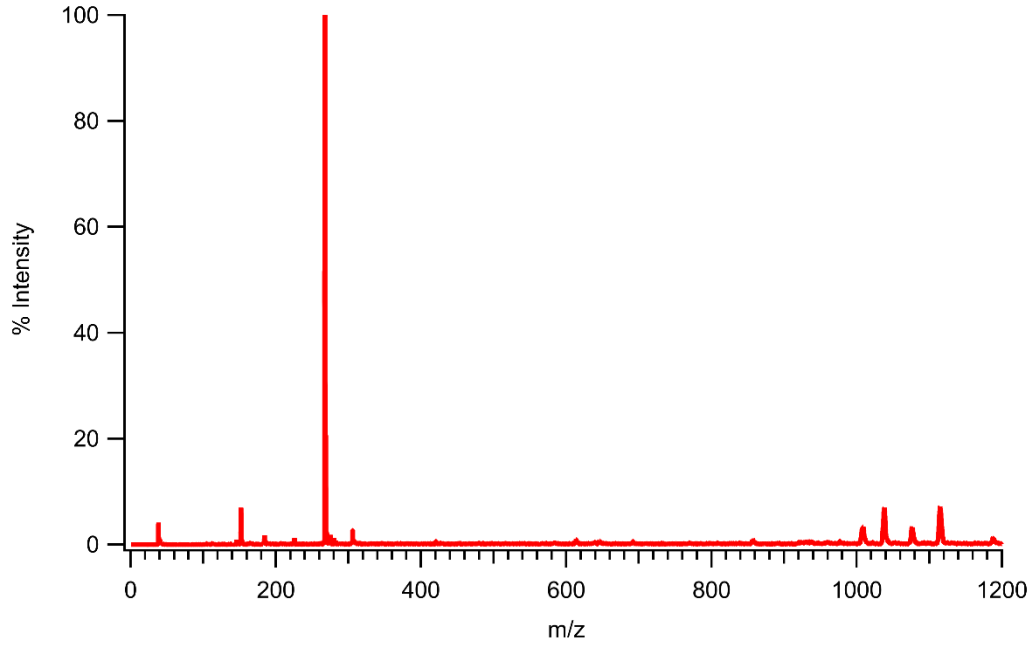

Figure S3-4 MALDI-TOF spectra of $[Tb(TPP)SalenK_2]^+$ with peak at m/z 269 is associated with salen-H^+.

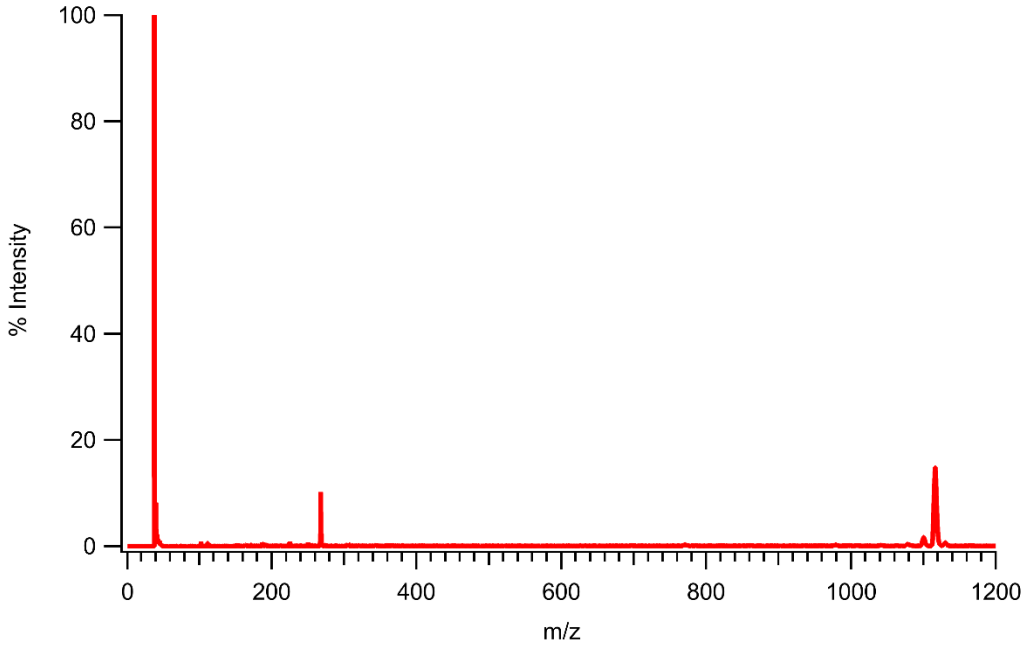

Figure S3-5 MALDI-TOF spectra of $[Dy(TPP)SalenK_2]^+$ with peak at m/z equal 269 is associated with salen-H^+ and at m/z equal 39 is attributed to K^+.

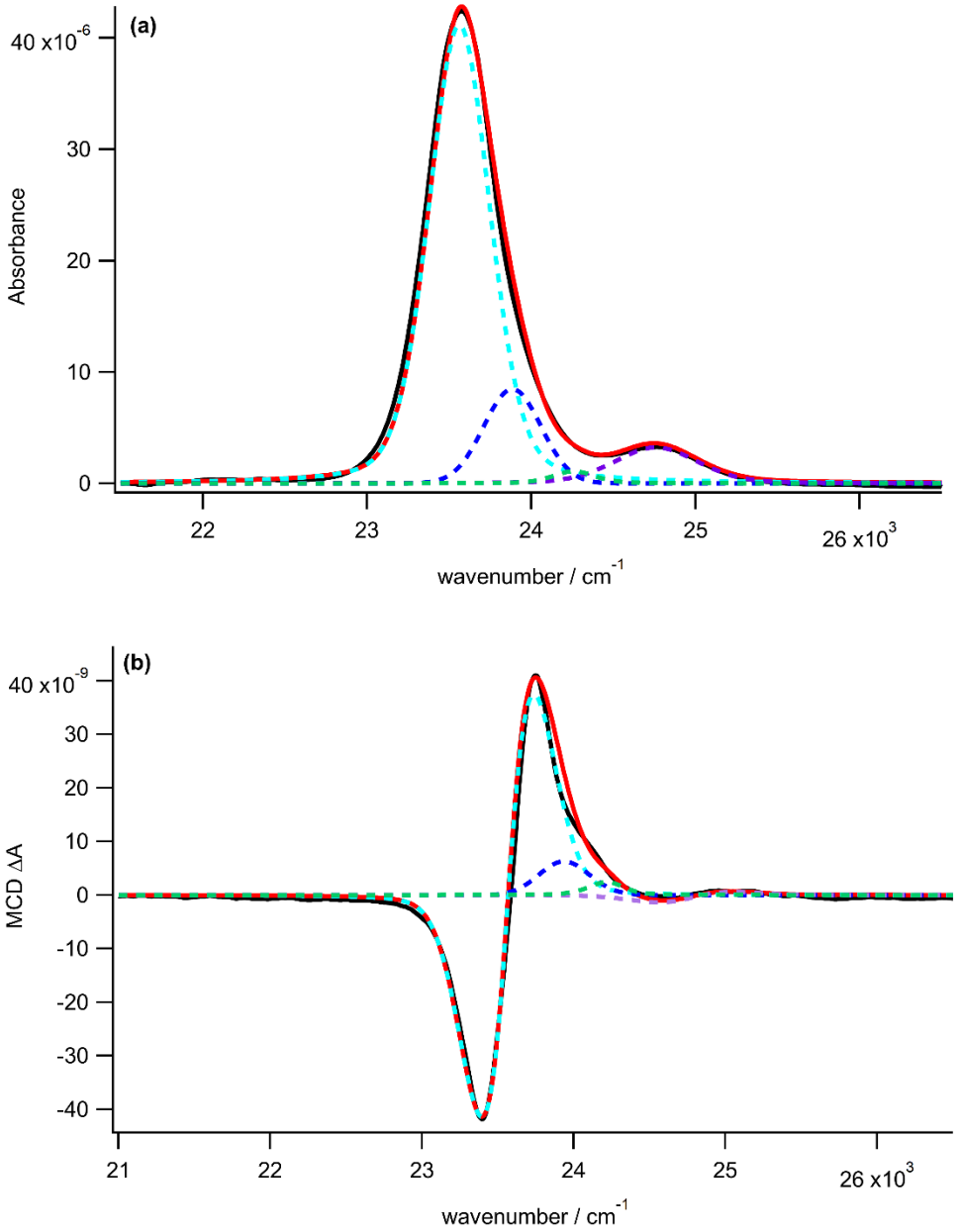

Figure S3-6 Band deconvolution of absorption (**a**) and MCD (**b**) of B(0,0) band spectra [Y(TPP)Salen]Cl at 1.5 K and under 1 T. Experimental spectra is shown in black while simulated band is in red color. The components that give the simulated band are in dashed lines.

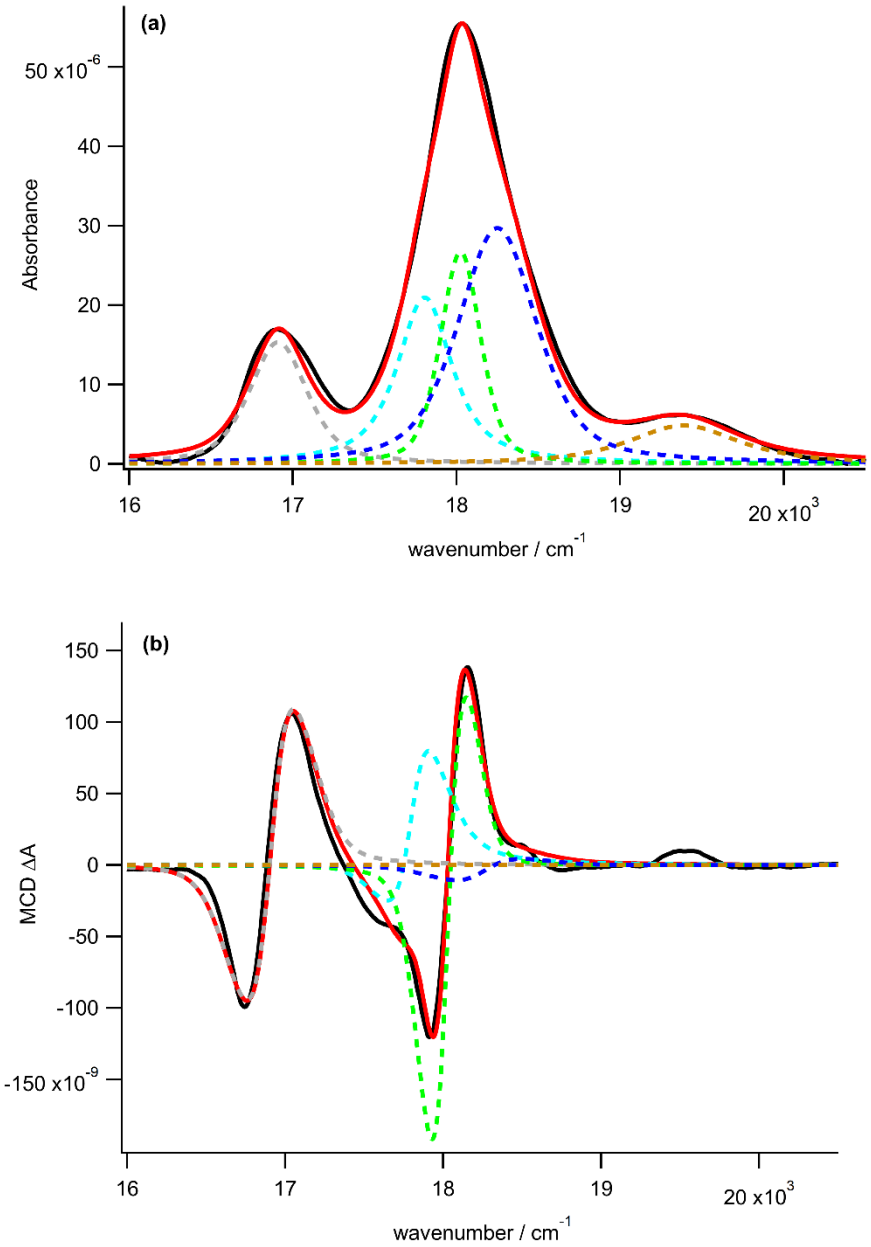

Figure S3-7 Band deconvolution of absorption (**a**) and MCD (**b**) of Q(0,0) and Q(1,0) band spectra [Y(TPP)Salen]Cl at 1.5 K and under 1 T. Experimental spectra is shown in black while simulated band is in red color. The components that give the simulated band are in dashed lines.

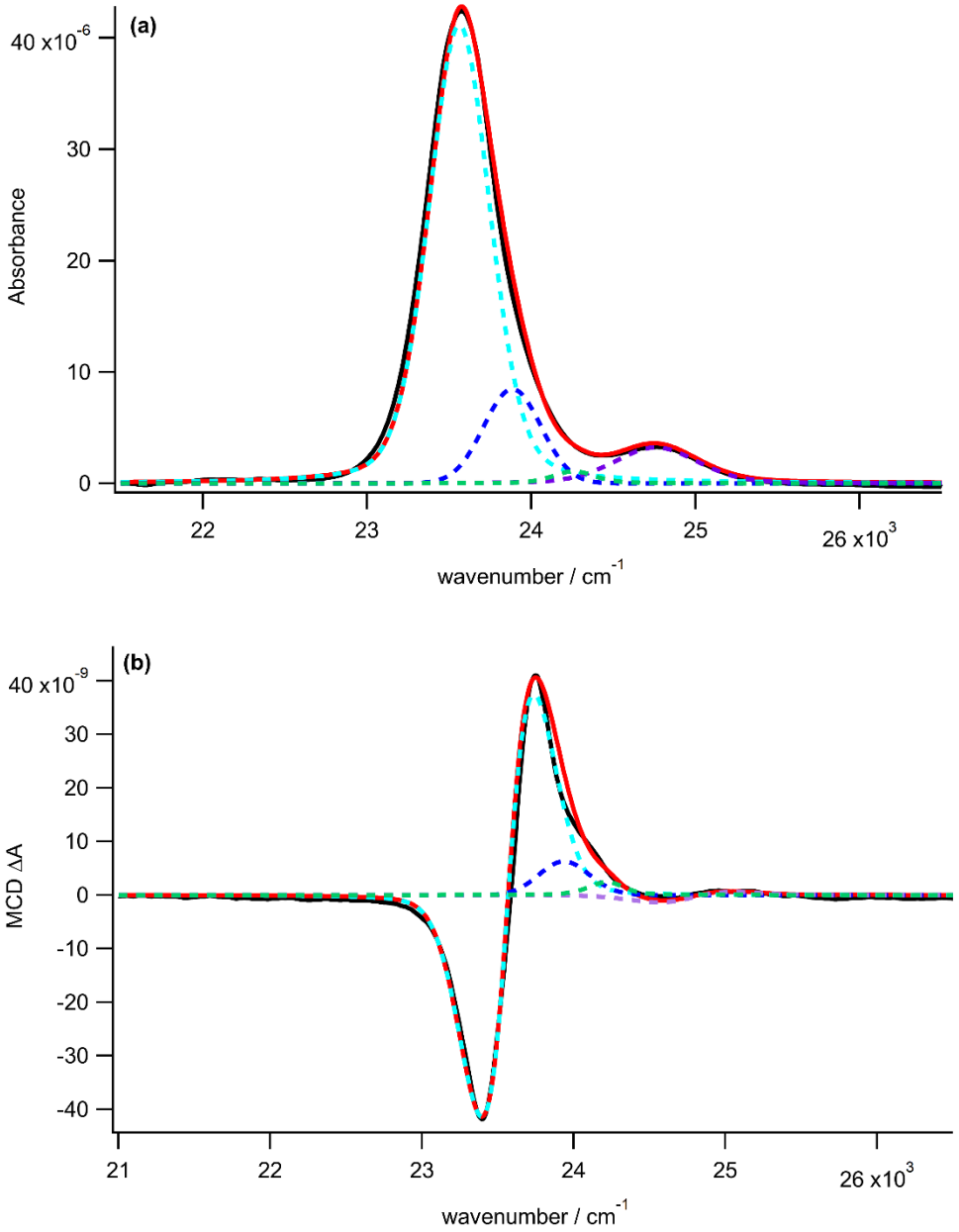

Figure S3-8 Band deconvolution of absorption (**a**) and MCD (**b**) of B(0,0) band spectra [Y(TPP)Salen]Cl at 1.5 K and under 1 T. Experimental spectra is shown in black while simulated band is in red color. The components that give the simulated band are in dashed lines.

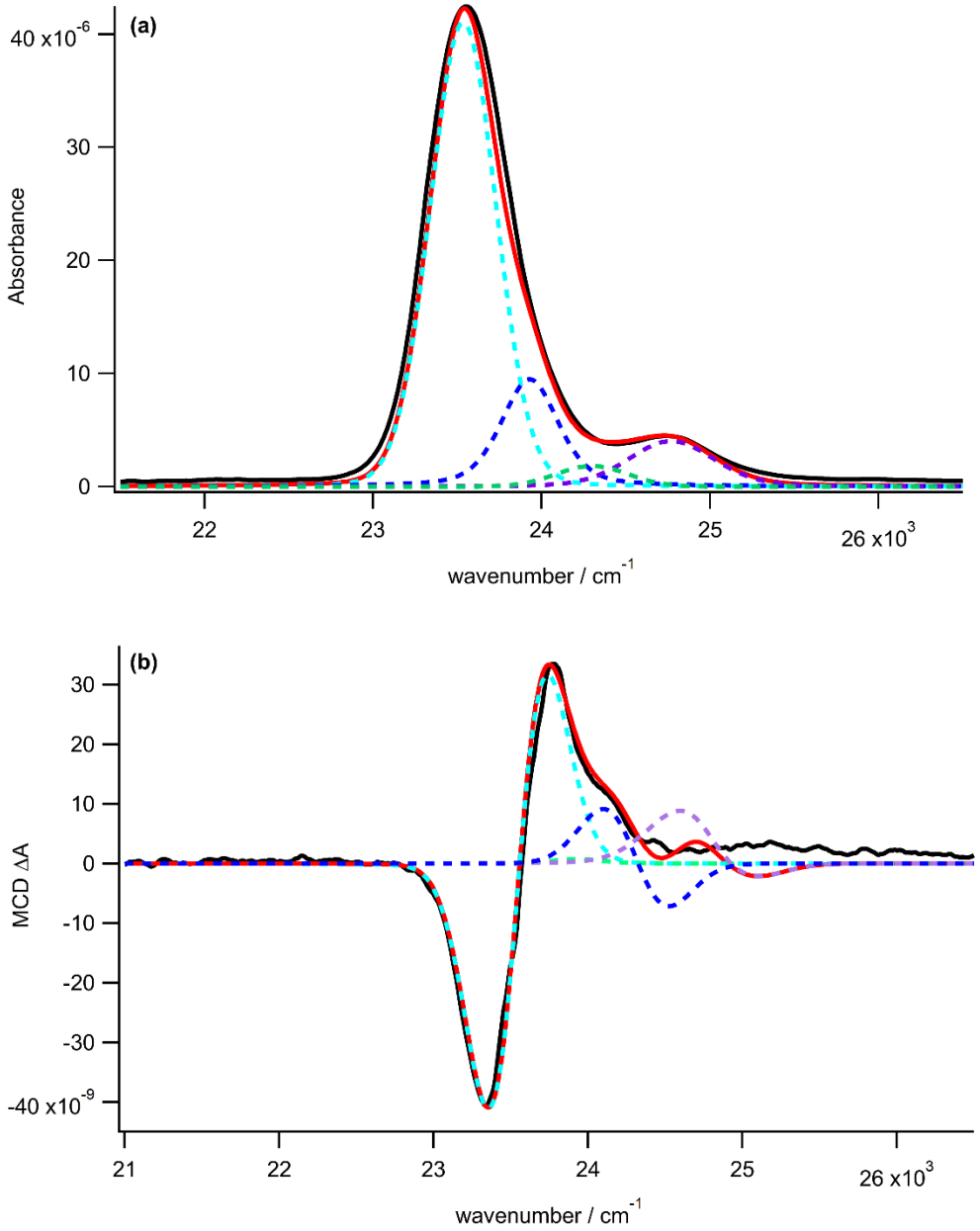

Figure S3-9 Band deconvolution of absorption (**a**) and MCD (**b**) of B(0,0) band spectra [Tb(TPP)Salen]Cl at 100 K and under 1 T. Experimental spectra is shown in black while simulated band is in red color. The components that give the simulated band are in dashed lines.

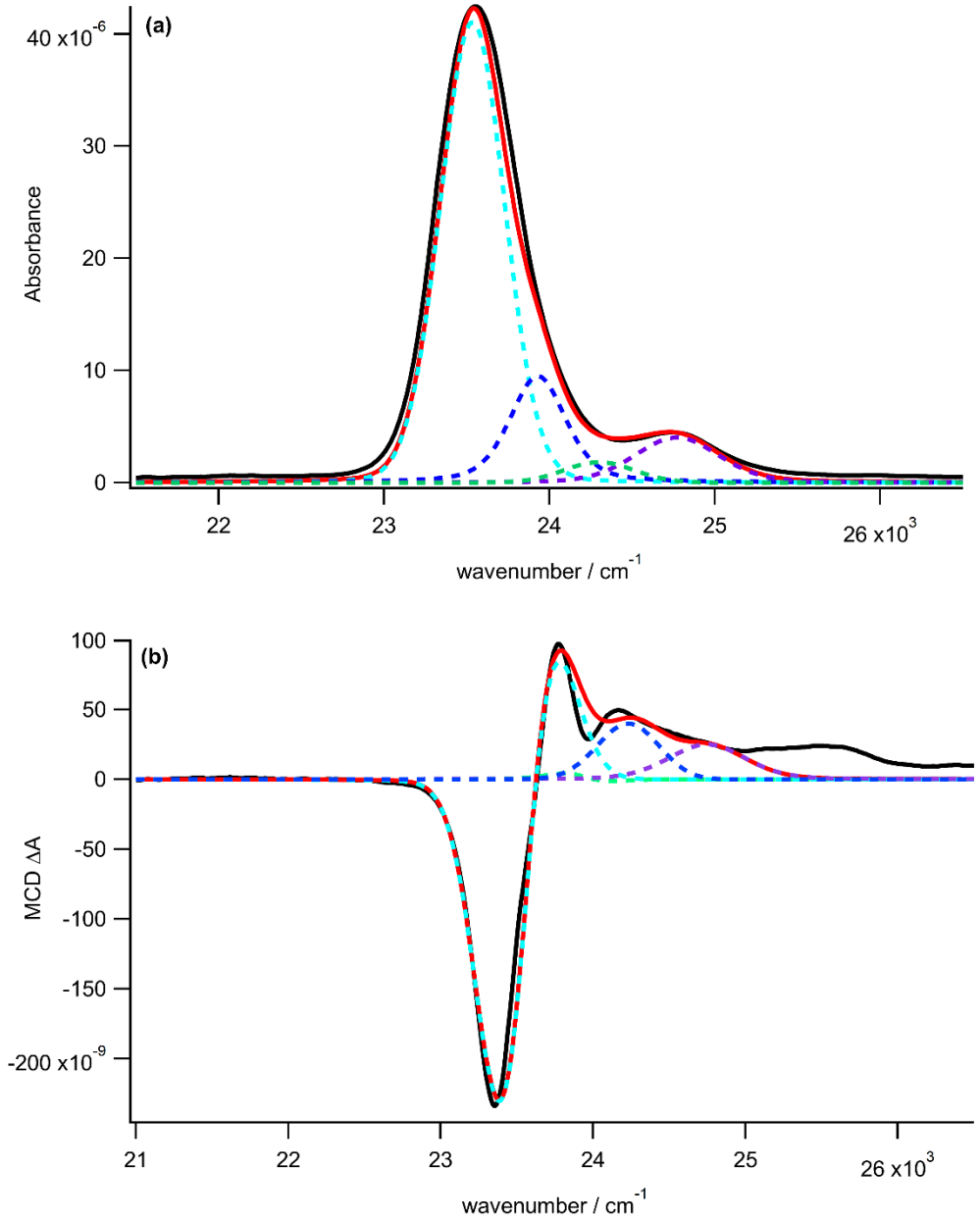

Figure S3-10 Band deconvolution of absorption (**a**) and MCD (**b**) of B(0,0) band spectra [Tb(TPP)Salen]Cl at 100 K and under 1 T. Experimental spectra is shown in black while simulated band is in red color. The components that give the simulated band are in dashed lines.

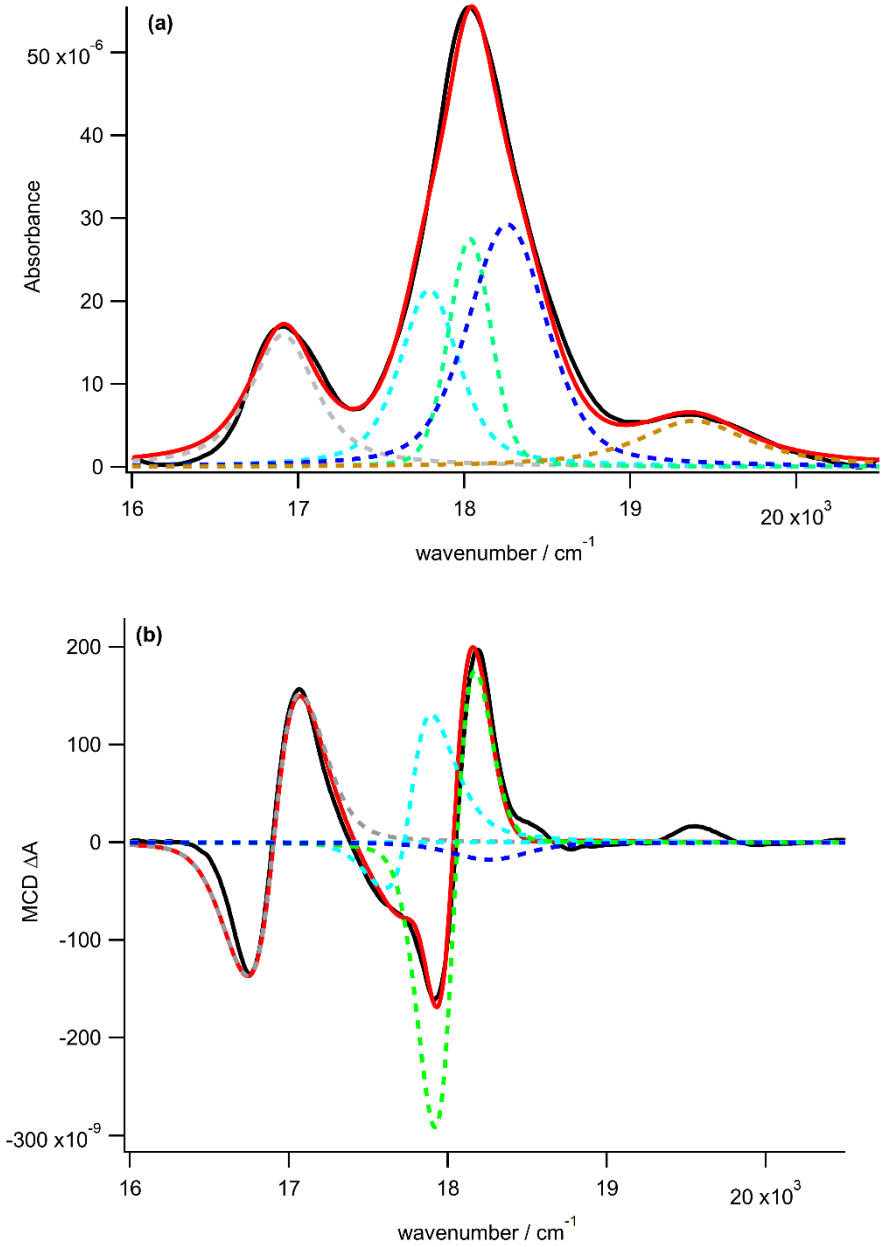

Figure S3-11 Band deconvolution of absorption (**a**) and MCD (**b**) of Q(0,0) and Q(1,0) band spectra [Tb(TPP)Salen]Cl at 100 K and under 1 T. Experimental spectra is shown in black while simulated band is in red color. The components that give the simulated band are in dashed lines.

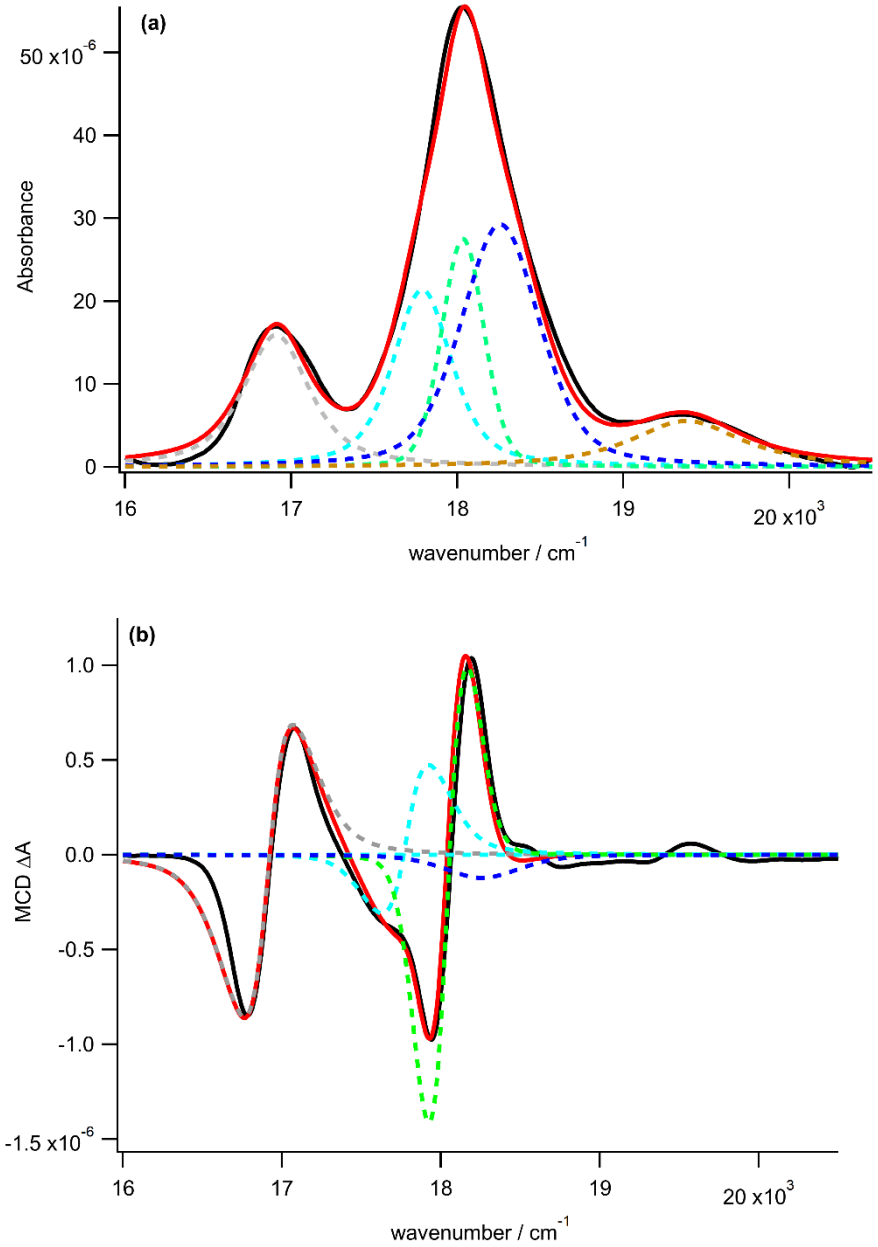

Figure S3-12 Band deconvolution of absorption (**a**) and MCD (**b**) of Q(0,0) and Q(1,0) band spectra [Tb(TPP)Salen]Cl at 1.5 K and under 1 T. Experimental spectra is shown in black while simulated band is in red color. The components that give the simulated band are in dashed lines.

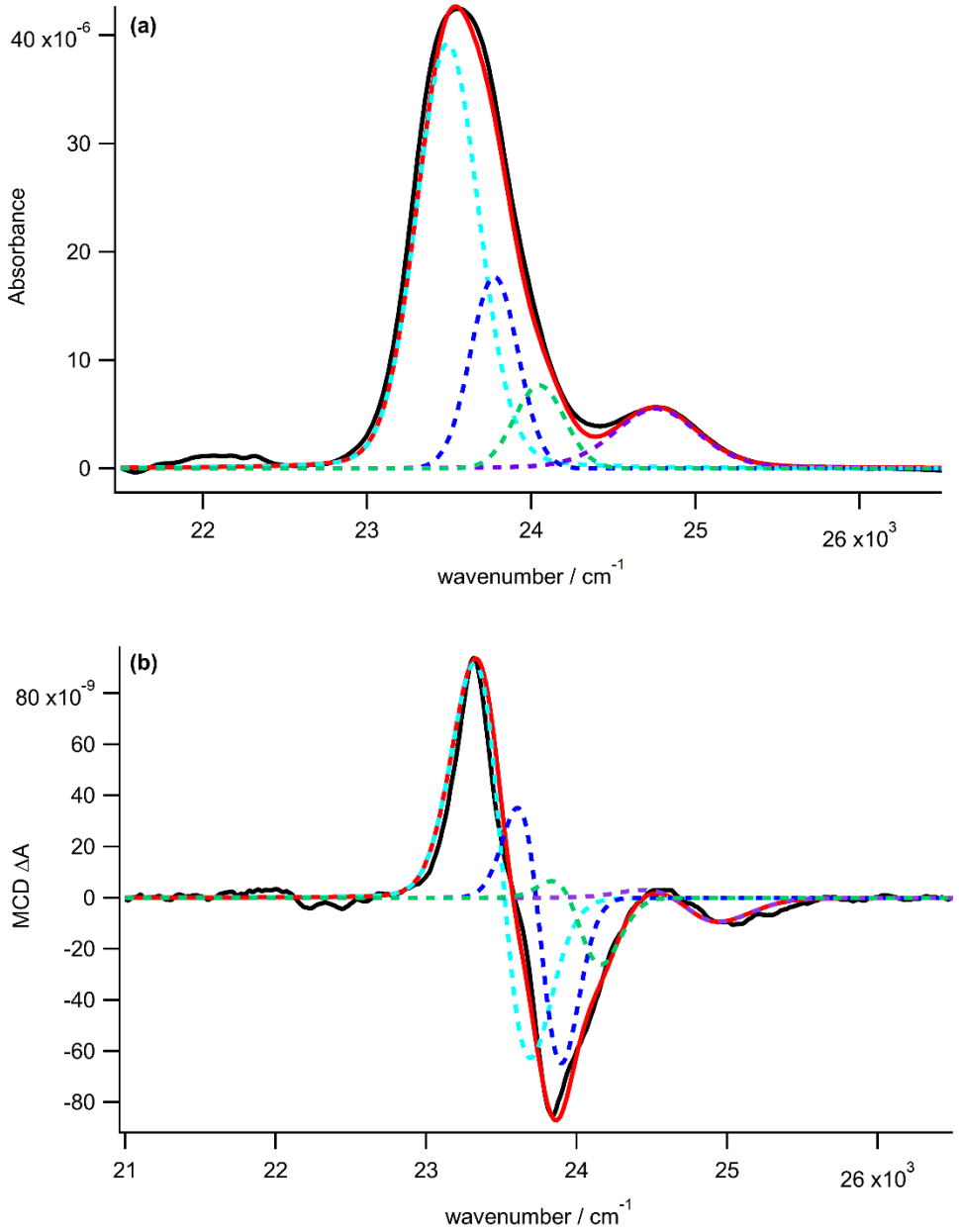

Figure S3-13 Band deconvolution of absorption (**a**) and MCD (**b**) of B(0,0) band spectra [Dy(TPP)Salen]Cl at 20 K and under 1 T. Experimental spectra is shown in black while simulated band is in red color. The components that give the simulated band are in dashed lines.

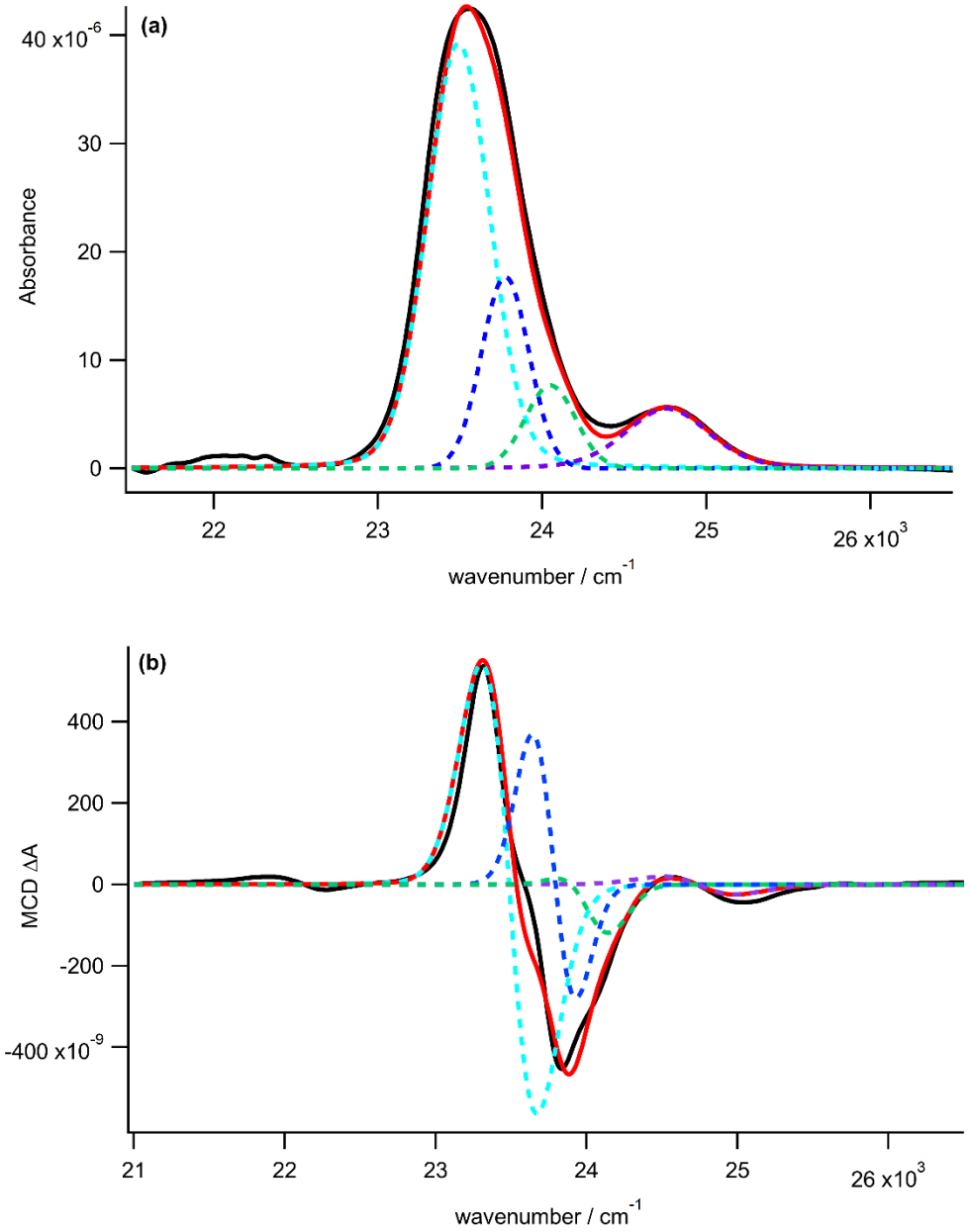

Figure S3-14 Band deconvolution of absorption (**a**) and MCD (**b**) of B(0,0) band spectra [Dy(TPP)Salen]Cl at 1.5 K and under 1 T. Experimental spectra is shown in black while simulated band is in red color. The components that give the simulated band are in dashed lines.

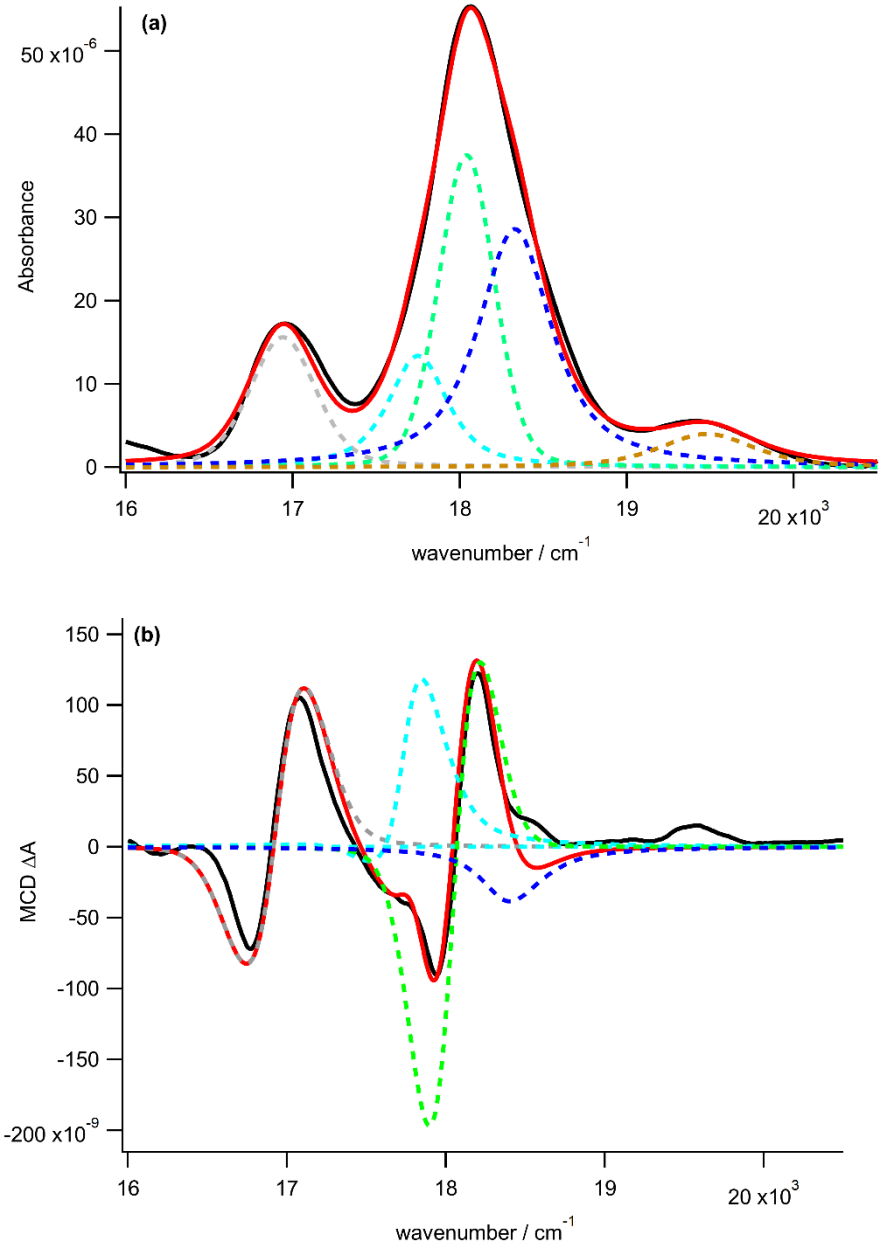

Figure S3-15 Band deconvolution of absorption (**a**) and MCD (**b**) of Q(0,0) and Q(1,0) bands spectra [Dy(TPP)Salen]Cl at 100 K and under 1 T. Experimental spectra is shown in black while simulated band is in red color. The components that give the simulated band are in dashed lines.

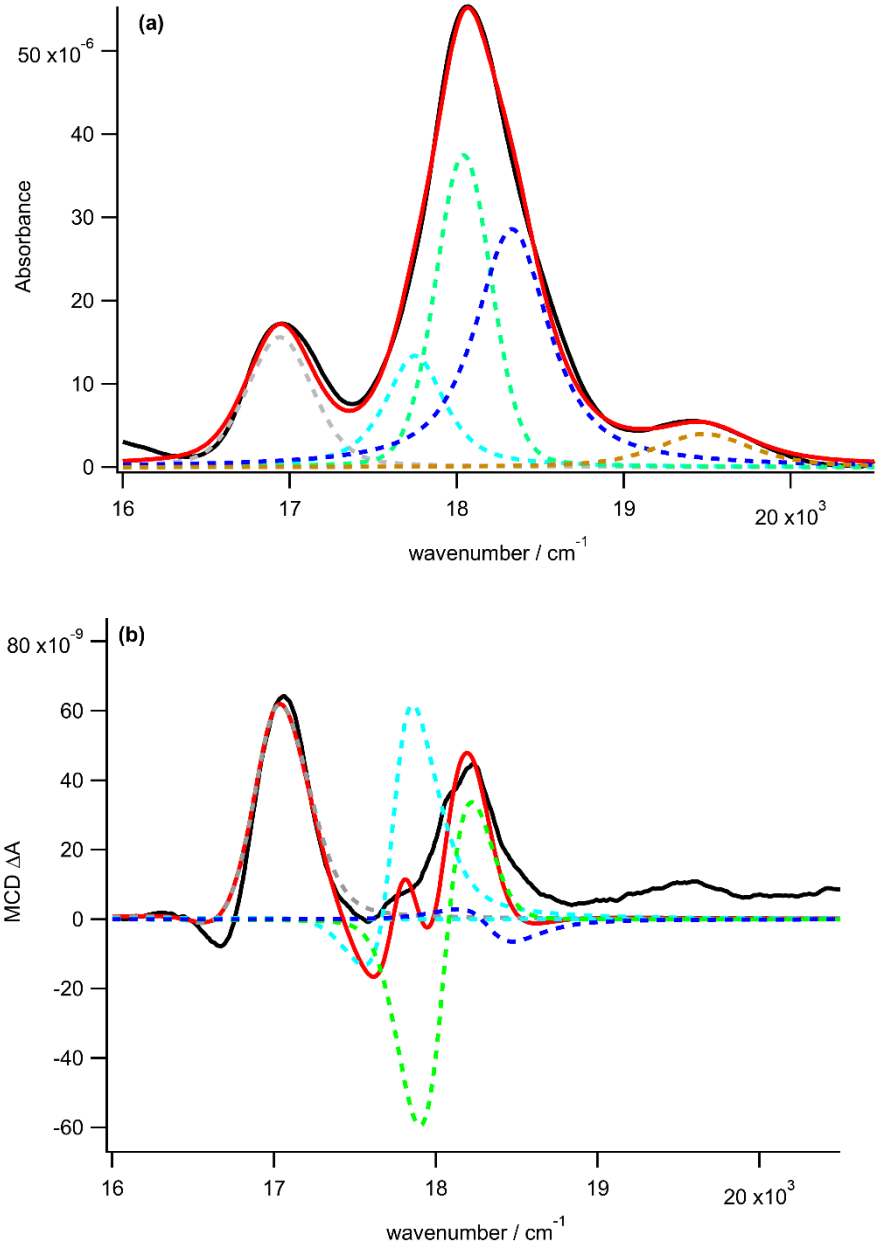

Figure S3-16 Band deconvolution of absorption (**a**) and MCD (**b**) of Q(0,0) and Q(1,0) bands spectra [Dy(TPP)Salen]Cl at 1.5 K and under 1 T. Experimental spectra is shown in black while simulated band is in red color. The components that give the simulated band are in dashed lines.

[Y(TPP)Salen]$^+$						
From	To	Oscillator Strength	Einstein Coefficient (sec^{-1})			Total A (sec^{-1})
			A_x	A_y	A_z	
1	2	4.14×10^{-3}	1.63×10^{5}	1.83×10^{6}	7.78×10^{3}	2.00×10^{6}
1	3	2.03×10^{-2}	7.38×10^{5}	9.01×10^{6}	1.39×10^{5}	9.89×10^{6}
1	4	4.32	5.21×10^{9}	8.81×10^{8}	3.17×10^{5}	6.09×10^{9}
1	5	4.38	1.02×10^{9}	5.42×10^{9}	1.80×10^{7}	6.46×10^{9}
2	4	4.09×10^{-2}	7.00×10^{6}	2.11×10^{6}	7.99×10^{5}	9.91×10^{6}
2	5	2.88×10^{-2}	1.82×10^{6}	5.83×10^{6}	1.21×10^{5}	7.77×10^{6}
3	4	2.24×10^{-2}	3.20×10^{3}	5.36×10^{6}	1.62×10^{4}	5.38×10^{6}
3	5	2.21×10^{-2}	4.02×10^{6}	1.54×10^{6}	3.56×10^{5}	5.91×10^{6}
4	5	3.50×10^{-3}	2.11×10^{3}	3.74×10^{2}	1.52	2.49×10^{3}

Table S3-1. Dipole transition strengths for [Y(TPP)Salen]$^+$ obtained from RASSCF/RASSI/single_aniso calculations.

		Q band					B band			
		Band 1	Band 2	Band 3	Band 4	Band 5	Band 6	Band 7	Band 8	Band 9
E_0 $(cm^{-1})^{\xi}$		16910	17805	18025	18250	19387	23562	23885	24260	24760
Γ $(cm^{-1})^{\xi}$		420	400	290	570	800	440	410	300	600
η^{ξ}		0.61	0.85	0.49	0.60	0.80	0.33	0.00	0.5	0.3
$\mathcal{D}_0$		0.34	0.48	0.390	0.89	0.22	23.50	4.01	0.45	2.47
Values obtained under 1 T										
T (K)		Band 1	Band 2	Band 3	Band 4	Band 5	Band 6	Band 7	Band 8	Band 9
100	$\mathcal{A}_1/\mathcal{D}_0$	4.11450	1.63544	2.51098	0.22472	0.00000	0.61843	0.14942	-0.22222	0.27037
	$\mathcal{B}_0/\mathcal{D}_0$	0.00117	0.00372	-0.00399	-0.00033	0.00000	-0.00011	0.00151	0.00666	0.00081
1.5	$\mathcal{A}_1/\mathcal{D}_0$	4.52595	1.59455	2.66199	0.22471	0.00000	0.66098	0.08591	-0.22222	0.27037
	$\mathcal{B}_0/\mathcal{D}_0$	0.00146	0.00388	-0.00447	-0.0003	0.00000	-0.00016	0.00151	0.00444	-0.00040
Values obtained at 1.5 K										
B (T)		Band 1	Band 2	Band 3	Band 4	Band 5	Band 6	Band 7	Band 8	Band 9
1	$\mathcal{A}_1/\mathcal{D}_0$	4.52595	1.59455	2.66199	0.22471	0.00000	0.66098	0.08591	-0.22222	0.27037
	$\mathcal{B}_0/\mathcal{D}_0$	0.00146	0.00388	-0.00447	-0.00033	0.00000	-0.00016	0.00151	0.00444	-0.00040
2	$\mathcal{A}_1/\mathcal{D}_0$	4.52595	1.59455	2.66199	0.22471	0.00000	0.66098	0.08591	-0.22222	0.27037
	$\mathcal{B}_0/\mathcal{D}_0$	0.00146	0.00367	-0.00383	-0.00033	0.00000	-0.00024	0.00151	0.00444	-0.00040
3	$\mathcal{A}_1/\mathcal{D}_0$	4.52595	1.59455	2.66199	0.22471	0.00000	0.66098	0.08591	-0.22222	0.27037
	$\mathcal{B}_0/\mathcal{D}_0$	0.00146	0.00367	-0.00383	-0.00067	0.00000	-0.00024	0.00151	0.00444	-0.00040
4	$\mathcal{A}_1/\mathcal{D}_0$	4.52595	1.59455	2.66199	0.22471	0.00000	0.66098	0.08591	-0.22222	0.27037
	$\mathcal{B}_0/\mathcal{D}_0$	0.00146	0.00408	-0.00435	0.00000	0.00000	-0.00024	0.00151	0.00444	-0.00040
5	$\mathcal{A}_1/\mathcal{D}_0$	4.52595	1.59455	2.66199	0.22471	0.00000	0.66098	0.08591	-0.22222	0.27037
	$\mathcal{B}_0/\mathcal{D}_0$	0.00146	0.00408	-0.00435	0.00000	0.00000	-0.00024	0.00151	0.00444	-0.00040
6	$\mathcal{A}_1/\mathcal{D}_0$	4.52595	1.63544	2.66199	0.22471	0.00000	0.66098	0.08591	-0.22222	0.27037
	$\mathcal{B}_0/\mathcal{D}_0$	0.00146	0.00408	-0.00435	0.00000	0.00000	-0.00024	0.00151	0.00444	-0.00040

Table S3-2. Parameters of B and Q bands determined by the band deconvolution of absorption and MCD spectra of [Y(TPP)Salen]Cl incorporated into PMMA.

		Q band					B band			
		Band 1	Band 2	Band 3	Band 4	Band 5	Band 6	Band 7	Band 8	Band 9
E_0 $(cm^{-1})^{\xi}$		16910	17780	18030	18260	19380	23535	23930	24300	24770
Γ $(cm^{-1})^{\xi}$		454	420	320	560	800	460	400	500	600
η^{ξ}		0.54	0.75	0.35	0.48	0.89	0.08	0.50	0.00	0.26
$\mathcal{D}_0$		0.41	0.53	0.49	0.86	0.29	25.50	5.95	1.20	3.47
Values obtained under 1 T										
T (K)		Band 1	Band 2	Band 3	Band 4	Band 5	Band 6	Band 7	Band 8	Band 9
100	$\mathcal{A}_1/\mathcal{D}_0$	6.67557	2.90903	3.94884	0.00000	0.00000	0.61487	0.00000	-3.33333	-1.15015
	$\mathcal{B}_0/\mathcal{D}_0$	0.00159	0.00625	-0.00653	-0.00137	0.00000	-0.00039	0.00016	0.00191	0.00287
1.5	$\mathcal{A}_1/\mathcal{D}_0$	34.92569	14.36420	20.47241	0.00000	0.00000	2.52317	-0.16798	-3.33333	-0.28753
	$\mathcal{B}_0/\mathcal{D}_0$	-0.01860	0.02381	-0.03746	-0.00137	0.00000	-0.00627	0.00050	0.044166	0.013226
Values obtained at 1.5 K										
B (T)		Band 1	Band 2	Band 3	Band 4	Band 5	Band 6	Band 7	Band 8	Band 9
1	$\mathcal{A}_1/\mathcal{D}_0$	34.92569	14.36420	20.47241	0.00000	0.00000	2.52317	-0.16798	-3.33333	-0.28753
	$\mathcal{B}_0/\mathcal{D}_0$	-0.01860	0.02381	-0.03746	-0.00137	0.00000	-0.00627	0.00050	0.044166	0.013226
2	$\mathcal{A}_1/\mathcal{D}_0$	20.91729	10.59407	13.58496	0.00000	0.00000	1.56934	-0.16798	-3.69166	-0.86261
	$\mathcal{B}_0/\mathcal{D}_0$	-0.00577	0.02699	-0.03259	-0.00137	0.00000	-0.00334	0.00016	0.024833	0.00747
3	$\mathcal{A}_1/\mathcal{D}_0$	16.06545	8.70900	10.52020	0.00000	0.00000	1.22341	-0.16798	-1.66666	-0.57507
	$\mathcal{B}_0/\mathcal{D}_0$	-0.00302	0.02343	-0.02655	-0.00137	0.00000	-0.00232	0.00142	0.01500	0.00575
4	$\mathcal{A}_1/\mathcal{D}_0$	13.52607	8.03415	9.02885	0.00000	0.00000	1.05959	-0.21165	-3.33333	-1.15015
	$\mathcal{B}_0/\mathcal{D}_0$	-0.00333	0.02343	-0.02441	-0.00137	0.00000	-0.00194	0.00125	0.01250	0.00345
5	$\mathcal{A}_1/\mathcal{D}_0$	12.06366	6.14908	7.54899	0.00000	0.00000	0.94199	-0.29161	-3.33333	-0.86261
	$\mathcal{B}_0/\mathcal{D}_0$	-0.00253	0.01401	-0.02265	-0.00327	0.00000	-0.00182	0.00125	0.01000	0.00431
6	$\mathcal{A}_1/\mathcal{D}_0$	11.05851	4.04007	6.36277	0.00000	0.00000	0.87053	-0.56324	-2.86250	-0.57507
	$\mathcal{B}_0/\mathcal{D}_0$	-0.00097	0.00782	-0.01066	-0.00137	0.00000	-0.00182	0.00091	0.01458	0.00287

Table S3-3. Parameters of B and Q bands determined by the band deconvolution of absorption and MCD spectra of [Tb(TPP)Salen]Cl incorporated into PMMA.

		Q band					B band			
		Band 1	Band 2	Band 3	Band 4	Band 5	Band 6	Band 7	Band 8	Band 9
E_0 (cm^{-1}) $^{\xi}$		16940	17750	18040	18330	19480	23490	23775	24050	24760
Γ (cm^{-1}) $^{\xi}$		467	420	392	525	670	450	340	360	600
η^{ξ}		0.37	0.75	0.22	0.86	0.66	0.18	0.00	0.00	0.30
$\mathcal{D}_0$		0.38	0.34	0.72	0.95	0.15	22.45	7.20	3.30	4.38
Values obtained under 1 T										
T (K)		Band 1	Band 2	Band 3	Band 4	Band 5	Band 6	Band 7	Band 8	Band 9
100	$\mathcal{A}_1/\mathcal{D}_0$	4.57630	2.93029	2.62127	-0.25166	0.00000	-0.10325	-0.03960	-0.25494	-0.30181
	$\mathcal{B}_0/\mathcal{D}_0$	0.00313	0.01259	-0.00302	-0.00262	0.00000	-0.00006	-0.00072	-0.00076	-0.00042
1.5	$\mathcal{A}_1/\mathcal{D}_0$	1.05822	1.81678	0.74084	-0.13894	0.00000	-9.74594	-9.28330	-3.76151	-3.66928
	$\mathcal{B}_0/\mathcal{D}_0$	0.00691	0.00553	-0.00117	-0.00018	0.00000	-0.00097	0.00892	-0.02504	-0.00141
Values obtained at 1.5 K										
B (T)		Band 1	Band 2	Band 3	Band 4	Band 5	Band 6	Band 7	Band 8	Band 9
1	$\mathcal{A}_1/\mathcal{D}_0$	1.05822	1.81678	0.74084	-0.13894	0.00000	-9.74594	-9.28330	-3.76151	-3.66928
	$\mathcal{B}_0/\mathcal{D}_0$	0.00691	0.00553	-0.00117	-0.00018	0.00000	-0.00097	0.00892	-0.02504	-0.00141
2	$\mathcal{A}_1/\mathcal{D}_0$	2.84598	1.98966	1.73408	0.22591	0.00000	-4.76839	-4.83969	-1.94333	-1.16232
	$\mathcal{B}_0/\mathcal{D}_0$	0.00509	0.00961	-0.00089	-0.00183	0.00000	-0.00104	0.00656	-0.01616	-0.00141
3	$\mathcal{A}_1/\mathcal{D}_0$	3.50642	2.33807	2.10530	0.22591	0.00000	-2.92714	-2.71102	-0.91303	-1.16232
	$\mathcal{B}_0/\mathcal{D}_0$	0.00454	0.01022	-0.00105	-0.00196	0.00000	-0.00032	0.00453	-0.01313	-0.00141
4	$\mathcal{A}_1/\mathcal{D}_0$	3.80859	2.31493	2.27827	0.33717	0.00000	-2.00379	-2.01146	-0.61000	-0.70650
	$\mathcal{B}_0/\mathcal{D}_0$	0.00360	0.00990	-0.00109	-0.00183	0.00000	0.00016	0.00326	-0.00779	0.00048
5	$\mathcal{A}_1/\mathcal{D}_0$	4.04587	2.54642	2.39653	0.22591	0.00000	-1.54708	-1.62788	-0.64545	-0.93441
	$\mathcal{B}_0/\mathcal{D}_0$	0.00447	0.01139	-0.00204	-0.00180	0.00000	-0.00014	0.00302	-0.00551	-0.00027
6	$\mathcal{A}_1/\mathcal{D}_0$	4.17951	2.60795	2.47721	0.22591	0.00000	-1.17324	-1.27091	-0.64545	-0.70650
	$\mathcal{B}_0/\mathcal{D}_0$	0.00386	0.01139	-0.00192	-0.00180	0.00000	-0.00007	0.00171	-0.00358	0.00071

Table S3-4. Parameters of B and Q bands determined by the band deconvolution of absorption and MCD spectra of [Dy(TPP)Salen]Cl incorporated into PMMA.

Chapter 4
Conclusion and Future Research

4.1 Conclusions

From this report, it can be concluded that replacement of cyclododecane ligands and Schiff-base ligands as the non-aromatic ligands in the Ln-tetraphenylporphyrin molecular systems can be done without any particular treatment during the synthesis process. Thus, VT-VH-MCD measurements of lanthanide-tetraphenylporphyrin containing different non-aromatic ligands i.e. 12-crown-4 ether, 1-aza-12-crown-4 ether, and salen could be carried out and the values of L_z and Δ_{JL} for each complex were calculated in order to know how the electronic interaction varied with different second ligands.

In the case of Ln-porphyrinoid compounds with cyclododecanes, both 12-crown-4 ether and 1-aza-12-crown-4 ether could be added and the formation of Ln-tetraphenylporphyrin with 12-crown-4 ether or with 1-aza-12-crown-4 ether with good purity. Furthermore, the values of L_z in all complexes in B(0,0), Q(0,0), and Q(1,0) bands remain unchanged, meaning different symmetry of the cyclododecane moiety did not affect the angular momentum of the porphyrin. However, smaller symmetry as in 1-aza-12-crown-4 ether was confirmed to enhance the electronic interaction Δ_{JL} in Tb and Dy. Particularly, for the Dy complexes, reversal of $\mathcal{A}_1/\mathcal{D}_0$ from positive to negative attributed to the antiferromagnetic character of Dy in Q bands area under temperature lowering was observed in [Dy(TPP)Azacrown]Cl and such reversal was not detected in [Dy(TPP)Crown]Cl.

When salen ligand was added to Ln-tetraphenylporphyrin, potassium hydroxide was added as a stabilizer. From VT-VH-MCD measurement, while L_z of B(0,0) band was relatively same with that of the cyclododecane complexes, L_z values of Q(0,0) band in [Ln(TPP)Salen]Cl demonstrated increment. Besides that, Δ_{JL} values of B(0,0) band of Tb and Dy were found to be in between those of [Ln(TPP)Crown]Cl and [Ln(TPP)Azacrown]Cl. However, [Tb(TPP)Salen]Cl and [Dy(TPP)Salen]Cl showed Δ_{JL} increase in Q(0,0) band compared to [Ln(TPP)Crown]Cl and this increase is more significant for [Tb(TPP)Salen]Cl since the Δ_{JL} exceeded that of [Ln(TPP)Azacrown]Cl as well. All the results can be presented in the tables below.

Compound	B(0,0)		Q(0,0)		Q(1,0)	
	L_z	Δ_{JL}	L_z	Δ_{JL}	L_z	Δ_{JL}
[Y(TPP)Crown]Cl	0.54	-	3.44	-	2.35	-
[Tb(TPP)Crown]Cl	0.63	0.81	3.61	5.24	2.83	3.63
[Dy(TPP)Crown]Cl	0.84	-3.19	3.53	-0.39	2.26	-0.26
[Y(TPP)Azacrown]Cl	0.61	-	3.5	-	2.25	-
[Tb(TPP)Azacrown]Cl	0.54	1.02	3.68	6.77	3.9	4.37
[Dy(TPP)Azacrown]Cl	0.28	-4.19	3.44	-3.24	1.03	-1.74
[Y(TPP)Salen]Cl	0.66	-	4.53	-	2.66	-
[Tb(TPP)Salen]Cl	0.53	0.66	6.26	9.31	3.45	5.77
[Dy(TPP)Salen]Cl	0.59	-3.50	4.85	-1.29	2.85	-0.71

4.2 Future Research Ideas

In this research report, the investigation of **J–L** interaction in lanthanide-porphyrinoid compounds are discussed without discussing the structural aspects of each complex. This is because single-crystals of all complexes still cannot be isolated. Thus, researches focusing on obtaining crystal structures are important in the future in order to examine how bond length between Ln with the non-aromatic ligands differ. Regarding the computational chemistry calculation, advance research should be conducted in how to reproduce Δ_{JL} of Ln-tetraphenylporphyrin containing asymmetric second ligand. Moreover, compared to Tb, Dy showed interesting reversal behaviour depending on the non-aromatic ligand under temperature variation in which MCD spectra in Q band region did not show reversal when the temperature was lowered. Hence, future research about modifying the antiferromagnetic behaviour in Dy-porphyrinoid systems only by adding various non-aromatic ligands is necessary and also how the behaviour influences the electronic interaction should be carried out.